Generation and characterization of FRET-based cGMP sensor knock-in mice for cGMP imaging

Dissertation

der Mathematisch-Naturwissenschaftlichen Fakultät

der Eberhard Karls Universität Tübingen

zur Erlangung des Grades eines

Doktors der Naturwissenschaften

(Dr. rer. nat.)

vorgelegt von

Lai Wen

aus Jiangxi, China

Tübingen

2014

Zusammenfassung

Die molekularbiologischen Vorgänge in einer Zelle sind hochgradig dynamisch und können in subzellulären Kompartimenten lokalisiert sein. Cyclisches Guanosinmonophosphat (cGMP) ist ein ubiquitär vorkommendes Signalmolekül, das viele physiologische Prozesse beeinflusst. Die Biosynthese von cGMP erfolgt durch Guanylylcyclasen, welche durch NO oder bestimmte Peptide stimuliert werden. Der Abbau von cGMP und die Beendigung der damit verbundenen Signale erfolgt durch Phosphodiesterasen (PDEs), die cGMP zu GMP hydrolysieren. cGMP-Signale regulieren unter anderem die Relaxation glatter Muskelzellen, die Aggregation von Blutplättchen und die neuronale Entwicklung und Plastizität. Allerdings ist die räumlich-zeitliche *in vivo*-Dynamik von cGMP-Signalen größtenteils unbekannt. Mittels herkömmlicher Detektionsmethoden, wie z. B. Radioimmunassays oder Enzym-gekoppelten Immunassays, kann cGMP nicht in lebenden Zellen oder Organismen in Echtzeit verfolgt werden. Seit Kurzem stehen aber Sensorproteine zur Verfügung, die Veränderungen der cGMP-Konzentration anhand ihrer Fluoreszenzänderungen messbar machen. Diese Sensoren bieten eine hervorragende Möglichkeit, cGMP in lebenden Zellen in Echtzeit mit hoher räumlicher Auflösung „sichtbar" zu machen und zu quantifizieren.

Im Rahmen dieser Arbeit wurden sog. „cGMP-Sensor Knock-in"-Mauslinien erzeugt, die es ermöglichen cGMP-Signale *in vivo* zu visualisieren. Hierzu wurde eine durch Cre-Rekombinase aktivierbare Expressionskassette verwendet, über die der Fluoreszenz-Resonanzenergietransfer (FRET)-basierte cGMP-Sensor cGi500 (<u>c</u>GMP-<u>I</u>ndikator mit einer EC_{50} von <u>500</u> nM für cGMP) unter Kontrolle des CAG-Promotors (cytomegalovirus early enhancer/chicken β-actin/β-globin) exprimiert wird. Das DNA-Konstrukt wurde mittels homologer Rekombination in embryonalen Stammzellen in den murinen Rosa26-Genlocus integriert. Je nachdem welche Strategie zur Aktivierung der Sensorexpression verwendet wurde, zeigten die Mäuse entweder eine allgemeine oder eine gewebespezifische Expression des Sensors, welche die Untersuchung von cGMP-Signalen *in vivo* ermöglichte. Durch Kreuzung der Knock-in-Mäuse mit einer Purkinjezell-spezifischen Cre-Mauslinie (L7-Cre) konnten Mäuse generiert werden, welche den cGi500-Sensor spezifisch in den Purkinjezellen des Cerebellums exprimieren. In der ubiquitär exprimierenden Mauslinie konnte der Sensor in verschiedenen Geweben und Zelltypen nachgewiesen

werden. Eine starke und einheitliche Expression des Sensors konnte z. B. in Glattmuskelzellen, Blutplättchen und Neuronen nachgewiesen werden, nachdem diese Zellen als primäre Zellkulturen aus dieser Mauslinie gewonnen worden waren. Mit Hilfe dieser neuen cGMP-Sensormauslinien können cGMP-Signale nun nicht nur in vielen Zell- und Gewebetypen, sondern erstmals auch in lebenden Säugetieren gemessen werden.

In der vorliegenden Arbeit konnten cGMP-Signale erfolgreich in Echtzeit und mit subzellulärer Auflösung visualisiert werden. Es ist zwar bekannt, dass der cGMP-Signalweg die Bifurkation von Axonen der Neurone in Hinterwurzelganglien (DRGs, engl.: "dorsal root ganglion") während der Embryonalentwicklung reguliert, aber der zugrunde liegende molekulare Mechanismus ist nicht vollständig geklärt. Die in dieser Arbeit durchgeführten FRET-Untersuchungen von lebenden embryonalen DRG-Neuronen zeigten, dass nur das natriuretische Peptid Typ C (CNP, engl.: "C-type natriuretic peptide"), nicht aber das atriale natriuretische Peptid (ANP) oder NO, die Bildung von cGMP stimulierte. Der Abbau von cGMP erfolgte in diesen Neuronen hauptsächlich durch PDE1 und PDE2. Die lokale Applikation von CNP am Wachstumskegel der embryonalen DRG-Neurone führte zu einer lokal begrenzten Produktion von cGMP, was darauf hindeutete, dass der Wachstumskegel cGMP-Signale unabhängig vom Soma der Zelle generieren kann. Diese lokale Erhöhung von cGMP könnte eine wichtige Rolle in der Wegfindung und Verzweigung der Axone der DRG-Neurone spielen, wenn diese während der Embryonalentwicklung in die Eintrittszone des Wirbelkanals vordringen.

Im letzten Teil der Arbeit wurden cGMP-Signale in murinen Blutplättchen untersucht, welche ein klinisch relevantes Modell für die Wirkung von cGMP-erhöhenden Pharmaka darstellen. cGMP-FRET-Versuche mit adhärenten Blutplättchen in einer Flusskammer zeigten, dass cGMP nach Applikation von NO, nicht aber nach ANP-oder CNP-Gabe, erhöht wurde, und dass die PDE2, PDE3 und PDE5 zum Abbau des NO-induzierten cGMPs beitrugen. Diese Daten bestätigten frühere Untersuchungen zum cGMP-Signalweg in Blutplättchen. Die Gabe von NO-freisetzenden Substanzen bewirkte einen schnellen und anhaltenden cGMP-Anstieg. Überraschenderweise führte eine Verringerung der Flussrate während der cGMP-Plateauphase zu einem schnellen Abfall der intrazellulären cGMP-Konzentration, was darauf hindeutete, dass die NO-induzierten cGMP-Signale durch Scherkräfte reguliert werden. Durch die gleichzeitige Messung von cGMP und Ca^{2+} konnte gezeigt werden, dass sich die Konzentrationen dieser sog. zweiten Botenstoffe (engl.: "second messenger")

gegenläufig verhalten. In Anwesenheit von NO führte die Scherbeanspruchung zu einem Anstieg von cGMP, dem ein Abfall des aggregationsunterstützenden Ca^{2+}-Signals folgte. Diese Ergebnisse legen den Schluss nahe, dass die Scherbeanspruchung als physikalischer Antikoagulationsfaktor die Plättchenaggregation reguliert. Dieser neu entdeckte Mechanismus der Scherkraft-abhängigen Regulation des NO/cGMP-Signalwegs könnte *in vivo* eine wichtige Rolle in der Hämostase und Thromboseentstehung spielen.

Zusammenfassend kann festgestellt werden, dass die im Rahmen dieser Arbeit generierten und charakterisierten cGMP-Sensor Knock-in-Mauslinien den großen Vorteil bieten, dass nun cGMP-Signale und damit verbundene biologische Vorgänge *in vivo* und in Echtzeit untersucht werden können. In Kombination mit neuen Methoden wie der Intravitalmikroskopie, und zusammen mit anderen genetischen Mausmodellen, sollten diese Mauslinien ein breites Anwendungsspektrum haben, um cGMP-abhängige Mechanismen unter physiologischen und pathophysiologischen Bedingungen weiter aufzuklären.

Summary

Molecular events in cells are highly dynamic and can occur locally in subcellular domains or compartments. Cyclic guanosine monophosphate (cGMP) is a ubiquitous molecule modulating a wide range of physiological processes. It is generated by guanylyl cyclases which are activated by NO or certain peptides. Phosphodiesterases (PDEs) degrade cGMP by hydrolyzing it to GMP, thereby deactivating cGMP-dependent pathways. Among other functions, cGMP regulates smooth muscle relaxation, platelet aggregation, and neuronal development and plasticity. However, the spatiotemporal dynamics of cGMP *in vivo* is largely unknown. Conventional methods for cGMP detection, such as radioimmunoassays or enzyme-linked immunosorbent assays are not able to monitor cGMP signals in real time in live cells or organisms. The recent development of sensor proteins, which detect cGMP via changes in fluorescence offers a great opportunity to visualize and quantify cGMP in real time and in intact living cells with high spatiotemporal resolution.

In this work, so-called cGMP sensor knock-in mice were generated to enable the visualization of cGMP signals *in vivo*. A Cre recombinase-activatable expression cassette of the fluorescence resonance energy transfer (FRET)-based cGi500 sensor (cGMP indicator with an EC_{50} value for cGMP of 500 nM) driven by the cytomegalovirus early enhancer/chicken β-actin/β-globin (CAG) promoter was integrated into the murine Rosa26 locus by homologous recombination in embryonic stem cells. Depending on the strategy to activate sensor expression, these mice showed either ubiquitous or tissue-specific sensor expression allowing for delineation of cGMP signaling *in vivo*. Upon crossbreeding with Purkinje cell-specific Cre (L7-Cre) mice, these sensor knock-in mice exhibited tissue-specific expression of cGi500 in Purkinje cells in the cerebellum. In the ubiquitously expressing mouse line, global cGi500 expression was demonstrated in various tissues and cell types. Primary cells, such as smooth muscle cells, platelets, or neurons isolated from the transgenic cGMP sensor mice confirmed strong and uniform sensor fluorescence. These new mouse lines allowed to robustly measure cGMP not only in multiple cell types and tissues, but also for the first time in living mammals.

In the present study, cGMP signals were also successfully visualized in real time with subcellular resolution. It is well known that the cGMP signaling pathway regulates axonal bifurcation in dorsal root ganglion (DRG) neurons during embryonic development, but the underlying molecular mechanism is not completely understood.

FRET experiments in live embryonic DRG neurons showed that only C-type natriuretic peptide (CNP) but not atrial natriuretic peptide (ANP) or NO stimulated cGMP generation. PDE1 and PDE2 were mainly responsible for cGMP degradation in these neurons. Local application of CNP to growth cones of embryonic DRG neurons increased cGMP only locally, indicating that cGMP can be generated in the growth cone independently of the soma. Local cGMP elevation may be critical for DRG sensory axon pathfinding and branching when they grow into the dorsal root entry zone of the spinal cord during embryonic development.

In the last part of this work, cGMP signals were studied in murine platelets, which represent a clinically important model for the action of cGMP-elevating antithrombotic drugs. cGMP FRET experiments with adherent platelets in a flow chamber showed that cGMP was elevated in response to NO but not ANP or CNP, and that PDE2, PDE3 and PDE5 contributed to the degradation of NO-induced cGMP. These data are in line with previous studies of cGMP signaling in platelets. Application of NO-releasing compounds led to a fast increase of cGMP followed by a sustained cGMP level. Surprisingly, reduction of the flow rate during this plateau resulted in a rapid decrease of the intracellular cGMP concentration, indicating that NO-induced cGMP in platelets was regulated by shear stress. Simultaneous measurements of cGMP and Ca^{2+} revealed that the concentration of these two second messengers had an inverse relationship. In the presence of NO, shear stress resulted in an increase of cGMP followed by a decrease of procoagulant Ca^{2+} signals. These findings suggest that shear stress functions as an anticoagulant physical factor in regulating platelet aggregation. This newly discovered shear stress-regulated NO/cGMP signaling pathway might play important roles in hemostasis and thrombosis *in vivo*.

In summary, the cGMP sensor knock-in mice generated and characterized in this work offer the unique advantage of imaging cGMP and associated biological events in real time *in vivo*. In combination with advanced microscopic techniques, such as intravital microscopy, and other genetic mouse models, these mouse lines should find widespread applications in elucidating cGMP-associated mechanisms under both physiological and pathophysiological conditions.

Table of contents

List of figures

List of tables

Abbreviations

A-DRG	Adult dorsal root ganglion
ANP	Atrial natriuretic peptide
BNP	Brain natriuretic peptide
bp	Base pairs
BRET	Bioluminescence resonance energy transfer
BSA	Bovine serum albumin
BSMCs	Bladder smooth muscle cells
CAG	Cytomegalovirus early enhancer/chicken β-actin/rabbit β-globin
CaM	Calmodulin
cAMP	Cyclic 3',5'-adenosine monophosphate
CFP	Cyan fluorescent protein
cGi	cGMP indicator
cGK	cGMP-dependent protein kinase
cGKII	cGMP-dependent protein kinase II
cGKIα/β	cGMP-dependent protein kinase I α/β
cGMP	Cyclic 3',5'-guanosine monophosphate
CNG	Cyclic nucleotide-gated
CNP	C-type natriuretic peptide
Cre	Cyclisation/recombination SSR
CSMCs	Colonic smooth muscle cells
DAG	Diacylglycerol
DEA/NO	2-(N,N-diethylamino)-diazenolate-2-oxide diethylammonium salt
DETA/NO	(Z)-1-[N-(2-aminoethyl)-N-(2-ammonioethyl)amino]diazen-1-ium-1,2-diolate
DMEM	Dulbecco's modified Eagle medium
DMSO	Dimethyl sulfoxide
DNA	Deoxyribonucleic acid
dNTP	Deoxynucleotide triphosphate
dpc	Days *post coitum*
DREZ	Dorsal root entry zone
DRG	Dorsal root ganglion (ganglia)
DTA	Diphtheria toxin fragment A
ECs	Endothelial cells
EDRF	Endothelium-derived relaxing factor
EDTA	Ethylenediaminetetraacetic acid
EIA	Enzyme-linked immunosorbent assay
EM-CCD	Electron multiplying charge-coupled device
eNOS	Endothelial NO synthase
ER	Endoplasmic reticulum
ES	Embryonic stem
F_{340}	Fluorescence intensity at 340 nm excitation
F_{380}	Fluorescence intensity at 380 nm excitation
F_{480}	Emission at 480 nm (CFP emission)
F_{535}	Emission at 535 nm (YFP emission)
Flp	Flippase
FPLC	Fast protein liquid chromatography
FRET	Fluorescence resonance energy transfer
FRT	Flp recombinase target sequence
G418	Geneticin
GAF	GAF domains from cGMP-specific phosphodiesterases, *Anabaena* adenylyl cyclases, and *E. coli* FhlA
GC	Guanylyl cyclase
GFP	Green fluorescent protein
GPIbα	Glycoprotein Ibα
H-NOX	Heme-nitric oxide and oxygen binding domain
IBMX	3-Isobutyl-1-methylxanthine
iNOS	Inducible NO synthase

IP$_3$	Inositol triphosphate
IP$_3$R	IP$_3$ receptor
IRAG	IP$_3$R-associated cGMP kinase substrate
LacZ	β-Galactosidase-coding lacZ gene
LIF	Leukemia inhibitory factor
loxP	Locus of X-over in P1
mRNA	Messenger RNA
MRP	Multidrug resistance protein
Neo^R	Neomcyin resistance gene
NGF	Nerve growth factor
NGS	Normal goat serum
nNOS	Neuronal NO synthase
NO	Nitric oxide
NOS	Nitric oxide synthase
ODQ	1H-[1,2,4]oxadiazolo[4,3-a]quinoxalin-1-one
ORF	Open reading frame
PBS	Phosphate-buffered saline
PCR	Polymerase chain reaction
PDE	Phosphodiesterase
PDL	Poly-D-lysine
Pen/Strep	Penicillin/Streptomycin
pGC	Particulate guanylyl cyclase
PPIX	Protoporphyrin IX
R	CFP/YFP emission ratio (F_{480}/F_{535}) or ratio of fluorescence intensity at 340 nm/380 nm excitation (F_{340}/F_{380})
RIA	Radioimmunoassay
RNA	Ribonucleic acid
ROI	Region of interest
ROSA	Reverse orientation splice acceptor
RT	Room temperature
SDS	Sodium dodecyl sulfate
sGC	Soluble guanylyl cyclase
SPER/NO	(Z)-1-[N-[3-aminopropyl]-N-[4-(3-aminopropylammonio)butyl]-amino]diazen-1-ium-1,2-diolate
SSR	Site-specific recombinase
TBS	Tris-buffered saline
Tris	Tris(hydroxymethyl)aminomethane
TRP	Transient receptor potential
TRPC3	Transient receptor potential channel 3
VASP	Vasodilator-stimulated phosphoprotein
VSMCs	Vascular smooth muscle cells
vWF	von Willebrand factor
YFP	Yellow fluorescent protein
β-ME	β-Mercaptoethanol

1 Introduction

1.1 cGMP signaling

Cyclic guanosine monophosphate (cGMP) is a ubiquitous intracellular second messenger that regulates many physiological processes including smooth muscle relaxation, platelet activation, neuronal plasticity and sensory axon bifurcation [1]. Ever since its first discovery in rat urine in the 1960s [2], extensive knowledge about cGMP has been gained throughout the whole signaling pathway as well as its physiological and pathological outcome [1, 3].

In the history of cGMP research, there were two seemingly isolated studies. In the 1970s, Murad and coworkers demonstrated that nitrogen-containing compounds like nitroglycerin, sodium nitroprusside and azide increase cGMP via soluble guanylyl cyclase (sGC), which in turn induces smooth muscle relaxation and vasodilatation. Their paper published in 1977 is a milestone of the cGMP and vascular studies. It shows that it is gaseous nitric oxide (NO) formed from these compounds that activates the sGC [4]. Another study led by Furchgott in 1980 found that the endothelial layer of blood vessels releases a substance upon treatment with acetylcholine that causes smooth muscle relaxation [5]. This mysterious substance was termed endothelium-derived relaxing factor (EDRF), because its chemical nature was unknown for many years. These two studies were unified with the identification of EDRF as NO [6, 7]. Firstly, the effect of EDRF like other nitrovasodilators on vasorelaxation was blocked by hemoglobin and myoglobin [8, 9], and in 1987 Ignarro et al. observed a peak shift of the absorption spectrum of deoxyhemoglobin from 433 to 406 nm indicating that the hemoglobin reacted with NO and formed nitrosyl hemoglobin [6]. These studies led to the conclusion that EDRF released from arteries and veins is NO. At the same time, another independent group led by Moncada also accounted NO for the biological activity of EDRF based on the chemiluminescent product of its reaction with ozone and the similarity of NO and EDRF in biological effects [7]. In 1998, the Nobel Prize for Physiology or Medicine was awarded to Furchgott, Ignarro and Murad for their discovery of NO as a vasodilator.

Today it is well known that NO is a gaseous signaling molecule in mammals, which activates its receptor sGC over 200-fold [10, 11]. Endogenous NO is synthesized by a family of enzymes called nitric oxide synthases (NOS). The NOS in the endothelium can be activated by acetylcholine-induced intracellular Ca^{2+} elevations [12]. NO synthesized in endothelial cells diffuses across membranes to target smooth muscle cells where it activates sGC, resulting in conversion of guanosine-5'-trisphosphate (GTP) to cGMP and thereby smooth muscle relaxation (**Figure 1**).
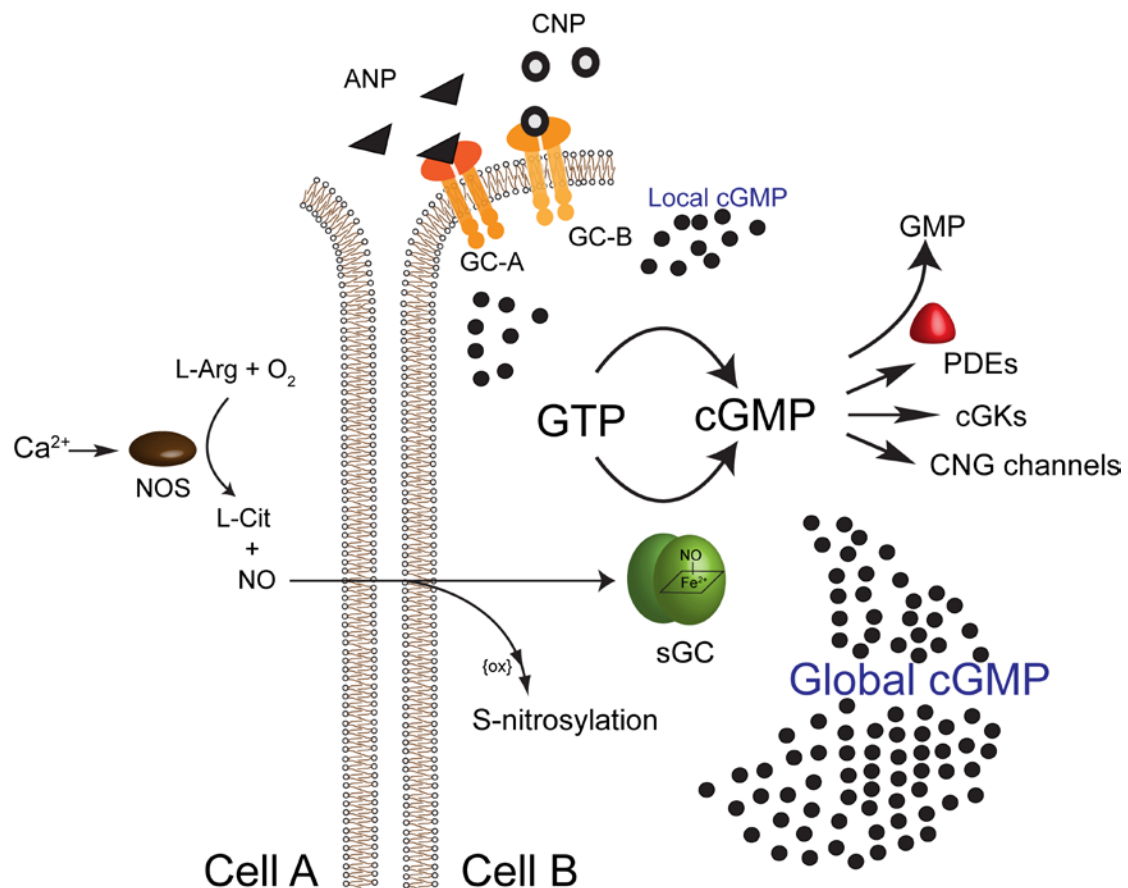
Figure 1. The cGMP signaling pathway.
NO synthesized by NOS in cell A (e.g., endothelial cells) diffuses across cell borders to a target cell B (e.g., smooth muscle cells or platelets). sGC activated by NO generates cGMP, which is degraded by PDEs. Local cGMP can also be generated at the plasma membrane by particulate guanylyl cyclases such as GC-A or GC-B activated by ANP or CNP, respectively. cGMP exerts its function via effector proteins including cGKs, PDEs and CNG channels. NO can also undergo oxidation and react with protein cysteine thiols, leading to S-nitrosylation of proteins. NOS, nitric oxide synthase. L-Arg, L-arginine. L-Cit, L-citrulline. sGC, soluble guanylyl cyclase. ANP, atrial natriuretic peptide. CNP, C-type natriuretic peptide. cGKs, cGMP-dependent protein kinases. PDEs, phosphodiesterases. CNG channels, cyclic nucleotide-gated channels.

During the isolation of guanylyl cyclases (GCs), it was found that both cytosolic and membrane fractions isolated from heart and lung contain GC activity [13, 14]. Later on, specific stimulation of guanylyl cyclases in the membrane was first shown in intestinal tissue with heat-stable toxin of *Escherichia coli* [15]. Therefore, two sites of cGMP generation exist. sGC located in the cytosol is activated by NO and particulate guanylyl cyclases (pGC) in the plasma membrane respond to natriuretic peptides such as atrial (ANP), brain (BNP), and C-type natriuretic peptide (CNP). Accumulating evidence suggests that cGMP produced by these two GCs has different functional outcomes, indicating the compartmentalization of cGMP signaling in cells [16]. On the other hand, cGMP can be removed either by degradation into GMP by phosphodiesterases (PDEs) or excreted by nucleotide transporters present in the plasma membrane [17]. cGMP exerts its effects through activation of multiple targets, such as cGMP-dependent kinases (cGKs), cyclic nucleotide-gated (CNG) ion channels, and PDEs [1, 18, 19].

1.1.1 cGMP generation

1.1.1.1 Nitric oxide

Nitric oxide is a heterodiatomic molecule acting as a gaseous signaling molecule in a vast variety of organisms. Endogenous NO is synthesized from L-arginine and oxygen by NOS enzymes. There are three members of NOS enzymes with different abundance in different tissues: neuronal NOS (nNOS, NOS-1), inducible NOS (iNOS, NOS-2) and endothelial NOS (eNOS, NOS3) [12]. Both nNOS and eNOS are constitutively expressed whereas the expression of iNOS can be induced when macrophages, vascular smooth muscle cells, or endothelial cells are exposed to lipopolysaccharides or cytokines. The activity of nNOS and eNOS is Ca^{2+}/Calmodulin (Ca^{2+}/CaM)-dependent. iNOS was first cloned from macrophages, and is generally independent of intracellular Ca^{2+}/CaM [20]. The physiological NO concentration is proposed to be ranging from 100 pM (or below) up to ~5 nM [21]. In many pathophysiological conditions, iNOS was found to play a prominent role in endotoxic shock, host defense and inflammatory disorders, where the NO concentration produced is also higher (~µM) as comparing to that generated by eNOS and nNOS [22, 23].

NO produced by NOS rapidly diffuses across cell membranes to target cells, where sGC gets activated. Because of the oxidizing nature of NO as a free radical, NO in physiological fluid has a short half-life of several seconds and it can easily change its

redox state. There was skepticism regarding whether the free radical NO or the secondary products are the physiologically relevant species [24]. However, among the redox forms of NO (NO^-, $NO^·$, NO^+), only the uncharged NO radical ($NO^·$) significantly activates sGC [24, 25].

Nitrite and nitrate compounds, such as nitroglycerin, have long been used as clinical therapies for angina pectoris, congestive heart failure, acute myocardial infarction and other cardiovascular diseases without knowing their mechanism of action [26]. Then it became clear that these drugs stimulate cGMP production by donating NO, which activates sGC, therefore relaxing the vascular smooth muscle and leading to vasodilation [4]. Multiple NO donors are available for research today [27]. NO exerts its function predominantly via sGC/cGMP signaling, but it could also react via cGMP-independent mechanisms, such as nitrosylation, the covalent attachment of the NO group to the thiol side chain of cysteine, forming nitrosylated proteins [28].

1.1.1.2 Soluble guanylyl cyclase

Soluble guanylyl cyclase (sGC), the only known receptor for NO, is a heterodimer consisting of two homologous subunits, an α-subunit and a heme-containing β-subunit [29]. The α-subunit has a molecular mass of 73-82 kDa, whereas the β-subunit weighs ~70 kDa [10, 30]. Although each subunit has two isoforms (α1, α2, β1 and β2), the β2 isoform, expressed preferentially in kidney does not form functional enzymes [31]. The heterodimer α1/β1 is more widely expressed throughout the body, including smooth muscle and platelets, while α2/β1 is most abundant in brain, uterus and placenta [32-35]. Catalytic activity requires both subunits. Single subunit expression of individual α1 or β1 cDNA in a heterologous cell system did not show NO-sensitive guanylyl cyclase activity, but only cotransfection of both α1 and β1 resulted in a marked increase in GC activity [36]. The sGC subunits are conserved among eukaryotes. Each subunit consists of four distinct regions. The β1 subunit contains an N-terminal heme-binding domain, a Per/Arnt/Sim (PAS) domain, a putative amphipathic helix/coiled-coil, and a C-terminal catalytic domain. sGC α1 has 30% sequence identity and a similar structural organization like β1, except that its N-terminus is of unknown function. The heme-binding domain of β1 is also termed heme-nitric oxide and oxygen binding domain (H-NOX) based on the ligand binding properties which are conserved among many similar proteins found in prokaryotes and eukaryotes [37, 38]. The rat sGC contains 690 and 619 amino acids of α1 and β1 subunit in length, respectively. The heme-binding domain is located at the residue 1 to ~194 on the β1 subunit [39, 40]. The ferrous heme is ligated to the binding domain via its proximal heme ligand,

histidine 105 (His[105], rat numbering) [41]. NO binds to the heme moiety and converts sGC into an active state leading to over 200-fold activation of the enzyme [11].

Studies with purified protein suggest that sGC is activated in a binary mode [42]. Binding of NO to the reduced Fe^{2+} heme of sGC at a diffusion-controlled rate initially forms a 6-coordinate NO-Fe^{2+}-His-complex. Subsequently, the Fe^{2+}-His bond breaks, resulting in a 5-coordinate nitrosyl-heme complex. This breakage of the Fe^{2+}-His bond is considered a key step, which brings about a conformational change of sGC, and finally full activation of the enzyme [37]. A reduced iron (Fe^{2+}) is essential for the activation of sGC by NO. Oxidation of heme Fe^{2+} to Fe^{3+} state strongly attenuates the enzymatic response to NO [25, 43].

The mechanism of action of several sGC activators supports this binary model of sGC activation. Protoporphyrin IX (PPIX) is the iron-free precursor of heme, which cannot form the bond to the His[105] due to the lack of iron in the porphyrin ring. Therefore, PPIX in substitution of heme forms a complex with sGC, where the axial His is unbound, resembling the 5-coordinate nitrosyl-heme-complex, which in turn activates sGC [44]. In addition to NO, another gaseous molecule, carbon monoxide (CO), can also bind to the H-NOX domain of sGC and activate the enzyme weakly, around 2-4 fold [45]. This is much lower compared to the potency of NO in sGC activation. The vast difference in activation is due to the different reaction between the two diatomic molecules with the ferrous heme of sGC. The binding of CO leads to the formation of a 6-coordinate Fe^{2+}-CO complex which represents the low-active state of sGC [37].

The importance of the NO/cGMP signaling pathway for cardiovascular physiology and diseases has propelled scientists to develop pharmacological compounds capable of directly stimulating the cGMP generator, sGC. These agents that target sGC can be categorized into heme-dependent sGC stimulators and heme-independent sGC activators. The sGC stimulator function relies on the presence of reduced Fe^{2+} heme within sGC, whereas sGC activators activate the enzyme when the heme iron is at its oxidized state (Fe^{3+}), or when the heme group is missing [46, 47]. sGC stimulators like YC-1 or its derivative Bay 41-2272 are from the indazole family. These compounds stabilize the nitrosyl-heme complex and synergize with NO, therefore increase the efficacy of NO dramatically [48, 49]. An inhibitory effect of Bay 41-2272 on PDE5 was also suggested [50]. On the other hand, sGC activators such as Bay 58-2667 and Bay 60-2770 selectively activate heme-oxidized or heme-free sGC, most likely by

mimicking the heme group to cause conformational changes similar to that elicited by NO bound to the heme moiety [47].

Several inhibitors have been found to selectively block NO-induced sGC activity. Out of them, the quinoxalin derivative 1H-[1, 2, 4] oxadiazolo[4,3-a]-quinoxalin-1-one (ODQ) is widely used due to its potency and selectivity [51]. ODQ does not inhibit membrane-bound guanylyl cyclase, adenylyl cyclase or PDE activity. NOS and other heme proteins are affected only at high ODQ concentrations. ODQ or its analog NS2028 are frequently used to obtain sGC-specific inhibition and to distinguish sGC/cGMP-dependent or -independent effects of NO.

Despite the importance of the NO-cGMP pathway in cardiovascular and neuro-degenerative diseases, the modulatory mechanisms of sGC are still poorly known [29, 52]. In particular, desensitization, the attenuated or abolished responsiveness of sGC to a second NO stimulation, is an unresolved issue that might underlie clinical NO tolerance during the development of oxidative vascular pathophysiology, atherosclerosis, and pulmonary hypertension [53, 54]. Similar to other nucleotide-converting enzymes, conversion of GTP to cGMP by sGC requires the divalent cations Mg^{2+} and Mn^{2+}. The heme domain of sGC is key to its regulation; enzyme stimulation by NO depends on the presence of a reduced heme moiety within sGC. Several other mechanisms have been suggested for sGC regulation, including phosphorylation, nitrosylation, translocation, or protein-protein interaction [37].

1.1.1.3 Particulate guanylyl cyclases

As mentioned above, intracellular cGMP levels can also be elevated through membrane-spanning particulate GCs. pGCs are a family of enzymes consisting of at least 7 members: GC-A, GC-B, GC-C, GC-D, GC-E, GC-F and GC-G. They share a basic topology characterized of an extracellular ligand binding domain, a short single transmembrane region, and an intracellular domain that contains the catalytic (GC) region at its C-terminal end [55, 56]. A homodimer is the minimal catalytic unit for guanylyl cyclase activity of pGCs. The common existence of extracellular binding domain implies that these enzymes function as receptors for specific ligands, but to date, only ligands for GC-A, GC-B, GC-C and GC-D have been identified. GC-A is the receptor for atrial natriuretic peptide (ANP) and B-type natriuretic peptide (BNP). GC-B binds C-type natriuretic peptide (CNP), and GC-C mediates the effect of guanylin, uroguanylin and heat-stable enterotoxin. Guanylin and uroguanylin are also extracellular ligands for GC-D in rodents, whereas GC-D in humans appears to be a

pseudogene. GC-E and GC-F are involved in phototransduction in the retina [55]. No extracellular ligands have been identified for GC-E, GC-F and GC-G, which are therefore presumed orphan receptors [56]. GC-A and GC-B are the best characterized membrane guanylyl cyclases. The order of preference of natriuretic peptide-dependent activation of GC-A is ANP≥BNP≫CNP, and that of GC-B is CNP≫ANP=BNP [55, 57].

ANP and BNP are cardiac hormones that are produced mainly in the atrium and ventricle, respectively, and both are released into the bloodstream [58]. The GC-A receptor is expressed in a variety of tissues and activated by circulating ANP and BNP, regulating cardiovascular homeostasis. Genetic deficiency of ANP or of its receptor GC-A in mice leads to arterial hypertension, hypervolemia and cardiac hypertrophy [59-62]. A BNP knock-out does not lead to hypertension or cardiac hypertrophy, but increases the susceptibility to cardiac fibrosis [63]. CNP does not circulate in the blood in appreciable amounts, rather it has local paracrine functions prominent in bone formation and sensory axon bifurcation [64]. Inactivation of GC-B leads to dysfunction in endochondral ossification and dwarfism [65]. The CNP/GC-B/cGKII signaling pathway is critical in long bone growth [66]. Instead, CNP/GC-B/cGKI is essential for sensory axon bifurcation in the spinal cord [67].

1.1.2 cGMP removal

At least three mechanisms are involved in the removal of intracellular cGMP: 1) The conversion of cGMP into GMP. cGMP hydrolysis catalyzed by PDEs represents the most prominent cGMP lowering action in cells. 2) Efflux of cGMP into the extracellular milieu. Since cGMP was first isolated from urine, it is reasonable that cells might extrude cGMP into the extracellular fluid. Indeed, efflux is observed in virtually all cell types. Several transporters located in the plasma membrane have been identified for the efflux process, including members of the multidrug resistance protein (MRP) family, MRP4/5/8 [68]. Although cGMP can be extruded by these transporters, this process is comparatively slower and quantitatively minor than the effects mediated by PDEs [17]. 3) Transit of cGMP through intercellular communication [69]. There are also other processes that can lower intracellular cGMP level in particular cells via cell-cell communication. cGMP in cumulus cells of ovarian follicle gets transported through gap junctions to neighboring oocytes, where cGMP inhibits PDE3 activity in cAMP degradation to arrest oocytes in meiosis prophase [70, 71].

There are 21 genes known that encode cyclic nucleotide phosphodiesterases (PDEs), and they were grouped into 11 gene families based on amino acid sequences,
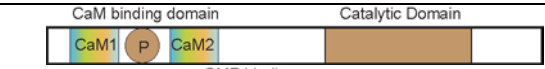
regulatory properties, and catalytic characteristics [69]. These PDEs catalyze the hydrolysis of the phosphodiester bond in cAMP and cGMP, producing 5`-AMP or 5`-GMP. PDEs 4, 7, 8 are highly specific for cAMP, PDEs 5, 6, 9 are highly specific for cGMP, and the remaining five families (PDEs 1, 2, 3, 10, and 11) hydrolyze both cGMP and cAMP, although with different affinities and efficiencies (**Table 1**) [69].

PDEs contain three functional domains, including a N-terminal regulatory domain, a conserved catalytic core and a C-terminus. The catalytic domain containing approximately 270 amino acids is highly conserved (18-46% sequence identity) within all mammalian PDEs. The amino acid sequences outside of this region differ significantly, which accounts for distinct regulatory features. PDEs 2, 5, 6, 10, 11 have tandem GAF domains. GAFs have been shown to function as allosteric cGMP binding sites (PDEs 2, 5, 6, 11), cAMP binding sites (PDE10), dimerization contacts (PDEs 2, 5, 6) and regulators of the catalytic site (PDEs 2, 5). These regulatory domains provide negative feedback and/or crosstalk between cGMP, cAMP, and Ca^{2+} in intact cells. For example, PDE2 is cGMP-stimulated cGMP/cAMP-specific; binding of cGMP to the allosteric site promotes the hydrolysis of cGMP or cAMP. Similarly, PDE10 is cAMP-stimulated cGMP/cAMP-specific. However, PDE3 is a cGMP-inhibited cGMP/cAMP-specific PDE; it has similar affinities for cGMP and cAMP, while the reaction rate for cGMP is ~10% that of cAMP. Thus, cGMP exerts competitive inhibition of cAMP hydrolysis and PDE3 is usually referred as "cGMP-inhibited" PDE. In the case of PDE1, the Ca^{2+}/CaM binding domain can be modulated by intracellular Ca^{2+} levels.

PDE5 and PDE6 have similarities in domain organization. Both enzymes contain tandem GAF domains, and GAF A is responsible for high-affinity allosteric cGMP binding. PDE5 has also subdomains including a single phosphorylation site (Ser^{92}, bovine; Ser^{102}, human) that can be phosphorylated by cGKI [72]. cGMP also increases its PDE5-dependent degradation by direct activation of the PDE5 enzyme through binding to GAFs [73]. PDE5 is highly expressed in smooth muscle [74], platelets [75], cerebellar Purkinje cells [76], gastrointestinal epithelial cells [77] and endothelial cells [78]. Because of its specificity for cGMP degradation, PDE5 has been targeted for drug development. For instance, PDE5 inhibitors like sildenafil (Viagra) are used for treatment of erectile dysfunction and pulmonary hypertension. PDE6 is highly concentrated in the outer segment of retina photoreceptors. PDE6 shares similar domain organization with PDE5, whereas the regulation of PDE6 is unique in the context of rod and cone photoreceptors. In darkness, the cGMP level is relatively high, keeping the cGMP-gated ion channels in the plasma membrane open. Light excitation

of the visual pigment, rhodopsin, activates the photoreceptor G-protein, transducin. Activated transducin translocates from the outer segment to the inner segment, where it binds to PDE6 and displaces the PDE6 inhibitory γ subunit from the catalytic site. The resulting PDE6 activation leads to a subsecond drop in cGMP concentration, closure of CNG channels and membrane hyperpolarization [79].

Table 1. Characteristics of cGMP phosphodiesterases

Phospho-diesterase	Regulatory feature	Substrate specificity	Structural organization
PDE1	Ca^{2+}/Calmodulin-stimulated	cGMP/cAMP	
PDE2	cGMP-stimulated	cGMP/cAMP	
PDE3	"cGMP-inhibited"	cGMP/cAMP	
PDE5	cGMP-activated	cGMP	
PDE6	Pγ-regulated	cGMP	
PDE9		cGMP	
PDE10	cAMP-stimulated	cGMP/cAMP	
PDE11		cGMP/cAMP	

CaM, Calmodulin binding domain. GAF, domains from cGMP-binding PDEs, *Anabaena* adenylyl cyclase, and *Escherichia coli* FhlA. Pγ, protein γ subunit. P indicates the position of phosphorylation sites.

The various PDE isozymes with distinct expression, localization, and regulation constitute a functionally diverse superfamily, which highlights the importance of cGMP and its crosstalk with other second messengers in signal transduction. The balance between cGMP synthesis and degradation is crucial to the regulation of a broad range of physiological functions.

1.1.3 cGMP signaling in embryonic DRG neurons

Neurons are highly specialized cells. Some landmarks of neuronal development include the genesis and differentiation of neurons from neuronal stem cells, polarization of axon and dendrites, axon guidance, axonal and dendritic branching and morphogenesis. Each neuron extends only one axon. However, each axon can further branch to connect to multiple targets, providing the anatomical basis for parallel information processing. At the tip of the growing axon is the highly motile structure termed growth cone. Axonal growth cones navigate through developing tissues to

reach the target areas, where they make synapses and create neural circuits in the body. During development, different modes of axonal branch formation are observed: 1) Splitting branching can occur at the growth cone by splitting or bifurcation of the growth cone into two daughter branches far apart, 2) outgrowth of collaterals from the axon shaft in a process called interstitial branching, 3) axonal terminals in the target region form tree-like arbors, designated as terminal branching or arborization [80, 81].

All three types of axonal branching can be found during the development of dorsal root ganglion (DRG) sensory neurons (**Figure 2A**). DRG sensory neurons reside in the dorsal root of the spine and project into the dorsal horn of the spinal cord. Unlike the majority of neurons found in the central nervous system, DRG neurons are pseudo-unipolar cells, unique among peripheral neurons in that they project one axonal branch to the periphery and another into the central nervous system during development. The afferent axons enter the spinal cord at the dorsal root entry zone (DREZ) between embryonic days 10-13 (E10-E13) in mice. The growth cones of the axons split into two daughter branches, displaying a pattern of T- or Y- shaped bifurcation (splitting branching). The resulting daughter axons grow over several segments in rostral or caudal directions, respectively, while remaining in the dorsolateral margin of the cord. Only after a waiting period, the collaterals sprout from these stem axons and penetrate into the gray matter (interstitial branching). At the termination zones, the collateral branches can further arborize (terminal branching) and connect with the target [80]. DRG neurons enable the body to sense touch, temperature, pain, limb movements and limb spatial position [82].

Axonal branching is tightly controlled in order to establish functional neural circuits. It has been shown that the CNP/GC-B/cGMP signaling pathway is involved in DRG neuron development [80]. CNP expression has a very specific timing and spatial confinement during DRG neuron development. It starts to get expressed at E9 during mouse development. It is at first more widely distributed in the whole quarter of the spinal cord at E10-11.5, when most of the DRG sensory neurons start to approach and grow into the spinal cord through the DREZ. At E12.5-E13.5, when DRG neurons have accomplished bifurcation, CNP becomes more concentrated in the dorsal-medial part and in cells located adjacent to the dorsal part of the central canal, where CNP might serve other functions [83]. Upon arrival of DRG neurons at the DREZ, secreted CNP activates GC-B on the membrane of DRG neurons [67]. Activated GC-B leads to a rise of intracellular cGMP, which has multiple effectors. cGKI is one of the major downstream targets activated by cGMP. Mammals express cGKI in two isoforms,

termed α and β, that differ in their N-terminal domains. In embryonic DRG neurons, cGKIα is highly expressed by sensory axons, with a similar localization pattern as GC-B, whereas most other neurons in the spinal cord are negative for cGKI. Furthermore, sensory axons at the DREZ express high levels of cGKI. cGKI expression is not only spatially restricted to DRG neurons, but also temporally confined to early developmental stages [84].
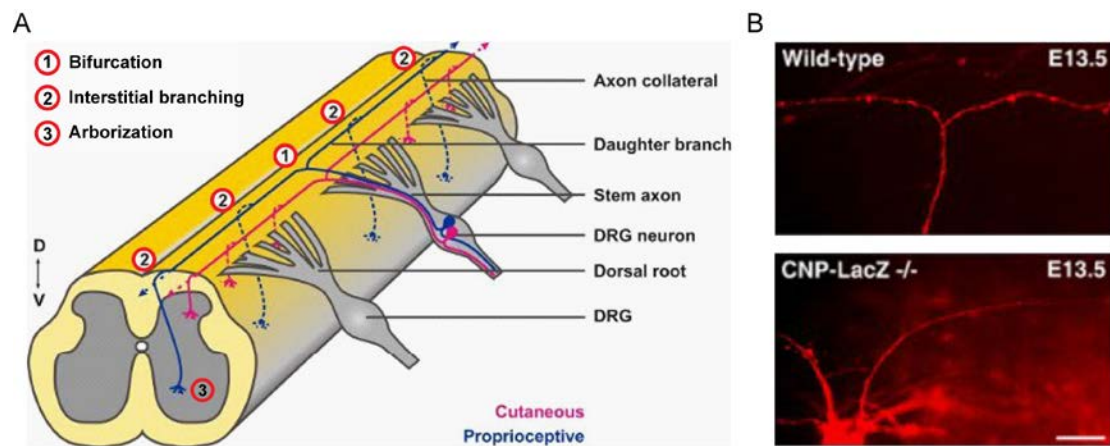
Figure 2. Axonal branching in DRG neurons.

A. Afferent axons of DRG neurons project into the DREZ of the embryonic spinal cord and at first display bifurcation at the growth cone. Secondly, the newly generated daughter branches form collaterals from the axon shaft after a waiting period by interstitial branching. Thirdly, the collaterals enter the dorsal grey matter and further arborize to form synaptic contacts. **B**. CNP-deficient mice show bifurcation defects. Figure modified from Schmidt H., et al., 2011 [85].

The deficiency of any one of the pathway components such as the ligand CNP, the receptor GC-B (also known as Npr2), or the cGMP-dependent protein kinase Iα (cGKIα) leads to identical axonal bifurcation defects of DRG sensory neurons *in vivo* [80]. In contrast to the wild type, the sensory neurons do not bifurcate but turn only in one direction, either rostral or caudal without preference (**Figure 2B**). However, the interstitial branching of collaterals from single stem axons remains unaffected. Therefore, the CNP/GC-B/cGMP signaling pathway is critical for bifurcation, but not for interstitial branching. Distinct molecular mechanisms are therefore accounted for bifurcation and interstitial branching [67, 83, 84]. *In vitro* experiments also supported the conclusion that the CNP/GC-B/cGMP/cGKIα pathway is important in axonal branching. Treatment of dissociated DRG neurons in culture with CNP, cGMP analogs and overexpression of cGKIα all promoted branch formation. Interestingly, CNP was also shown to attract growth cone turning [86, 87]. DRG neurons represent an important model for studying axon branching and wiring of the nervous system.

1.1.4 cGMP signaling in platelets

Platelets are anucleate cell fragments that are derived from megakaryocytes, a hematopoietic precursor cell residing in the bone marrow, and circulate in the blood stream. Many reports have shown the involvement of platelets in various physiological and pathological processes, such as hemostasis and thrombosis, atherosclerosis, and immune responses [88]. The primary task of platelets is to form a thrombus to prevent blood loss upon vascular injury. Normal endothelium, which provides a non-adhesive surface for thrombus formation, contains mainly three thromboregulators: NO [6, 7], prostacyclin (prostaglandin I2) [89], and ectonucleotidase CD39 [90].

Platelet aggregation occurs in emergent response to vascular injury, which causes the extracellular matrix proteins underneath the endothelium to be exposed. Exposed collagen triggers platelet adhesion and activation [91]. Multiple platelet membrane receptors for collagen exist. Initial platelet tethering to the vessel wall is considered to occur via interaction of the platelet glycoprotein GPIa-IIa receptor (integrin $\alpha_2\beta_1$) with collagen, which allows further binding to collagen via the GPVI receptor. The platelets adhered to the vessel wall are subjected to frictional force resulting from blood flow. Shear stress is important in platelet adhesion and activation [92]. At high shear rates, as found in arteries and arterioles, GPVI and collagen interaction is not sufficient to initiate binding to collagen, and binding of the GPIb-IX-V receptor to von Willebrand factor (vWF) that is mobilized on collagen becomes critical for platelet arrest [92, 93]. Platelet adhesion initiates their subsequent activation. Multiple signaling events occur after activation and converge into common signaling pathways, resulting in platelet shape change and granule secretion. Activated platelets release ADP, thrombin and thromboxane A2, which have prothrombotic properties, i.e. they stimulate the activation of new platelets as well as increase platelet aggregation by activation of the glycoprotein complex GPIIb/IIIa (integrin $\alpha_{IIb}\beta_3$, fibrinogen receptor) in the platelet membrane. Circulating ligands, including fibrinogen and vWF bind to these receptors on adjacent platelets, further strengthening and expanding platelet aggregation and thrombus formation. Concomitantly, exposed tissue factor in the endothelium initiates a second pathway to generate thrombin, which activates platelets but also converts fibrinogen to fibrin, stabilizing platelet-platelet aggregate formation [91].

The two sides of the same coin are hemostasis and thrombosis; platelets participate in hemostasis at sites of vascular injury in physiological conditions, while excessive or overstimulated platelets lead to pathological consequences, like thrombosis,

myocardial infarction, and stroke [91]. Thus, thrombus formation, an otherwise beneficial function in preventing blood loss, may lead to artery or vein occlusion causing life-threatening disease conditions. Therefore, the mechanisms regulating platelet activation and inhibition are of essential interest to preclinical and clinical research.

It is commonly accepted that the cyclic nucleotides cGMP and cAMP play an inhibitory role in the regulation of platelet activation, representing two of the most important physiological pathways to limit thrombus formation. The intact endothelium produces NO and prostacyclin, which binds to sGC and G_s-protein-coupled prostacyclin receptors in circulating platelets, respectively. Activation of sGC leads to cGMP synthesis, whereas prostacyclin leads to adenylyl cyclase (AC) stimulation resulting in cAMP generation [94]. PDEs take part in the regulation of cyclic nucleotide concentrations. So far, three PDE subtypes have been identified in platelets, cGMP-stimulated cGMP/cAMP-degrading PDE2, "cGMP-inhibited" cGMP/cAMP-degrading PDE3, and cGMP-stimulated, cGMP-degrading PDE5. These PDEs regulate platelet cGMP and cAMP levels and contribute to the crosstalk between cGMP and cAMP signaling [95, 96]. Elevated cyclic nucleotide levels then activate the corresponding cGMP- and cAMP-dependent protein kinases, respectively.

Human platelets express only cGKIβ, whereas both cGKIβ and a small amount of cGKIα was found to be expressed in mouse platelets [97, 98]. Many cGKI substrates including vasodilator-stimulated phosphoprotein (VASP) and IP3 receptor-associated cGMP kinase substrate (IRAG) are also abundantly expressed in platelets. Mice deficient for cGKI, VASP, or IRAG showed impaired NO-cGMP dependent inhibition of platelet aggregation *in vivo*. cGKI inhibits intracellular Ca^{2+} release in platelets through regulation of IRAG and the inositol-1,4,5-trisphosphate (IP_3) receptor. Intracellular Ca^{2+} transients in platelets were not affected by NO or cGMP in IRAG-deficient platelets [98-100].

As mentioned above, it is generally accepted that the NO-cGMP signaling pathway inhibits platelet activation [101]. NO donors and cGMP analogs exhibit a strong inhibitory role in platelet activation *in vitro*. sGC total knock-out mice show a prominent reduction in bleeding time, suggesting an inhibitory role of sGC [102]. However, a stimulatory role of the NO/cGMP signaling pathway has also been proposed [103, 104]. Dating back to the 1970s, many platelet agonist such as collagen, vWF and thrombin

have been shown to promote cGMP generation in platelets during aggregation with stirring [104, 105]. Recently, Li et al. showed GPIb stimulation activates cGKI, leading to activation of extracellular-related kinase, which is required for platetelet integrin $\alpha_{IIb}\beta_3$ activation [104]. Moreover, sGC knock-out in megakaryocytes showed prolonged bleeding times, indicating that sGC plays a stimulatory role [103]. X. Du and colleagues therefore proposed biphasic roles of NO/cGMP signaling in platelet thrombus formation. Low concentrations of NO synthesized by platelet NO synthase during platelet activation may be stimulatory, whereas high concentrations of NO supplied by exogenous vascular cells result in a second phase of inhibition in platelet aggregation, through inhibition of store Ca^{2+} release by cGMP/cGKI [98, 99] as well as through possible inhibition of cAMP degradation by elevated cGMP [103, 104]. The biphasic role of the NO/cGMP pathway might therefore fine-tune activation and inhibition to stimulate robust hemostatic thrombus formation upon vascular injury while inhibiting overgrowth of the thrombus.

1.2 cGMP measurement and FRET imaging

1.2.1 Conventional methods

Since the isolation and identification of cGMP, rapid progress has been made due to the development of quantitative biochemical assays for cGMP detection. Conventional biochemical methods to determine the cellular cGMP concentration include radioimmunoassays (RIA) or non-radioactive approaches such as enzyme-linked immunosorbent assays (ELISA or EIA) [106-108].

RIA has been used for quantification of total cGMP concentrations in various cells and tissues. This cGMP detection method is based on the competition of an unknown amount of unlabeled cGMP for the sample to be assayed and a defined amount of tracer-labeled (usually ^{125}I-labeled) cGMP for binding to an anti-cGMP antibody. Increasing amounts of unlabeled cGMP from samples compete and displace ^{125}I-labeled cGMP and the radioactive signal decreases proportional to the unlabeled cGMP in a sample. Thus, by drawing a calibration curve, the amount of cGMP in a sample can be determined.

The drawbacks of RIA related to handling of radioactive compounds led to development of the non-radioactive EIA. EIA is based on the competition between free cGMP and a non-radioactive cGMP tracer (cGMP conjugated with enzymes such as alkaline phosphatase or acetylcholinesterase). The cGMP-bound antibody complex further binds to a secondary antibody that has been previously attached to a plastic well. Because the concentration of the cGMP tracer is held constant, the amount of cGMP tracer that is able to bind to the antibody will be inversely proportional to the cGMP concentration in the sample. A colored product generated by the conjugated enzyme is detected, and the amount of cGMP concentration can be determined with the help of a calibration curve.

Besides the direct detection of cGMP as described above, an indirect and simple approach utilizing the western blot of VASP phosphorylation by cGKs has been also practiced in many cell and tissue samples [99, 109, 110]. Immunohistology using antibodies against cGMP has also been applied in fixed cells or tissue sections [111, 112]. Both RIA and EIA are highly sensitive and specific in detecting cGMP, with almost no cross-reaction with other nucleotides, including cAMP. However, all these biochemical methods are endpoint assays requiring large amounts of cells or tissues.

The necessity of cell disruption causes the loss of spatial-temporal dimensions. Thus, these methods are not well suited to study dynamic cGMP signals within a living cell. To overcome these limitations in real-time analysis of cGMP dynamics at a subcellular level, methods to visualize cGMP in live cells have been developed [113].

1.2.2 Optical imaging and FRET-based cGMP biosensors

Knowledge of the *in vivo* concentrations, distribution and mobilization of ions, signaling molecules and metabolites is critical for understanding how the body functions in both healthy and diseased states. Live cell imaging is one of the areas that has deepened our view on the dynamic regulation of signaling networks in living cells. This is largely pushed forward by the advancement of microscopic techniques as well as by the discovery of green fluorescent protein (GFP) [114].

Before various fluorescent protein-based indicators were available, simple organic dyes had been used for live cell imaging. One prominent member for optical imaging is Fura-2. Fura-2 is a fluorescent dye, which allows ratiometric measurements of the intracellular Ca^{2+} concentration [115]. It was the first widely used dye for Ca^{2+} imaging, and is still in popular use nowadays. The compound is an aminopolycarboxylic acid containing an 8-coordinate tetracarboxylate chelating site with stilbene chromophores. Fura-2 has two different fluorescent states depending on Ca^{2+} binding. When Fura-2 is free of Ca^{2+}, it has an absorption maximum at 380 nm. Once bound with Ca^{2+}, its maximal absorption shifts to 340 nm. However, the emission maximum for both forms is the same at ~515 nm. Upon Ca^{2+} elevation in the cells, the fluorescence intensity at 515 nm during excitation at 340 nm (F_{340}) increases, whereas the fluorescence intensity at 515 nm during 380 nm excitation (F_{380}) decreases. Thereby, ratiometric imaging is possible, and the ratio ($R=F_{340}/F_{380}$) is taken as a measure of intracellular Ca^{2+} levels. The brighter fluorescence and selectivity for Ca^{2+} over other divalent cations makes Fura-2 a useful indicator for Ca^{2+} imaging.

The discovery and subsequent molecular engineering of GFP and its variants (**Figure 3**) has revolutionized many areas of biology. The principal advantage of fluorescent protein-based sensors over simple organic dyes is that they can be genetically expressed and, thus, they can be tagged with signaling peptides, fused with other proteins, targeted to subcellular compartments and even introduced into a wide variety of tissues and intact organisms. GFP has been successfully used for many years as a reporter for gene expression, protein trafficking and localization [114]. Recently, the various sensors utilizing GFP and its variants has been successfully developed [116].

These sensors can be used to monitor complex processes, including concentrations of second messengers [117], protein dynamics (e.g., protein-protein interactions [118], G-protein [119] and protein kinase activation [120]), as well as biophysical parameters (e.g., membrane potential [121] and molecular tension [122]).
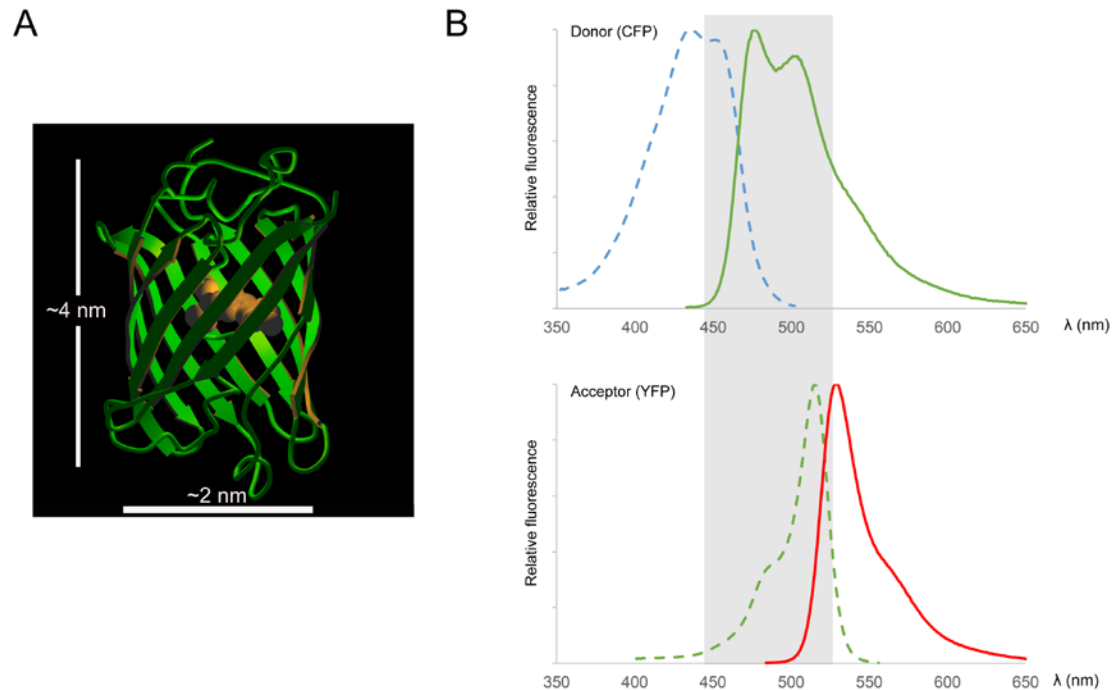
Figure 3. Overlap of the excitation and emission spectra of donor and acceptor.

A. Crystal structure of GFP. The protein consists of 11 β strands forming a hollow cylinder, and a single α-helix, which bears the chromophore and runs along the axis. GFP variants, including cyan or yellow fluorescent protein (CFP or YFP) have a similar structure. **B**. Excitation (dotted line) and emission (solid line) spectra of CFP and YFP are shown. To allow FRET to occur, donor (CFP) emission and acceptor (YFP) excitation spectra must overlap, as highlighted by the grey box. Figure adapted from R. Tsien's website (http://www.tsienlab.ucsd.edu).

In the last decades, the development of optical imaging based on fluorescent proteins and fluorescence resonance energy transfer (FRET) microscopy has become a powerful tool for analysis of live cells. FRET is a distance-dependent quantum mechanical phenomenon characterized by radioactiveless transfer of energy from a donor fluorophore to an acceptor fluorophore through dipole-dipole coupling [114]. For FRET to occur, several parameters must be met: 1) a proper spectral overlap of the donor and the acceptor. There must be a substantial overlap (>30%) between donor`s emission spectrum and acceptor's excitation spectrum, but both excitation spectra should be separated enough to allow independent excitation (**Figure 3B**); 2) the donor and acceptor fluorophores need to be in a favorable spatial orientation and close proximity, usually at a distance <10 nm (**Figure 4**). CFP and YFP is such a pair of donor and acceptor of popular choice [123].

Förster calculated that the efficiency of the FRET process (E) depends on the inverse sixth power of the distance between donor and acceptor,

$$E = 1/(1 + r^6/ R_0^6)$$

with R_0 (Förster distance) being the characteristic distance at which 50% of the energy is transferred (typically 2-6 nm) and r being the actual distance between donor and acceptor. R_0 is dependent on the extent of spectral overlap, the quantum yield of the donor and the relative orientation of donor and acceptor [114, 124]. Because of the $1/r^6$ dependence, the FRET efficiency is very sensitive to r. For example, if the donor-acceptor distance r is half R_0, then the FRET efficiency is 98.5%, close to maximal; if r=R_0, then E=50%; note that for distances greater than R_0, the efficiency drops sharply close to zero. Since FRET relies on the distance of the acceptor and donor, it has been widely used to investigate molecular interaction, for example, protein-protein interactions. Another successful area has been the engineering of FRET-based indicators for second messengers, including Ca^{2+}, cAMP and cGMP [116].

A variety of cGMP biosensors, either based on FRET or non-FRET techniques, have been developed. One type of biosensors is built on CNG channels [125, 126]. CNG channels are non-selective cation channels in the plasma membrane activated by both cGMP and cAMP [127]. Increase of cGMP at the plasma membrane can be indirectly monitored by electrophysiological recordings of cation currents, or by measuring Ca^{2+} influx through CNG channels with fluorescent dyes [125, 126]. However, the low selectivity for cGMP over cAMP limits their application.

Other non-FRET sensors for cGMP include bioluminescence resonance energy transfer (BRET)-based sensors, and the single fluorescent protein-based sensor FlincG. A resonance energy transfer can also occur between a bioluminescent protein (a donor enzyme such as luciferease) and a fluorescent protein (e.g., a GFP derivative). In contrast to FRET, energy is transferred from a non-fluorescent donor in BRET [128]. One recent BRET cGMP sensor is derived from the GAF-A domain of PDE5 [129]. Although signals from BRET pairs are generally weaker and require supply with appropriate chemical substrates, the donor does not require any excitation light, which has the advantage of eliminating the concern of autofluorescence as well as possible light interference in some tissues, such as the retina. Another non-FRET-based single fluorescent sensor for cGMP is called FlincG, which comprises the cGMP-binding domain of cGKI fused to a circularly permutated GFP. With this sensor, cGMP is monitored by single fluorescence intensity changes caused by conformational changes upon cGMP binding [130]. FlincG has a high cGMP sensitivity. But it is not ratiometric

imaging, therefore making the data interpretation difficult, especially considering the detrimental influence of pH on the sensor [131] and potential artifacts caused by tissue movement during intravital imaging.

Most FRET-based cGMP sensors are unimolecular proteins derived from either partially truncated cGKI containing the cGMP-binding domain, or from the PDE GAF domain, flanked by the donor and acceptor fluorophores, typically CFP and YFP. These sensors differ in kinetic properties, sensitivity and selectivity for cGMP (**Table 2**). The first FRET-based cGMP sensor called CGY-Del1 is based on the cGKIα, with 47 amino acids truncated on the N-terminus to prevent dimerization. The conformational change of cGKI upon binding of cGMP to the binding domain results in the separation of the flanked CFP and YFP, thereby changing the FRET efficiency. However, the selectivity of CGY-Del1 for cGMP over cAMP is rather low [132]. Efforts had been undertaken to improve different versions of cGMP sensors. The GAF domains from PDE2 or 5 were also fused to CFP and YFP by Nikolaev et al. to generate cGMP FRET sensors [133, 134]. For example, cGES-DE5 shows high cGMP selectivity, fast kinetics and good FRET signal amplitude. However, the sensitivity to cGMP is still quite low (cGMP EC_{50}=1.5 µM) [113, 135, 136].

Table 2. Characteristics of FRET-based biosensors for cGMP imaging

Sensors	Donor-Acceptor	Sensitivity		Selectivity	ΔFRET, max,%	Ref.
		cGMP EC_{50} (µM)	cAMP EC_{50} (µM)	$\frac{cGMP\ EC_{50}}{cAMP\ EC_{50}}$		
CGY-Del1	CFP-YFP	0.020	0.152	7.5	24	[132]
Cygnet-2	CFP-YFP	1.9	185	100	40	[137]
cGi500	CFP-YFP	0.5	>100	>200	77	[138]
cGi3000	CFP-YFP	3	>100	>30	72	[138]
cGi6000	CFP-YFP	6	>1,000	>166	57	[138]
cGES-cGKIB	CFP-YFP	5	485	100	30	[133]
cGES-DE5	CFP-YFP	1.5	630	420	40	[133]
RedcGES-DE5	Sapphire/RFP	0.04	>100	>1,000	15	[134]

The recently generated cGMP sensors cGi500, 3000 and 6000 (cGis, <u>cG</u>MP <u>i</u>ndicator with an EC_{50} of 500 nM, 3,000 nM or 6,000 nM, respectively) by Russwurm et al. show great promise for real-time imaging of cGMP by displaying fast kinetics and high selectivity for cGMP over cAMP [138]. cGi500 shows a higher affinity and greater dynamic range than most other cGMP FRET sensors that have so far been described [138]. cGis consist of the tandem cGMP-binding domains of cGKI sandwiched by CFP and YFP. Upon cGMP binding, FRET decreases. The measured FRET efficiency can therefore be taken as evaluation of the cGMP level (**Figure 4**).
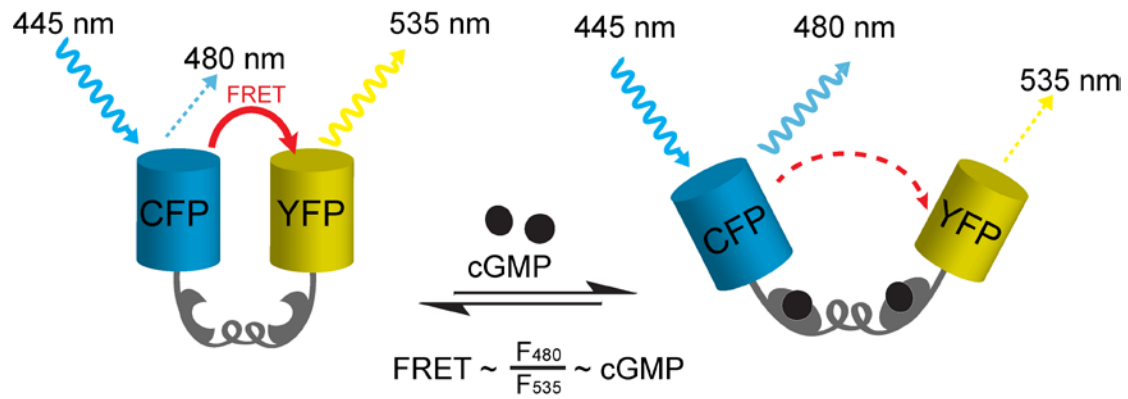
Figure 4. Working principle of the FRET-based biosensor cGi500.

cGi500 is a cGMP indicator consisting of the engineered cGMP-binding domain of cGKI sandwiched by CFP and YFP. Without cGMP binding, CFP and YFP are close to each other, FRET occurs from excited CFP to YFP. Upon cGMP binding, cGi500 undergoes a conformational change leading to separation or reorientation of CFP and YFP. The FRET efficiency is reduced. Thereby, light emission from YFP at 535 nm gets reduced, while emission from CFP at 480 nm gets increased. The ratio of emission at 480 nm and 535 nm (F_{480}/F_{535}) can be taken as a measure of FRET efficiency, which represents the cGMP level.

Multiple FRET microscopy techniques are available. In the simpler case, a FRET microscope can be built from an epifluorescence microscope. FRET multiphoton microscopy permits intravital imaging with deep tissue penetration and represents an emerging area of *in vivo* analysis of signaling events under physiological conditions [139].

1.3 Gene targeting and mouse generation

Mice play an important role in biomedical research. As a model organism, the mouse is genetically similar to the human species, and most human genes and signaling pathways are conserved in the mouse. Thus, the mouse offers an exceptional tool to understand genotype-phenotype relationships that are relevant for revealing the biologic role of these genes in humans. Since the first trial of transgenic mouse generation by R. Jaenisch in 1974 [140], the landscape of biological research has changed enormously. Genomic modification in mice has been made possible by random transgenesis or gene targeting. This has been achieved by the development of several technologies: 1) transgenic mice, 2) pluripotent embryonic stem (ES) cell culture, 3) knock-out mice, 4) tissue- and time-specific knock-outs, and 5) inducible gene expression systems.

1.3.1 Random transgenesis versus gene targeting

Mutant mice are traditionally generated by either using random mutagenesis [141] or gene targeting methods [142] (**Figure 5**). Random transgenesis is typically used for overexpression of specific proteins or reporter systems. Classically, an exogenous DNA fragment (transgene) is introduced into fertilized oocytes via pronuclear microinjection [143-145]. The transgene will integrate randomly into the genome and may be transmitted through the germline to the offspring (**Figure 5A**). It could happen that either a single copy or more commonly, multiple numbers of copies are randomly inserted into primarily one site of the genome. Gene expression varies with the location of transgene integration due to the chromosomal accessibility and the copy number [146]. Although random transgenesis gained wide applications in creating gain-of-function mutations thanks to its lower technical requirements, random insertion may cause unwanted effects, such as inactivation of host genes, which complicates the analysis.

By contrast, gene targeting modifies the genome at a defined locus [147-149]. It has become a well-established technique to create animal models for human diseases or study gene function at the level of the whole animal. Mouse generation by gene targeting takes advantage of the *in vitro* culture system of pluripotent ES cells. Genetic modification can be introduced into ES cells via a DNA targeting vector. The targeting vector is usually designed to carry selectable markers and 2 homologous arms flanking the targeted genomic sequence (**Figure 5C**). In that way homologous pairing occurs between the targeting vector and the genomic sequence, and a homologous

recombination event replaces the genomic sequences with vector sequences containing additional modifications (e.g., the neomycin resistance (neo^R) gene). The frequency of homologous recombination is low, approximately 1 in 1,000 cells that are transfected with the targeting vector [142]. The targeted ES cells can be enriched following a positive-negative selection protocol based on two selection markers: A positive selection marker, such as neo^R gene is used to select for cells that have integrated the targeting vector, while a negative marker, such as the cell-toxic diphtheria toxin fragment A (DTA) gene, eliminates cells carrying the transgene at non-homologous sites [142, 150]. By injecting targeted ES cells into blastocysts, chimeric mice can be generated, which transmit the mutant gene to their progeny.
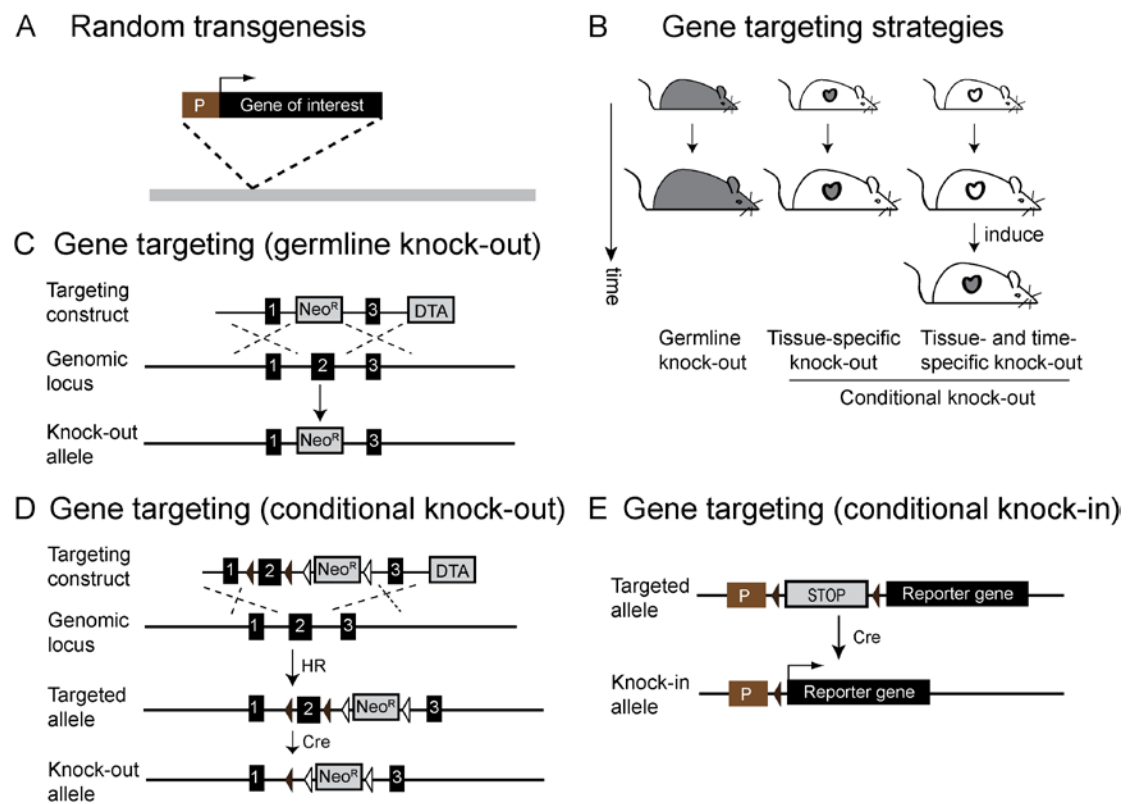
Figure 5. Genomic modification by random transgenesis and gene targeting.
A. Schematic representation of random transgenesis. Gene of interest driven by promoter (P) integrates into the genome at a random site. **B**. Strategies for targeted transgenesis. Germline knock-out: the knock-out allele replacing one or more exons with a selectable marker is carried in every cell through germline to adulthood. Tissue-specific knock-out: the knock-out allele is introduced in somatic cells of a specific tissue. Tissue- and time-specific knock-out: the knock-out allele is inducible in a specific tissue; inactivation occurs at a specific time upon induction. The specific tissue in which the gene is mutated is shown in grey. **C**, **D**. Genomic engineering of a germline knock-out or conditional (tissue- and time-specific) knock-out. **E**. Conditional knock-in, as exemplified by reporter knock-in, is a variation of conditional knock-out, whereby the transgene is inserted into a locus with or without an exogenous promoter. Transgene expression is conditionally activated upon Cre-mediated excision of a floxed STOP cassette. P, promoter; HR, homologous recombination; Cre, Cre recombinase; Neo^R, Neomcycin resistance gene; DTA, diphtheria toxin A; Filled triangles, loxP sites; Empty triangles, FRT (Flp recombinase target) sequences.

Gene targeting in ES cells was most commonly used to disrupt a chosen gene in the mouse, termed gene knock-out. Conventional germline knock-out deletes genes in all cells throughout all developmental stages (**Figure 5B and C**). Inactivation of many genes leads to lethality in embryonic or early postnatal stage, which makes the investigation of gene function in adulthood impossible [151]. Also, a null mutant in the whole body can sometimes make the interpretation difficult. For example, it could be hard to tell if a phenotype of the heart is linked to the gene ablation in the heart *per se* or in the brain indirectly. In combination with a designated site-specific DNA recombination system, such as Cre-loxP or Flp-FRT, gene targeting can be used to generate mutations in a way that allows separate evaluation of a gene`s function in specific tissues (conditional knock-out) (**Figure 5B and D**) [152]. The most commonly used site-specific recombinase Cre catalyzes recombination between two 34 bp loxP recognition sites [153, 154]. The FLP-FRT recombination system works similarly to the Cre-loxP system [155]. The conditional knock-out practically relies on the crossing of two mouse strains, one strain carrying the loxP- or FRT-flanked target gene and an additional strain expressing the site-specific recombinase Cre or Flp. Tissue-specific Cre expression will catalyze the excision of DNA flanked by directly repeated loxP recognition sites (floxed), therefore deleting the target gene in a spatially confined manner, resulting in tissue-specific knock-outs [156, 157]. Time- and tissue-specific knock-outs or inducible tissue-specific knock-outs were reported by R. Feil et al. [158], and others [159]. This is achieved by the induction of recombination with a ligand-dependent Cre recombinase, so called CreER and its evolved version CreER^{T2}, a fusion of Cre recombinase to a mutated ligand-binding domain of the human estrogen receptor [158, 160]. This fusion protein, CreER^{T2}, can be activated by synthetic 4-hydroxytamoxifen, but not endogenous estradiol. The cytoplasmic CreER^{T2} translocates into the nucleus upon the administration of tamoxifen, resulting in tamoxifen-induced Cre recombination of loxP sites [161]. Combining tissue-specific expression of a CreER^{T2} recombinase with time-specific delivery of tamoxifen, the excision of floxed chromosomal DNA can be controlled both spatially and temporally [162]. Many transgenic mice expressing the Cre or CreER^{T2} recombinase with different spatial and temporal patterns have been generated. Genetic engineering including conditional and inducible gene targeting provides a powerful tool to analyze gene functions.

1.3.2 Reporter knock-in

Besides knock-out generation, gene targeting can also be used to manipulate any chosen mouse gene locus in any desired manner, ranging from point mutations to large

fragment replacements [142]. The knock-in approach allows precise insertion of an exogenous reporter gene into the genome, so that the expression of the reporter acquires the transcriptional regulation of the targeted gene locus. Reporter knock-ins allow for analysis of gene expression patterns, detection of Cre or Flp activity, labelling specific cell types and tracking cell fate, or reporting other molecular events such as the concentration dynamics of second messengers [163].

A reporter knock-in is actually a variation of standard knock-out strategy. The knock-in introduces an exogenous DNA fragment, meanwhile it typically results in disruption of the endogenous gene. Although losing one copy of most genes does not necessarily cause a detectable phenotype, this is not always the case. One strategy to circumvent this is to use an internal ribosomal entry site (IRES) so that the endogenous and the reporter gene can be expressed bicistronically from the same mRNA [164]. However, the expression levels for the open reading frames before and after the IRES often vary drastically. Another promising strategy is to link self-cleaving 2A peptide between open reading frames of the endogenous and the reporter gene. The posttranslational self-cleavage of the peptide results in equal levels of two proteins [163, 165].

The Gt(ROSA)26Sor (Rosa26) locus has been established as the preferred integrating site for expression of exogenous transgenes without giving rise to any detectable phenotypic effect [166]. The ubiquitous transcriptional activity of the locus suggests that the genomic region maintains an open and permissive chromatin configuration, therefore allowing generalized expression of the inserted transgene in any tissue throughout the embryonic stage to adulthood. Many reporter genes have been knocked into the Rosa26 locus, and Rosa26-LacZ is the first of this kind. The Cre-activatable lacZ gene was introduced into the first intron of the Rosa26 locus forward transcript. The presence of a strong splice acceptor allows for transgene expression to be driven by the endogenous ubiquitous Rosa26 promoter [166]. Simulating the original promoter trap insertion, other reporter genes including enzyme markers (for example, alkaline phosphatase [167], luciferase [168]), and fluorescent proteins (for example, YFP [169]) have also been integrated into the Rosa26 locus. Expression of the reporter genes is usually blocked by a loxP-flanked STOP fragment placed before the expression cassette and after the Rosa26 promoter. When used in conjunction with a Cre recombinase-expressing line, successful Cre-mediated excision is indicated by reporter expression in Cre-expressing tissues and their descendants (**Figure 5E**). These mice serve as useful Cre reporter strains. LacZ expression is especially useful due to its high adaptability as well as simple detection methods for beta-galactosidase

using antibodies (e.g., [170]) or biochemical reactions [166]. However, expression of reporters directly from transgenes driven by the endogenous Rosa26 promoter is weak in the adult [171]. Many studies utilizing these lines require the aid of histochemical methods, or immunostaining of the reporter protein. An efficient way to achieve higher universal expression for *in vivo* visualization, in particular in adult mice, is to introduce a strong exogenous promoter such as the CAG (Cytomegalovirus early enhancer/chicken β-actin/rabbit β-globin) promoter together with the exogenous reporter expression cassette into the Rosa26 locus [171].

Nowadays, numerous transgenes have been integrated into the Rosa26 locus to achieve cell type-specific expression for *in vivo* imaging. For instance, optogenetic proteins targeted to this locus allow for precise manipulation of neuronal activity [172]. More and more Rosa26 transgenic mouse lines with sophisticated transgene design serve for multiple purposes, such as labeling different cell types as well as genetic fate mapping. Several recent mouse lines represent the current advance of reporter knock-ins. The Mosaic Analysis with Double Markers (MADM) method in mice is used for sparse marking of genetically defined neuron populations [173]. The Rosa26-mT/mG mouse allows for double marker labeling by switching from one fluorescent protein to another. It labels not only cells after Cre-mediated recombination but also non-recombined cells with green or red fluorescent proteins targeted to the cell membrane, respectively [174]. The R26R-Confetti mouse is very useful in labeling cells in the brain as well as other organ systems through stochastic Cre-mediated activation of one out of four fluorescent proteins [175]. Another category of reporter systems based on fluorescent proteins has been developed to detect molecular signaling events, such as Ca^{2+} mobilization, and many of them have also been knocked into the Rosa26 locus [176]. Genetically encoded Ca^{2+} indicators allow time lapse imaging of Ca^{2+} in defined cell types and even subcellular compartments by targeting the indicators to subcellular domains [177]. Imaging with these sensor proteins has greatly improved our knowledge of Ca^{2+} in physiology and neuroscience. A transgenic mouse approach with tissue-specific sensor expression enabled Ca^{2+} imaging virtually in all kinds of cell types [176], which has been especially useful to pinpoint the function of particular cell types in the nervous system. More than two decades after the first targeted transgenic mouse and over one decade after the discovery of the Rosa26 locus, the field of gene targeting including reporter knock-in is still expanding.

1.4 Aim of the work

The role of cGMP as a second messenger in a broad range of (patho-)physiological processes is widely appreciated. In concert with other second messengers such as cAMP, Ca^{2+} and phophoinositides, cGMP plays a central role in maintaining homeostasis in numerous cells and tissues in response to changing physiological conditions. Unlike proteins, which can be simply tagged with other fluorescent proteins for *in vivo* tracking, small molecules like cGMP have mainly been detected by conventional destructive methods like RIA or EIA, which generate only end point data and lack spatial resolution. Instead, *in vivo* imaging can capture quantitative information in real time at subcellular resolution and do so noninvasively and repeatedly in the same living cells or in an intact organism where the physiological circuit functions, offering insights that cannot be revealed using *in vitro* approaches.

Thus, the major objective of this work was to generate and characterize for the first time transgenic mice expressing the FRET-based cGMP indicator cGi500 ubiquitously or in a Cre-activatable tissue-specific fashion, so that cGMP could be visualized *in vivo*. Prior to our publication in 2013 [178], there had been no reports about the generation of transgenic mice that express cGMP sensors.

With these newly generated cGi500-expressing mouse lines, we aimed to perform robust cGMP imaging in a broad range of cell types, and prove the functionality of these sensor mice. Characterization of our new cGMP sensor mice should demonstrate that cGi500 sensor expression could be activated in a Cre-dependent manner and was sufficient to monitor physiological cGMP signals in live cells. Specifically, platelets and neurons were of main interest for the present study. cGMP imaging had already been performed in isolated primary cells such as smooth muscle cells by transfecting these cells with cGMP biosensors. However, transfection might generate unwanted side effects and many cell types including neurons and platelets cannot easily be transfected. Moreover, cGMP signals can change very rapidly, for example, as measured in platelets by RIA [75, 179]. cGMP sensor-expressing primary cells would allow repeated quantification of cGMP in real time in the same living sample with subcellular resolution and under relatively native conditions.

The CNP/GC-B/cGMP/cGKI signaling pathway is fundamental for DRG sensory axon bifurcation when projecting into the DREZ during nervous system development. However, the molecular mechanism underlying this process are not completely

understood. We hypothesized that the growth cone alone can detect CNP and elevate cGMP locally and independently from the soma. cGMP activates cGKI and potentially triggers cytoskeleton remodeling, such that the growth cone travels along the DREZ and bifurcates to form two branches. The test of this hypothesis requires subcellular imaging of cGMP at higher resolution, which could potentially be performed with our novel cGMP sensor-expressing mice. The aim was, therefore, to establish a local drug application system, which would mimic the local CNP exposure of the axonal growth cone, and to analyze the spatiotemporal cGMP dynamics at the same time.

To image cGMP signals in platelets, we wanted firstly to establish a flow chamber system, so that cGMP could be measured in platelets under flow. With the established imaging system, the present work aimed to answer the following questions: Are cGMP signals in platelets affected by flow/shear stress? Does flow/shear stress regulate Ca^{2+}? What are the relationships between the two second messengers, cGMP and Ca^{2+}? etc. Answers to these questions should provide new insights into platelet biology under flow conditions.

Overall, our aim has been to understand cGMP biology under (patho-)physiologically relevant conditions. With these newly generated cGMP sensor mice, we can now watch cGMP by intravital FRET imaging in the context of a living complex mammalian organism.

2 Materials and Methods

2.1 Materials

2.1.1 Common chemicals, reagents and antibodies

0.4% Trypan blue	Life Technologies
10×Trypsin/EDTA	Life Technologies
100×Penicillin/Streptomycin (Pen/Strep)	Life Technologies
2-propanol	Carl Roth
37% Hydrochloric acid (HCl)	Carl Roth
Agarose	Biozym Biotech
Boric acid	Carl Roth
Bovine serum albumin (BSA)	Carl Roth
Chloroform/isoamyl alcohol	Carl Roth
D-Glucose	Carl Roth
DMEM Glutamax^{TM}	Life Technologies
Dimethyl sulfoxide (DMSO)	Carl Roth
Diethylether	Carl Roth
Ethanol	Carl Roth
Fetal Bovine Serum (FBS)	Life Technologies
F12 culture medium	Life Technologies
Glutamine	Life Technologies
Horse Serum	Life Technologies
Hoechst 33258	Sigma-Aldrich
KpnI	New England Biolabs
N-Lauroylsarcosine sodium	Sigma-Aldrich
Paraformaldehyde (PFA)	Carl Roth
Phenol/chloroform/isoamyl alcohol	Carl Roth
Antibodies	
Alexa 555, Goat anti-Mouse	Life Technologies
Alexa 488, Goat anti-Rabbit	Life Technologies
Mouse anti-mouse β-III-Tubulin	Promega
Rabbit anti-mouse cGKI	Customized [180]

2.1.2 Common buffers and solutions

0.5 M EDTA pH 8.0
Dissolve 186.1 g disodium ethylenediaminetetraacetic acid dihydrate (Na$_2$EDTA·2 H$_2$O) in 800 mL H$_2$O, add NaOH pellets until the solution reaches pH 8.0 and EDTA is dissolved. Adjust volume to 1 L. Autoclave and store at room temperature (RT).

1×Trypsin/EDTA
10×Trypsin/ETDA (0.5% / 0.2%, Life Technologies) 3 mL, add 27 mL PBS, store at 4 °C.

10×TE pH 8.0
100 mM Tris-Cl (100 mL/L 1 M Tris-Cl pH 8.0), 10 mM EDTA (20 mL/L 0.5 M EDTA, pH 8.0), autoclave and store at RT.

10×RT buffer
10×RT-buffer (pH 8.0) contains 500 mM KCl, 100 mM Tris, 15 mM MgCl$_2$ and 2 mM dNTP-mixture. Store at −20°C.

10×Reaction buffer S
10×Reaction buffer S (PEQLAB) contains 100 mM Tris-Cl pH 8.8, 500 mM KCl, 0.1% Tween-20, 15 mM $MgCl_2$, store at −20°C.

1,000×Hoechst 33258
Dissolve Hoechst 33258 (Sigma-Aldrich) at 1 mg/mL in H_2O, store 1 mL aliquots at −20°C.

1 kb ladder DNA marker
Add 250 µL 1 kb ladder (Life Technologies) to 8.25 mL 1×DNA loading dye, store 500 µL aliquots at 4°C.

1 M Tris-Cl pH 6.8/7.4/8.0
Dissolve 121.14 g tris(hydroxymethyl)aminomethane (Tris) in 1 L H_2O, adjust pH to 6.8/7.4/8.0 with concentrated HCl. Autoclave and store at RT.

20% SDS
Dissolve 200 g sodium dodecyl sulfate (SDS) in 1 L H_2O at 60°C in a water bath. Store at RT.

3 M NaOAc pH 5.5
Dissolve 40.83 g $CH_3COONa \cdot 3 H_2O$ in 100 mL H_2O, adjust pH to 5.5 with acetic acid. Autoclave and store at RT.

5×TBE
Make 450 mM Tris-borate, 10 mM EDTA by weighing 54 g Tris and 27.5 g boric acid and dissolving both in approximately 900 mL H_2O. Add 20 mL of 0.5 M EDTA (pH 8.0) and adjust the solution to a final volume of 1 L. Store at RT.

5 M NaCl
Dissolve 292.2 g NaCl in 1 L H_2O. Autoclave and store at RT.

6×DNA loading dye
30% glycerol, 10% 10×TE, 0.05% bromophenol blue, 0.05% xylene cyanol. Store at 4 °C.

70% Ethanol
Mix 70 mL ethanol (analytical grade) and 30 mL H_2O, store at −20°C.

Ethidium bromide
Prepare 10 mg/mL in H_2O, store at 4°C, light protected.

Proteinase K
Prepare 50 mg/mL proteinase K in 1×TE, store at −20°C.

PBS Buffer

Component	Final conc.	Volume/weight
NaCl	135 mM	40 g
KCl	3 mM	1 g
$Na_2HPO_4 \cdot 2H_2O$	8 mM	7.1 g
KH_2PO_4	2 mM	1.2 g
H_2O		ad 10 L

Adjust pH to 7.4, aliquot, autoclave and store at RT

2.2 Generation of transgenic mice by gene targeting

Transgenic mouse generation by gene targeting in mouse embryonic stem (ES) cells is now a well-established technique. The protocol varies from lab to lab. But in general, it includes the construction of a targeting vector, ES cell culture, electroporation of the targeting vector into ES cells, drug selection of ES clones, and PCR or Southern screening and identification of correctly targeted ES clones. After their identification, the ES cells are expanded so that they can be injected into mouse blastocysts to generate chimeric mice. Breeding steps are needed to achieve germline transmission of the mutant allele to the progeny (**Figure 6**). The whole procedure follows standard protocols from the Feil lab as also described by S. Feil [181] and M. Thunemann [182]), and by others [183, 184].

2.2.1 Gene targeting in ES cells

2.2.1.1 Construction and preparation of targeting vector

The construction of pR26-CAG-cGi500(L2) from pROSA-mT/mG [174] was performed by A. Vachaviolos, B. Birk and M. Thunemann, and described in detail in A. Vachaviolos` diploma thesis [185] and M. Thunemann`s PhD thesis [182]. Here the methods part starts with the preparation of targeting vector DNA for electroporation into ES cells.

1) Linearize about 100 µg of targeting vector DNA with the restriction enzyme KpnI according to the manufacturer's instructions.
2) Precipitate linearized DNA with 1/10 volume 3M NaOAc pH 5.5 and 2.5 volumes absolute ethanol. Wash twice with 70% ethanol. Aspirate 70% ethanol and leave the pellet for drying under sterile conditions in a tissue culture hood. Resuspend the DNA pellet at 1 µg/µL in sterile PBS. Store the linearized targeting vector at −20°C.

2.2.1.2 Preparation of irradiated MEFs as feeder cells

Murine embryonic fibroblasts (MEFs) as feeder cells produce leukemia inhibitory factor (LIF) and many other factors, which are necessary to support ES cells at their pluripotent state [186]. Before every step of ES cell seeding, MEF feeders should be prepared. The feeder cells should also be resistant to neomycin-related G418 so that they can survive the drug selection during gene targeting. Neo[R]-expressing MEFs used here were derived from embryos of the SMIβ rescue mouse [110].

MEF medium

Component	Final conc.	Volume/weight
DMEM	90%	450 mL
FBS	10%	50 mL

Store at 4 °C for up to 1 month.

1) Set up matings with 2-4 males carrying the neomycin resistance gene (neo^R-/-, SMIβ rescue here) and separate plug-positive females in the next morning (0.5 day post coitum, dpc).

2) Sacrifice 1-2 pregnant female mice at 13.5 dpc. Spray the abdomen with 70% ethanol. Open the abdominopelvic cavity and collect the uterine horns and transfer them into a 10-cm Petri dish with ice-cold PBS.

3) Make a longitudinal incision of the uterine wall with small, straight scissors and cut away each amniotic sac from the placenta and collect the embryos in a new Petri dish with ice-cold PBS.

4) Decapitate the embryos; remove tail, limbs and blood-containing inner organs. Wash the carcasses 2 times in PBS.

5) Transfer the carcasses into the opening of a 50-mL falcon tube. Thoroughly mince each carcass with sterile scissors.

6) Suspend minced embryos in 1×trypsin/EDTA (1 mL per embryo). Incubate the tube in a 37°C water bath for 10 min. Shake the tube at 2 min intervals vigorously.

7) Add MEF medium (2 mL per embryo) and spin in a tabletop centrifuge (Eppendorf 5417C/R) for 5 min at 300 g.

8) Resuspend the cell pellet into 10 mL MEF medium and transfer the suspension to two 175-cm^2 flasks per embryo, filling each flask with a total of 20 mL medium.

9) Leave the cells at 37°C and 6% CO_2 (Innova-170 CO_2 incubator, New Brunswick Scientific). The next day, cultures should be 30-50% confluent. When the flasks become 90-100% confluent (4-6 days after initial seeding), expand the cultures.

10) Wash twice with PBS and add 5 mL trypsin/EDTA. After 5 min at 37°C, resuspend the cells in 6 mL MEF medium. Take out 9 mL from every flask to a 50 mL tube. Add 18 mL to the flask with the remaining 2 mL cell suspension. Leave it to grow until 100% confluent.

11) Centrifuge down the cells in the 50-mL tube (1,000 rpm, 5 min). Resuspend cells with MEF medium (4 mL per 175-cm^2 flask).

12) Leave cells to settle down and irradiate them with a dose of 5,000 Rad (50 Gray) using a Gammacell 1000 device (Nordion) in the institute of cell biology, University of Tübingen.

13) Centrifuge the cells at 1,000 rpm, 5 min. Resuspend cells in 3 mL freezing medium (90% MEF medium+10% DMSO) per flask. Distribute equally into 3 cryogenic vials (1 mL/vial). Place them at –80°C. The next day, store vials in liquid N_2.

14) Repeat the procedure for up to 6 passages for each embryo preparation.

2.2.1.3 ES cell culture

ES cell gene targeting can be used to generate transgenic mice, because these cells are pluripotent and can contribute to the germline so that the mutant allele is passed to the progeny. The maintenance of ES cell pluripotency during culture is of critical importance for the success of mouse generation. ES cell culture contains several handling steps including thawing, passaging, and freezing. The general guideline for optimal ES cell culture is that undifferentiated colonies should have uniform appearance with well-defined edges, owing to 3-dimensional growth. Constant monitoring of cells under a microscope every day is key to maintain undifferentiated ES cell culture, and thereby germline competence of ES cells.

ES-FBS
ES cell culture-tested FBS (Life Technologies, Cat. no. 10270-10), heat inactivated (30 min at 56°C water bath, shake every 10 min), store in 50 mL aliquots at −80°C.

500×LIF
Stock, $0.5x10^6$ U/mL: dilute 1 mL (1×10^7 U) mouse leukemia inhibitory factor (LIF; Millipore GmbH) with 19 mL MEF medium, store in 1 mL aliquots at 4°C.

Figure 6. Transgenic mouse generation through gene targeting in ES cells.

A. ES cell culture during gene targeting. R1 ES cells with 129/Sv background are thawed at low passage to 25-cm^2 flask (T25) and passaged once to 75-cm^2 flask (T75). Cells dissociated from a T75 flask are electroporated with linearized targeting vector and plated at low density on ten 10-cm dishes, followed by G418 drug selection. ES clones are picked into 96-well plates, and 2 replica (plate A and B) are prepared. Plate A is frozen at 60-80% confluence and store in a -80°C freezer. Plate B is further passaged to 3 plates as replica (plate B, C and D). They can be used for DNA extraction and Southern blot screening. Identified targeted ES cell clones are thawed from plate A into a 24-well plate. Further expansion and freezing is necessary before the ES cells can be used for blastocyst injection. **B**. Generation of gene targeted mouse. Targeted ES cells are injected into blastocysts from wild type C57BL/6 mice and re-implanted into CD1 surrogate mothers, which give birth to chimeric mice with cells contributed from the ES cells (+/-, appearing as agouti fur) and the host embryo (+/+, appearing as black fur). Chimeras are further crossed with C57BL/6 mice. Germline transmission is expected to occur in agouti-colored offspring and is genotyped with a PCR reaction. The animals carrying the transgene are established as a new targeted mouse line.

A. Gene targeting in ES cells
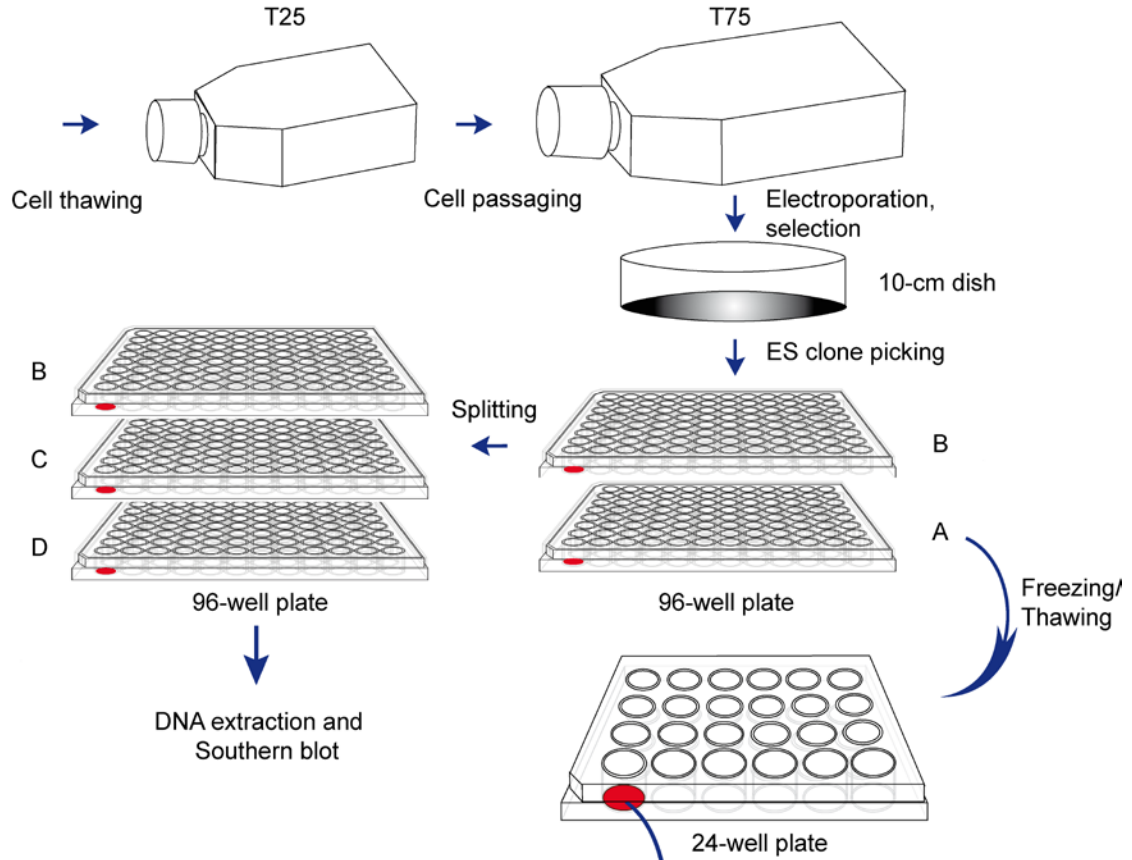
B. Generation of gene targeted mouse
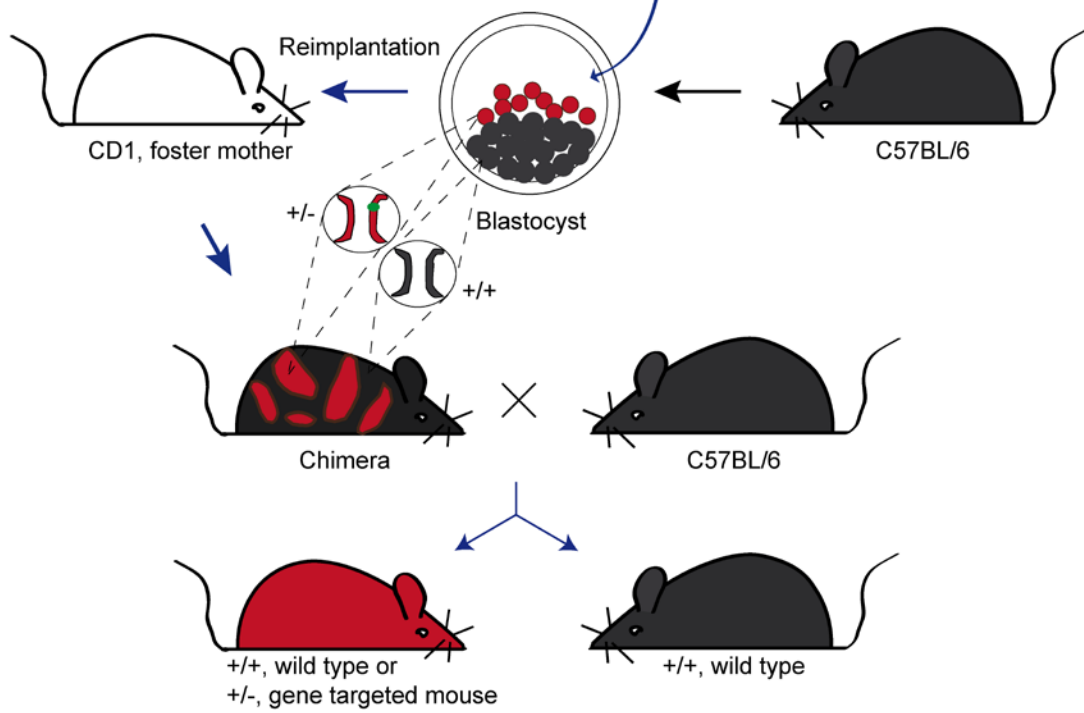
500×β-Mercaptoethanol (β-ME)
Stock, 50 mM: add 70 µL 2-mercaptoethanol (β-ME) to 20 mL PBS, sterilize by filtration, store in 1 mL aliquots at −20°C.

100×G418
Stock, 40 mg/mL: dissolve 1.6 g Geneticin®/G418-Sulfate in 40 mL PBS, sterilize by filtration, and store in 5 mL aliquots at −20°C.

ES cell culture medium (ES medium)

Component	Final conc.	Stock	Volume/weight
DMEM	80%		400 mL
FBS	20%		100 mL
LIF	1,000 U/mL	500×	1 mL
β-ME	0.1 mM	500×	1 mL

Store at 4 °C for up to 1 month.

Table 3. Specification, medium and trypsin volume for cell culture vessels

Flask	Surface Area	Medium	Trypsin
T25	25 cm^2	5 mL	2 mL
T75	75 cm^2	15 mL	5 mL
T175	175 cm^2	20 mL	8 mL
10-cm dish	55 cm^2	10-15 mL	5 mL
6-well plate	6x9 cm^2=54 cm^2	2-3 mL	1 mL
12-well plate	12x3.5 cm^2=42 cm^2	1-1.5 mL	0.5 mL
24-well plate	24x2.3 cm^2=55 cm^2	0.5-1 mL	0.3 mL
96-well plate	96x0.32 cm^2=29 cm^2	100-200 µL	50 µL

General requirements and procedures for cell culture include:

➢ Cell cultures are throughout incubated at 37°C and 6% CO_2. All media, PBS and 1×trypsin/EDTA should be pre-warmed to 37°C before use.

➢ Feeder cells should be thawed and plated 6-24 hours before ES cell seeding, and conditioned with LIF-containing ES medium for ≥1 h.

➢ Cell thawing: place immediately the frozen stocks in a water bath at 37°C; transfer the cell suspension into 4 mL ES medium, centrifuge for 5 min at 1,000 rpm, and resuspend the pellet in ES medium. Plate the cells onto culture vessels. Recommended medium volumes for various culture vessels are given in **Table 3**.

➢ Medium change: every day or every other day, depending on the culture density.

➢ ES cell culture used for mouse generation should always be subconfluent (~70%). It should be avoided to have the ES cells overgrown, as indicated by the yellowish color of the medium.

- ES cell passaging: wash the cells once with PBS and dissociate with 1×trypsin/EDTA for 3-5 min. Pipette up and down several times to obtain single cells. Stop trypsinization by addition of 1-2 volumes ES medium. Insufficient dissociation will result in cell clumps after reseeding. Over-trypsinization leads to cell death or loss of pluripotency. Centrifuge at 1,000 rpm for 5 min. Replate cells at a dilution of 1:3 to 1:6. Note down the passage number.
- Cell freezing: dissociate cells with 1×trypsin/EDTA, stop trypsinization with ES medium, centrifuge down cells and resuspend in freezing medium (90% ES medium+10% DMSO). Distribute cells from a culture area of 12.5 cm^2 to each cryogenic vial (1 mL/vial). Place them in a Styrofoam box at –80°C. The next day, store vials in liquid N$_2$.

Low passage (P14) of R1 ES cells (genetic background: 129/Sv x 129/Sv-CP, [187]) was used in this study.

1) Thaw feeder cells prior to ES cell culture to a 25-cm² flask (T25); each vial of feeder cells can be thawed to an area of 50-100 cm².
2) Thaw R1 ES cells onto the feeder cells in the T25 flask. Let the ES cells grow to 60–80 % confluence.
3) Passage cells to a 75-cm² flask (T75), let them grow to 60–80 % confluence.
4) Wash cells twice with PBS, detach them with 3 mL 1×trypsin/EDTA, resuspend in a 15-mL tube, and add 7 mL ES medium.
5) Centrifuge for 5 min at 1,000 rpm, resuspend in 10 mL PBS.
6) add 10 µL trypan blue to an aliquot of 10 µL cells in PBS, count cells in a hemocytometer (vitality should be greater than 95%, and cell yields from a T75 flask are 1-2×10^7).
7) Centrifuge again for 5 min at 1,000 rpm and resuspend cells in PBS to a density of 0.5−1×10^7/mL.

2.2.1.4 Electroporation

1) Mix 1 mL ES cell suspension with 20-50 µg targeting vector and transfer 800 µL cells into an electroporation cuvette (d = 4 mm, Bio-Rad). Remove potential air bubbles.
2) Electroporate at 230 V and 500 µF with Gene Pulser Xcell Electroporation System (Bio-Rad). The time constant should be between 5-8 ms.
3) Leave cells for 5 min in the cuvette at RT. Transfer cells to 9 mL ES medium, resuspend and plate cells onto ten 10-cm dishes with pre-seeded feeder cells.

2.2.1.5 Selection

1) 24 h after electroporation, change to ES medium with 300 µg/mL G418 (ES/G418 medium) for selection.

2) Change the medium every day or every other day for the first week depending on the amount of cell death.

3) 7-9 days after electroporation, pick the colonies.

2.2.1.6 Isolation of drug-resistant ES clones

Most of the ES clones will die, and drug-resistant ES cells will appear after 3-4 days of selection with G418. 7-9 days after electroporation, ES clones will be ready for picking. Picking of ES cell colonies can be done in 1-2 days, and 100-400 clones can be isolated per day. Suitable ES clones should have a sharp-edged morphology due to their three dimensional structure, while the center of the clone is relatively darker. The colonies are picked into round-bottomed 96-well plates for dissociation and then distributed to two flat-bottomed 96-well plates (replica A and B), one growing for freezing and another for further passaging. Avoid cross-contamination of the wells.

A. Picking of ES clones

1) 1 day prior to colony picking, thaw feeder cells to two 96-well plates in 100 µL ES/G418 medium.

2) Prepare a round-bottomed 96-well plate with 50 µL PBS.

3) Place a stereomicroscope (Stemi 2000C with transmitted-light unit S, Carl Zeiss Microscopy GmbH) inside a tissue culture hood. Set a 20 µL pipette to 2-3 µL.

4) Scan for a suitable colony under the stereomicroscope and interrupt the feeder monolayer around the colony using a 200-µL tip. Detach the colony and draw it with as little as possible ES medium. Transfer the colony to a well of the PBS-filled round-bottom 96-well plate. Repeat this step until 96 colonies are isolated (assuming the picking time is less than 1 hour).

5) Add 50 µL 2×trypsin/EDTA, incubate for 10 min at 37°C, pipette up and down ~10 times with a multichannel pipette to disaggregate the ES cells. Add 100 µL ES/G418 medium. Resuspend, and transfer 90 µL cell suspension to each replica of the two 96-well plate (A and B) seeded with feeder cells. Place the plate back to the incubator.

6) Change medium the next day.

7) ~3 days after plating, freeze plate A at 60-80% confluence. ~4 days after plating, passage plate B at 90-100% confluence to plate B, C and D.

B. Freezing

1) Remove medium from plate A, wash once with 180 µL PBS, incubate with 30 µL 1×trypsin/EDTA at 37°C, add 180 µL freezing medium (90% ES Medium + 10% DMSO) and resuspend.

2) Seal the plate tightly with autoclave tape, and freeze cells slowly at −20°C for 1-3 h. Store the plate at −80°C for up to 2 months.

C. Passaging

1) Add 150 µL ES/G418 medium to two new 96-well plates without feeder cells

2) Remove medium from plate B, wash once with 180 µL PBS, incubate with 50 µL trypsin/EDTA at 37°C for 10 min, add 100 µL ES medium and resuspend.

3) Transfer 50 µL of the cell suspension from plate B to the plates C and D each, then add another 150 µL ES/G418 medium to plate B.

4) Grow cells to 100% confluence (~4 days). Remove the medium, wash the cells twice with 150 µL PBS and allow the cells to dry. Store dried cells at −20°C or continue with isolation of genomic DNA,

2.2.1.7 Screening and identification of targeted ES clones

A. Extraction and digestion of genomic DNA from ES cells in a 96-well plate

DNA lysis buffer

Component, final conc.	Stock	Volume/weight
10 mM NaCl	5 M	1 mL
10 mM Tris, pH 7.4	1 M	5 mL
10 mM EDTA	0.5 M	10 mL
0.5% Sarcosyl		2.5 g
H_2O		ad 500 mL

Store at RT. Add 0.25 mg/mL proteinase K before use.

Ethanol/NaCl

For one 96-well plate, add 150 µL 5 M NaCl to 10 mL ethanol (pre-chilled to −20°C).

1) Defreeze a 96-well plate stored in -20°C for ~5 min at RT.

2) Add 50 µL DNA lysis buffer with proteinase K to each well of 96-well plates with a multichannel pipette.

3) Seal the plate tightly with saran wrap. Incubate the plate overnight at 55°C in a box with water-soaked tissue towels.

4) The next day, cool down the plate to RT, and then add ice-cold 100 µL ethanol/NaCl, and precipitate the DNA for ≥1 h at RT. Then, precipitated DNA

will stick to the plastic surface of the 96-well plate. DNA strings can be checked under a microscope with lower-power magnification.

5) Discard ethanol by inverting the plate onto paper towels. The DNA should adhere to the plate. Wash the precipitated DNA 2-3 times with 100 μL 70% ethanol (pre-chilled to −20°C), air dry the DNA for 1 h at RT. Screen wells for complete evaporation of ethanol to prevent the interference of remaining ethanol with restriction digestion. The plate with dried DNA can be stored at −20°C.

6) Prepare the restriction digest mixture (per well),

Restriction enzyme buffer (NEB1/2/3/4)	5 μL
100×BSA	0.5 μL
Restriction enzyme	1 μL (20 U)
H_2O	43.5 μL
Total	50 μL

7) Add the digestion mixture to the dried genomic DNA in the 96-well plate (50 μL/well) with a multichannel pipette, tap the plate to ensure the surface of each well is covered with the mixture.

8) Wrap the plate tightly with saran wrap, and incubate overnight at 37°C. The next day, store DNA at −20°C or continue with gel electrophoresis and Southern blot.

B. Southern blot

0.2 M HCl
Add 20 mL 37% HCl to 980 mL H_2O.

0.5 M NaOH/1.5 M NaCl
Dissolve 20 g NaOH and 87.5 g NaCl in 1 L H_2O.

0.5 M Tris/3 M NaCl pH 7.4
Dissolve 60.58 g Tris, 175.3 g NaCl in 1 L H_2O, adjust pH to 7.4 with HCl.

10×Labeling buffer with octadeoxyribonucleotides (NEB), store at −20°C.

1 M Na_2HPO_4: Dissolve 177.99 g Na_2HPO_4 in 1 L H_2O.

1 M NaH_2PO_4: Dissolve 137.99 g NaH_2PO_4 in 1 L H_2O.

2×SSC, 0.1% SDS
100 mL/L 20×SSC, 5 mL/L 20% SDS.

20×SSC
Dissolve 175.3 g NaCl, 88.2 g trisodium citrate dihydrate in 1 L H_2O.

50×TAE
400 mM Tris-acetate (242 g/L Tris, 57.1 mL/L acetic acid), 50 mM EDTA (100 mL/L 0.5 M EDTA pH 8.0).

Church buffer

1% BSA, 0.5 M phosphate buffer, pH 7.2 (193.5 mL 1 M Na_2HPO_4 and 56.3 mL 1 M NaH_2PO_4), 7% SDS, 50 mM EDTA, H_2O to 500 mL. Store in 50 mL aliquots at −20°C. Preheat and add ssDNA to a final concentration of 0.1 mg/mL (10 µL/mL 10 mg/mL ssDNA) before use.

dCTP, $α^{32}P$ (3000 Ci/mmol, 10 mCi/mL, EasyTide; Perkin-Elmer, Rodgau, Germany), store at 4°C.

dNTP mixture

Mix equal parts of 200-fold dilutions of 100 mM dATP, dGTP and dTTP (PEQLAB), store in 25 µL aliquots at −20°C.

Filter paper: Whatman 3MM gel blotting paper, 0.34 mm×460 mm×570 mm.

Klenow Fragment: 3′→5′ exo-Klenow fragment (5,000 Units/mL; NEB), store at −20°C.

LSC: Liquid scintillator cocktail UltimaGold (Perkin-Elmer).

Hybond N⁺ Membrane: 20 cm×3 m (GE Healthcare).

NICK columns: illustra NICK™ columns with sephadex G-50 (GE Healthcare).

RNase: Prepare 10 mg/mL RNase H in 1×TE, store in 1 mL aliquots at −20°C.

ssDNA: Prepare 10 mg/mL salmon sperm DNA (Roche), store in 1 mL aliquots at −20°C. Denature for 5 min at 99°C to obtain single-stranded DNA (ssDNA) before use.

1) Take out the plates from the incubator and add 10 µL 6×loading dye to each well of the 96-well plate. Leave them at 4°C until electrophoresis or at −20°C for longer storage.

2) Prepare 0.8% agarose gels with four rows á 26 lanes in 500 mL 1×TAE without ethidium bromide.

3) Load 50-55 µL of the digested genomic DNA onto the agarose gel.

4) Run the gel at 80-100 V until the diagnostic wild type and mutant band are adequately segregated.

5) Stain the gel for 15 min with ethidium bromide (0.01 mg/mL in 1×TAE).

6) Destain the gel for 10-20 min in H_2O.

7) Photograph the gel together with a ruler.

8) Perform depurination by soaking the gel in 0.2 M HCl for 10 min on a shaking platform (color change of bromophenol blue from blue to yellow). Wash with H_2O.

9) Perform denaturation with 0.5 M NaOH/1.5 M NaCl for 45 min. Wash with H_2O.

10) Perform neutralization for 0.5 M Tris/3 M NaCl pH 7.4 for 30 min. Wash with H_2O.

11) Cut a Hybond N⁺ nylon membrane for each gel piece while gels are incubating.

12) Southern transfer was built up as follows (from bottom to top):

> Buffer reservoir (2 L 10×SSC) in black tank with gel tray (tray is upside down),
> Filter paper on top of the gel tray, filter paper dips into the buffer reservoir,
> Agarose gel (upside down),
> Hybond N⁺ membrane (pre-wetted with 10×SSC),
> Parafilm around the membrane (no contact between filter papers above and below the membrane),
> Filter paper (six sheets),
> Two stacks of paper towels,
> Gel chamber lid with ~1 kg weight on top.

13) The next day, disassemble the Southern blot, label pockets and the membrane.

14) Dry the membrane for 3 h at 80°C.

15) Cut the membrane to the correct size to remove lanes with DNA markers to prevent from background hybridization of marker DNA.

16) Store the membrane in saran wrap at 4°C.

C. Hybridization

Hybridization was carried out in a roller bottle in a hybridization oven (OV1, Biometra) at 60°C. The ROSA26-5` probe was an EcoRI digestion product of 'pCR-II-Rosa5` probe' (gift of R. Kühn). Radioactive DNA probes were labelled with α[^{32}P]dCTP by random primed reaction.

1) Transfer the membrane into a hybridization tube with the membranes separated with nylon spacer mesh (Biometra GmbH). Add 10×SSC into the tube and roll until the membranes get spread onto the tube wall.

2) Meanwhile, denature ssDNA at 99°C for 5 min, and chill on ice.

3) Replace the 10×SSC solution with 20 mL pre-warmed Church buffer containing 10 µL/mL denatured ssDNA. Prehybridize the membrane in the oven for ≥60 min at 60°C.

4) During prehybridizaiton, label the DNA probe. Dilute 100 ng of the probe template DNA in 33 µL H$_2$O. Denature the probe for 5 min at 99°C, chill on ice (2-5 min), and spin down. Perform the labeling reaction:

10×labeling buffer	5 µL
dNTP mixture	6 µL
α[^{32}P]dCTP	5 µL
Klenow fragment	1 µL (5 U)
denatured probe	33 µL
Total	50 µL

Incubate for ≥60 min at 37°C.

5) About 10 min before the labeling reaction is done, remove storage buffer from NICK columns, wash once with 3 mL 1×TE, and pass through another 3 mL 1×TE to equilibrate the column.

6) Take a 1 µL aliquot from the labeling reaction to 10 mL LSC. Add 30 µL 1×TE to the remaining labeling reaction (~50 µL), load the dilution on the NICK column and collect fractions upon buffer addition,

Fraction 1: 320 µL 1×TE (death volume, no radioactivity),

Fraction 2: 500 µL 1×TE (with labeled probe),

Fraction 3: 800 µL 1×TE (with free α[^{32}P]dCTP).

7) After mixing and centrifugation of the fractions, measure the radioactivity of 1 µL aliquots in 10 mL LSC of each fraction and the labeling reaction in a liquid scintillation analyzer (2500 TR, Packard).

8) Denature the probe (fraction 2) for 5 min at 99°C. Chill for 2-5 min on ice.

9) Discard the prehybridization buffer, add new pre-warmed Church buffer with the labeled, denatured probe and hybridize overnight at 60 °C.

10) The next day, remove hybridization buffer. Wash twice with pre-warmed 2×SSC, 0.1% SDS at 60°C for 10 min; twice with 0.4×SSC, 0.1% SDS;

11) Detect the activities above the unwrapped membranes with a scintillation counter. Wash until each membrane of 40-80 Bq is detected. Wash with 0.4×SSC, 0.1% SDS at 70°C, if necessary.

15) Wrap membranes with Saran foil. Place the membrane inside an exposition cassette with the DNA facing a cleared phosphor screen. Expose the screen for 3-7 days.

12) Read the phosphor screen in the Bioimaging Analyzer System (in the institute of cell biology, University of Tübingen).

2.2.1.8 Expansion of targeted ES clones

The targeted ES clones identified by Southern blot should be thawed and expanded as soon as possible. Multiple frozen stocks should be prepared for each clone. The expanded targeted clones are re-verified by Southern blot.

1) The 96-well plate that contains the targeted ES clones are taken out from the -80°C freezer and wrapped with plastic foil (to prevent from water leaking into the plate) and placed into a 37°C water bath to thaw the cells.

2) Transfer suspension of the targeted ES clone into a 24-well plate with feeder cells and ES medium (without G418). Change medium after 1-2 days.

3) At 60-80% confluence, passage the ES cells to a 6-well plate.

4) At 60-80% confluence, freeze a part of the cells (3-4.5 cm²/vial) and passage the remaining cells again to a 6-well plate. Expand the cells for a secondary targeting or use them for blastocyst injection.

2.2.1.9 Cre-mediated excision in ES cells

To obtain Cre-activated transgene expression in both ES cells and mice, Cre excision is performed in ES cells by transiently expressing Cre in targeted ES cells. Therefore another round of electroporation of a Cre-expressing plasmid (i.e. pIC-Cre [157]) is performed with the targeted ES cells. The ES cells are plated at low densities with different dilutions, so that single clones can be isolated as described in 2.2.1.6.

1) Prepare 20-50 µg Cre-expressing plasmid.

2) Expand a targeted ES clone to a T75 flask.

3) Harvest ES cells at 60-80% confluence and perform electroporation with a Cre-expressing plasmid as described in 2.2.1.4. Plate cells onto 10-cm dishes at dilutions of 1:100 and 1:1,000.

4) 5-7 days later, pick ES clones and prepare replica plates as described in 2.2.1.6.

5) Verify Cre recombination in ES clones by Southern blot as described in 2.2.1.7.

2.2.2 Blastocyst injection

Pluripotent ES cells can contribute to all three germ layers including the germ line, through which the transgene is transmitted so as to establish a new transgenic mouse line. The production of knock-in or knock-out mice usually involves tetraploid aggregation or blastocyst injection. Blastocyst injection is the most common method carried out for the generation of chimeric mice from genetically modified ES cells. ES cells of lower passage (<P25) are more likely to have higher potential for germline transmission and should be kept for injection. ES cells are injected into the morula- or blastocyst-stage embryos. These embryos are reimplanted into the uterus of pseudopregnant mothers, which are expected to give birth to chimeric mice. Three mouse lines are required, C57/Bl6 for donating host embryos, CD1 females (aged ≥8-12 weeks) as foster mothers, and vasectomized FVB/N male mice (≥10 weeks). The ES cell injection and reimplantation were performed by Dr. S. Feil.

Analgesia: carprofen (4 mg/kg).

Narcosis antidote: naloxon (1.2 mg/kg), flumazenil (0.5 mg/kg), atipamezol (2.5 mg/kg).

Narcosis: fentanyl (0.05 mg/kg), midazolam (5.00 mg/kg), medetomidin (0.50 mg/kg).

Holding pipette: VacuTip holding capillary (Eppendorf).

Injection pipette: TransferTip ES (Eppendorf).

Transfer pipette: 1.5 mm O.D. ×1.17 mm I.D, made from glass capillaries (Clark Electromedical Instruments, Warner Apparatus)

M2 medium (Sigma-Aldrich).

Mineral oil: light oil (neat), suitable for mouse embryo cell culture (Sigma-Aldrich).

Surgical suture: Ethicon Vicryl P-3/5-0 (Johnson & Johnson Medical GmbH).

2.2.2.1 Mouse and blastocyst preparation

1) To obtain 3.5 dpc host embryos for microinjection, mate 30 male C57BL/6 with two C57BL/6 females each in the evening four days before injection. Check females for the appearance of copulation plugs in the next morning (0.5 dpc) and separate plug positive females for blastocyst collection at 3.5 dpc.

2) 2.5 days before injection, mate CD1 females to vasectomized FVB/N male mice to obtain pseudopregnant mothers for reimplantation of blastocysts injected with ES cells.

3) On the day of injection, sacrifice 3.5 dpc donor female mice, harvest uterine horns in PBS, flush them using a syringe filled with DMEM in a syringe with a bended 22G injection needle, wash once with DMEM and collect the embryos with an embryo transfer pipette under a stereomicroscope. Transfer the embryos to a micro drop of M2 medium in a 35 mm Petri dish and place the dish in an incubator at 37 °C, 10% CO_2.

2.2.2.2 Preparation of ES cells for injection

1) Thaw one vial of ES cells (typically containing cells frozen from 3-4.5 cm^2; P21 for primary targeted, and P28 for Cre-recombined ES cells) to 6-well plate.

2) Passage once at dilutions of 1:3, 1:10, and 1:20 to ensure the availability of ES cells with appropriate confluence on the day of injection. Freeze the remaining ES cells (3-4.5 cm²/cryovial).

3) On the day of injection, choose the best undifferentiated cells with 60% confluence for dissociation. Resuspend cells in 3-5 mL of ES medium. Divide 1-1.5 mL for injection and the remaining for DNA isolation and Southern blot.

4) Centrifuge down the ES cells in a 1.5-mL tube at 1,000 rpm for 5 min. Resuspend in 50 µL ES medium.

2.2.2.3 Injection of ES cells into blastocysts

1) Prepare an injection chamber (80 mm × 25 mm) with a glass coverslip (24 mm × 60 mm) attached at the bottom by Vaseline. The injection chamber on the microscope stage is cooled to 10°C with a circulating water bath. Add two drops of M2 medium covered with mineral oil. One drop is used for injection needle cleaning, and the other larger drop for placing the blastocysts and ES cells.

2) Transfer all (e.g., 30) blastocysts and ~10 µL of the ES cell suspension into the larger drop.

3) Tune the holding and injection pipette starting at 5x objective to be aligned in a line and adjust the pipette tips in parallel to the surface of the plate.

4) At 100× magnification, move the tip of the injection pipette to round and healthy-looking ES cells and load the pipette with cells, avoid larger fibroblast cells.

5) At 100× magnification, orient the blastocyst with the help of the injection pipette so that the inner cell mass is facing against the injection pipette, hold the blastocyst with the holding pipette by aspirating gently.

6) At 100× or 200× magnification, eject ~10 ES cells into the blastocoel cavity. The blastocyst cavity will collapse right after injection.

7) Move the injected blastocyst to the upper side of the drop.

8) After repeating the whole injection procedure, transfer all injected embryos to a dish with ES medium, and incubate for 1-6 h at 10% CO_2 and 37°C.

2.2.2.4 Embryo re-implantation

The uterine transfer of injected blastocysts into E2.5-day-old pseudopregnant recipient females would allow embryos to develop to term.

1) Anesthetize a 2.5 dpc pseudopregnant foster mouse.

2) Disinfect the skin in the back of the mouse. Make a small ~1 cm incision in the skin on the back about 1 cm away from the thigh area of the hind limb under a stereomicroscope. Cut through the muscle underneath until reaching peritoneal cavity.

3) Gently pull out the ovary by the nearby fat pad and lay the ovary oviduct and upperpart of uterus out onto the back for surgery. With a 22G gauge needle attached to a 1-cc syringe make a hole in the uterus.

4) Load the transfer pipette with injected blastocysts.

5) Insert the transfer pipette through the hole and place the embryos inside the uterus. Place the ovary and uterus back into the body.

6) Close the wound and inject antidote and analgesia. Place the mouse on a 37°C slide warmer until it wakes up.

7) Place the mouse in a cage allow it for further recovery. Chimeras are expected to be born in around 20 days.

2.2.3 Mouse breeding and husbandry

The chimeric mice can be determined by the coat color of the progeny mice. R1 ES cells are derived from a 129/Sv mouse strain with agouti-colored fur (A^w/A^w genotype),

while C57BL/6 mice have black fur (a/a genotype). Therefore, blastocyst injection should result in chimeras with both the host wild type cells (black, a/a) and ES cell-derived cells (agouti, A^w/A^w). Coat color and percentage of agouti pattern can be determined about 1 week after birth. A higher degree of chimerism is more likely but not a guarantee to have ES cell-derived gametes and *vice versa*. Chimeras are mated to C57BL/6 to achieve germline transmission. Germline transmitted offspring can be identified by the agouti coat color. Black pups can only be derived from the wild type C57BL/6 host embryos. Since the genetically modified ES cells are heterozygous for the transgene, half of the resulting agouti-colored first generation pups are expected to be tested positive by genotyping PCR (see 2.3.1). To transfer the modified allele to a standard inbred strain, mice are further backcrossed to C57BL/6N animals.

All mouse lines are housed in a conventional mouse facility in the Interfaculty Institute for Biochemistry at 22°C and 50-60% humidity in a 12 h light/12 h dark cycle with free access to standard rodent chow and tap water. Adult male and female mice are used for experiments. The mouse lines generated in this work are the cGi500 sensor knock-in mice, namely R26-CAG-cGi500(L2) and R26-CAG-cGi500(L1) on a mixed 129Sv/C57BL6N genetic background.

2.3 Characterization and analysis of transgenic mice

2.3.1 Identification of germline transmission and genotyping

Germline transmission of the targeted alleles was identified by PCR analysis of genomic DNA isolated from transgenic mice. PCR-based genotyping of ear biopsies was done with primers ROSA10 (5'-CTCTGCTGCCTCCTGGCTTCT), ROSA11 (5'-CGAGGCGGATCACAAGCAATA), and ROSA4 (5'-TCAATGGGCGGGGGGTCGTT) [173]. ROSA10 and ROSA11 amplify a 330-bp fragment of the wild type ROSA26 locus, while ROSA10 and ROSA4 amplify a 250-bp fragment of the R26-CAG-cGi500(L2) or R26-CAG-cGi500(L1) allele (see also **Figure 8A**, page 63).

When R26-CAG-cGi500(L2) was crossed with Cre mouse lines (e.g., L7-Cre mouse [188]), primer pairs Cre800 (5'-GCTGCCACGACCAAGTGACAGCAATG) and Cre1200 (5'-GTAGTTATTCGGATCATCAGCTACAC) were used for genotyping PCR of Cre transgene. Cre800 and Cre1200 amplify a fragment of 402 bp.

2.3.1.1 DNA extraction from mouse tissue for genotyping PCR

1) Prepare proteinase K digestion mix:

Proteinase K (50 µg/µL, Roth)	1 µL
10×Reaction Buffer S (Peqlab)	5 µL
H$_2$O	44 µL
Total	50 µL

2) Incubate ear punch tissue samples in 50 µL digestion mix, 55 °C, overnight.

3) Centrifuge at 12,000 rpm for 5 min.

4) Transfer the supernatant into a new 0.5 mL PCR tube.

5) Inactivate proteinase K activity and denature DNA for 15 min at 95°C.

6) Use 2 µL of the supernatant for PCR and store the remaining at −20°C.

2.3.1.2 Genotyping PCR

PCR reaction:

A. for R26-CAG-cGi500(L2) or (L1),

Taq polymerase	0.3 µL
10×RT buffer	2.5 µL
Rosa10（25 µM）	0.3 µL
Rosa11（25 µM）	0.3 µL
Rosa4 （25 µM）	0.3 µL
DNA	2.0 µL
H$_2$O	19.3 µL
Total	25 µL

B. for Cre transgene,

Taq polymerase	0.3 µL
10×RT buffer	2.5 µL
Cre800（25 µM）	0.3 µL
Cre1200（25 µM）	0.3 µL
DNA	2.0 µL
H$_2$O	19.6 µL
Total	25 µL

PCR program:

A. for R26-CAG-cGi500(L2) or (L1),   **B**. for Cre transgene,

94°C, 5 min	94°C, 5 min
94°C, 10 s ⎫	94°C, 10 s ⎫
65°C, 30 s ⎬ 35 cycles	58°C, 30 s ⎬ 35 cycles
72°C, 30 s ⎭	72°C, 30 s ⎭
72°C, 5 min	72°C, 5 min

2.3.1.3 Agarose gel electrophoresis:

1) Prepare 2% agarose gels with ethidium bromide.
2) Add 5 µL of 6× loading dye to the PCR product.
3) Load 15 µL of the mixture to the wells and run the gel at 120-150 V in 1×TBE buffer for ~45 min.
4) Photograph the gel under a UV detection system.

2.3.2 Confirmation of correct targeting by Southern blot

2.3.2.1 Preparation of DNA samples from small mouse tissue samples or ES cell pellets

DNA lysis buffer for tissue samples or ES cell pellets

Component, final conc.	Stock	Volume/weight
20 mM Tris-Cl, pH 8.0	1 M, pH8.0	1 mL
5 mM EDTA	0.5 M, pH 8.0	5 mL
1% SDS	20%	25 mL
400 mM NaCl	5 M	40 mL
H_2O		ad 500 mL

Store at RT. Add 0.4 mg/mL proteinase K before use.

1) Collect dissociated ES cells or tissue samples. Tissue samples can be 2 mm of tail biopsies or about 100-200 mg tissue from a sacrificed mouse.
2) Add 1 mL/55 cm^2 cells or 4 mL/100 mg tissue of DNA lysis buffer, and incubate at 55 °C with agitation in a water bath overnight.
3) Add the same volume of phenol/chloroform/isoamyl alcohol; shake for 30 min on a shaker.
4) Centrifuge at 13,000 rpm, 5 min at RT.
5) Transfer the upper aqueous phase to a new tube. Add the same volume of chloroform/isoamyl alcohol. Shake for 30 min on a shaker.
6) Centrifuge at 13,000 rpm, 5 min at RT.

7) Transfer the upper aqueous phase to a new tube. Add the same volume of chloroform/isoamyl alcohol. Shake for 15 min on a shaker.

8) Transfer the upper aqueous phase to a new tube. Add the same volume 2-propanol. Shake for 30 min on a shaker.

9) Centrifuge for 10 min at 10,000 rpm and 4°C.

10) Wash the DNA twice with 70% Ethanol.

11) Dry the DNA pellet under vacuum (Eppendorf Concentrator 5301) for 10 min at 40°C.

12) Re-dissolve in 50 µL (tail tip biopsy, small tissue samples, ES cell pellets) up to 300 µL (larger tissue samples).

13) Estimate DNA concentration with a final dilution of 1:100 by UV spectroscopy. Store DNA at –20°C.

2.3.2.2 Enzymatic restriction of genomic DNA

5-10 µg of DNA are digested at 37°C overnight. The digestion reaction is

Restriction enzyme buffer (NEB1)	5 µL
100×BSA	0.5 µL
KpnI	1 µL (20 U)
DNA + ad H_2O	43.5 µL
Total	50 µL

Southern blot with the digested DNA is performed as described in 2.2.1.7B.

2.3.3 Histology

For the analysis of fluorescence in organs, mice are anesthetized with isoflurane and sacrificed by cervical dislocation. Organs are isolated in ice-cold PBS and whole-mounts are observed with a fluorescence stereomicroscope with a EGFP filter set (Discovery, Carl Zeiss Microscopy GmbH, kindly provided by MPI Tuebingen). Organs are further processed for sectioning; mounted sections are detected under an epi-fluorescence microscope with a YFP filter set (excitation filter 497/16 nm, 516 nm dichroic mirror, and emission filter 535/22 nm) or a mT red fluorescence filter set (excitation filter 543/22 nm, 565 nm dichroic mirror, and emission filter 610/75 nm).

10×TBS
1 M Tris, 1.5 M NaCl; dilute 1:10 for 1×TBS, adjust pH7.4, store at RT.

30% Sucrose
Dissolve 30 g sucrose in 100 mL PBS, store at 4°C.

4% PFA
Work inside a fume hood. Weigh 4 g paraformaldehyde (PFA) in 100 mL PBS. Heat while stirring to 55-57°C until the PFA gets dissolved. Allow the solution to cool down and aliquot into 5-10 mL in 15-mL tubes. Store at -20°C. Thaw it at 37°C before use.

Mounting medium
Shandon ImmuMount (ThermoFisher HealthCare)

Normal goat serum
(NGS; Axxora, Enzo Life Sciences GmbH), store in 1 mL aliquots at 4°C

SuperFrost Plus glass slides (Thermo Fisher)

Tissue-Tek
Tissue-Tek O.C.T. compound (Sakura Finetek GmbH).

1) Fix the dissected tissue with precooled 4% PFA, 4°C for 16-24 h.

2) Dehydrate with 30% sucrose ≥16 h at 4°C (until the tissue sinks to the bottom of the tube).

3) Embed organs in TissueTek O.C.T. compound. Freeze the embedded samples in liquid nitrogen, and store them at −20°C.

4) Cut cryosections (e.g., 10 μm) on a cryostat (Microm, Thermo Fisher, AG Jansen). Mount the sections on SuperFrost Plus glass slides. Dry them briefly at RT. Continue with next steps or store them at -20°C.

5) Encircle the slides with a hydrophobic pen.

6) Rinse slides in 1×TBS for 3 times, 15-30 min each.
   Steps 7-12 are optional for immunostaining of sections.

7) Rinse slides in 1×TBS-T (0.25% Triton X-100 in TBS) once, 15 min.

8) Block with 3% normal serum (varied with species of secondary antibody) in TBS-T for at least 60 min at RT.

9) Incubate with primary antibodies in 3% normal serum/TBS for 24-72 h, at RT.

10) Rinse in TBS for 3 times, 15 min each.

11) Incubate with secondary antibodies in 3% normal serum/TBS for 60 min at 4°C.

12) Rinse in TBS for 3 times, 15 min each.

13) Wash once with H_2O.

14) Mount with mounting medium and cover with a glass coverslip.

2.3.4 Isolation of primary cells

2.3.4.1 Smooth muscle cells

Smooth muscle cells (SMCs) were isolated from aorta (vascular SMCs, VSMCs), and colon (colonic SMCs, CSMCs). Aortic or colonic smooth muscle tissue was digested into single cells and plated to glass coverslips. Cells were grown at 37°C and 6% CO_2 for 5-7 days and serum-starved for 24 h before microscopic/FRET analysis.

10 mg/mL Collagenase
Dissolve 100 mg collagenase (Sigma-Aldrich) in 10 mL Ca^{2+}-free medium, aliquot to 0.5 mL and store at −20°C.

10 mg/mL Hyaluronidase
Dissolve 100 mg hyaluronidase (Sigma-Aldrich) in 10 mL Ca^{2+}-free medium, aliquot to 0.5 mL and store at −20°C.

100 mg/mL BSA
Dissolve 0.5 g BSA in 5 mL Ca^{2+}-free medium, sterilize by filtration, aliquot to 0.5 mL and store at −20°C.

100 mg/mL DTT
Dissolve 0.5 g dithiothreitol (DTT) in 5 mL Ca^{2+}-free medium, sterilize by filtration, aliquot to 0.5 mL and store at −20°C.

7 mg/mL Papain
Dissolve 100 mg papain (Sigma-Aldrich) in 14.29 mL Ca^{2+}-free medium, aliquot to 0.5 mL and store at −20°C.

SMC culture medium

Component	Final conc.	Volume/weight
DMEM	90%	445 mL
FCS	10%	50 mL
Pen/Strep		5 mL

Ca^{2+} free medium

Component	Final conc. (mM)	Volume/weight
Na-Glutamate Monohydrate (Merck)	85	15.91 g
NaCl	60	3.5 g
HEPES	10	2.38 g
KCl	5.6	0.42 g
$MgCl_2 \cdot 6H_2O$	1	0.2 g
H_2O		ad 1 L

Enzyme solution A

Component	Final conc. (µg/µL)	Stock (µg/µL)	Volume/weight
Papain	0.7	7	100 µL
BSA	1	100	10 µL
DTT	1	100	10 µL
Ca^{2+}-free medium			ad 1 mL

Enzyme solution B

Component	Final conc. (µg/µL)	Stock (µg/µL)	Volume/weight
Hyaluronidase	1	10	100 µL
Collagenase	1	10	100 µL
BSA	1	100	10 µL
Ca^{2+}-free medium			ad 1 mL

1) Dissect aorta and colons from mice and wash with 1×PBS.

2) Isolate the smooth muscle tissue under a stereomicroscope. Clean aorta of adjacent fatty tissue, cardiac tissue, lung tissue and blood in PBS under a stereomicroscope. For colon, remove remaining feces from the colon by flushing with PBS using a syringe with a bended needle. Remove remaining mesenteries, fat, and blood vessels. Peel off the smooth muscle layer from the enteric tissue.

3) Cut aorta/colon into small pieces.

4) Incubate tissues for 45 min with enzyme solution A in a water bath at 37 °C, use 1 mL for 1-4 aorta; 1.5 mL for 1-4 colons.

5) Invert every 10 min during incubation.

6) Centrifuge for 2 min at 200 g at RT.

7) Remove and discard supernatant carefully.

8) Treat tissues with enzyme solution B, use same volume as in step 4.

9) Incubate in the water bath at 37 °C again for 5-10 min, depending on age of the mice and quality of enzymes. Resuspend after 5 min every 2-3 min using a pipette until a turbid suspension is formed.

10) Add 10 mL culture medium to the aorta cell suspension in a 15-mL tube to stop the digestion.

11) Spin down the cells in a centrifuge for 7 min at 200 g at RT.

12) Remove supernatant, resuspend the cell pellet with 0.5 mL culture medium per aorta.

13) Count cells and control viability with trypan blue, $1-2.5 \times 10^5$ cells can be expected per aorta, the viability should be higher than 90%; and a higher yield for colon.

14) Dilute cells at 6×10^4 VSMCs/mL, 3×10^4 CSMCs/mL. Seed cells at densities of 1.8×10^4 VSMCs/cm^2, and 0.9×10^4 CSMCs/cm^2. For example plate 1.0 mL of each cell suspension to 20 mm coverslips in 12-well plates.

15) Grow cells at 37 °C with 6% CO_2 in a cell culture incubator.

16) After 3-4 days, check attachment of the cells in a microscope and change culture medium. After 5-7 days, cells reach ≥70% confluence and are ready for analysis.

2.3.4.2 Tail tip fibroblasts

The tail tip fibroblasts were obtained from adult mouse tail. The mouse tail was skinned, minced and plated onto a 12-well plate with glass coverslips. Cells were maintained for 7-10 days in DMEM containing 10% FBS before microscopic/FRET analysis.

1) Cut the tail from an adult mouse and wash with PBS.

2) Incise the tail dermis lengthwise with an injection needle, peel off the superficial dermis and cut the tail into 1 cm pieces.

3) Place 1-2 pieces into a 12-well plate with coverslips and 500 µL culture medium containing 10% FBS.

4) Incubate at 37 ℃, 6% CO_2 for 5 days without movement.

5) Remove the tail piece and change with 1 mL culture medium.

2.3.4.3 Isolation of DRG neurons

DRG neurons reside in the dorsal root ganglion. The mouse spinal cord consists of 8 pairs of cervical, 13 pairs of thoracic and 4 pairs of sacral DRGs totaling to 60 ganglia. In E10-E13, the afferent axons reach the DREZ of the spinal cord and display a stereotyped pattern of T- or Y-shaped bifurcation. E12.5 DRG neurons are suitable for the analysis of axonal branching [85]. Normally, cells from one E12.5 embryo are sufficient for plating 6 wells of a 6-well plate.

Ethanol (96%)
Use 96 mL of absolute Ethanol, make volume with H_2O to 100 mL.

1 M HCl (3.2%)
Add 4.1 mL 37% HCl to 45.9 mL H_2O. Prepare freshly under a fume hood.

150 mM Borate buffer
Dissolve 1.67 g Boric acid in 180 mL H_2O, adjust to pH 8.3 with NaOH and store at 4°C.

1 mg/mL Poly-D-lysine
Dissolve 10 mg poly-D-lysine (PDL, Sigma-Aldrich) in 10 mL H_2O and shake thoroughly. Aliquot to 0.5 mL and store at -20°C.

Horse serum
Life Technologies, heat-inactivated (30 min at 56°C). Aliquot to 50 mL and store at −20°C.

Laminin (20 µg/mL)
Sigma-Aldrich, dilute 1mg in 50 mL PBS. Aliquot to 2 mL and store at -20°C.

0.4 g/mL Glucose
Dissolve 4 g D-glucose in 10 mL DMEM at 37°C for 30 min, filter sterilize and store at 4°C.

NGF (50 µg/mL)
Dissolve 5 µg NGF (Alomone labs) in 100 µL PBS. Aliquot to 20 µL and store at -80°C

DRG culture medium

Component	Final conc.	Stock	Volume/weight
DMEM+F12 medium	80%		4.5 mL+4.5 mL
Horse serum	10%		1 mL
2 mM Glutamine	1x	100x, 200 mM	100 µL
Pen/Strep	1x	100x,	100 µL
Glucose	8 mg/mL	4 g/mL	20 µL
NGF	50 ng/mL	50 µg/mL	10 µL

Prepare freshly before dissection of DRGs, store at 4°C.

A. Pretreatment of glass coverslips

1) Dissolve 4 pellets of NaOH in 10 mL H_2O.
2) Add 35 mL ethanol 96%.
3) Fill a 250 mL plastic container with this solution and agitate 25-50 coverslips overnight on a shaker.
4) Wash 5-10 times with H_2O.
5) Agitate overnight in 1 M HCl.
6) Wash 5-10 times with H_2O.
7) Store the clean coverslips (e.g., Ø30 mm) in 96% ethanol or dry it before use.

B. Coating of coverslips

One day before dissection, coat the coverslips with poly-D-lysine (PDL), and change to laminin the next morning.

1) Remove the desired number of sterile coverslips, drip off superfluous ethanol. Place coverslips in a 6-well plate under a sterile hood.
2) Dilute 1:10 from 1 mg/mL PDL to 100 µg/mL with 150 mM Borate buffer and pipet 150 µL onto one coverslip. Alternatively, add 100 µL of 100 µg/mL PDL onto one coverslip and cover with another.
3) Put the plate into the incubator at 37°C for 4 hours.
4) Wash 3 times with autoclaved water and dry for 30 min.
5) Pipet 150 µL laminin (20 µg/mL) onto a coverslip and incubate at 37°C over night. Alternatively, pipette 100 µL of laminin onto one coverslip and cover with another.
6) The next day, before use, wash 2 times with sterile H_2O and once with PBS. Do not let laminin dry.

C. Dissection of embryonic DRGs

1) Mate 4-6 C57BL/6N females with 2-3 either wild type C57BL/6N or sensor transgenic male mice, and separate plug-positive females at 0.5 dpc.
2) On the day of DRG neuron preparation (12.5 dpc). Prepare an ice box with ice and cold PBS, a 2 mL-tube with 900 µL PBS.
3) Sacrifice pregnant mouse by cervical dislocation. Open the abdominopelvic cavity, isolate the bilateral uterine horns and transfer them into a 10-cm Petri dish with ice-cold PBS.

4) Incise the uterine wall lengthwise with small, straight scissors and peel away amniotic sac from the placenta and cut the umbilical cord. Transfer the embryos in a new Petri dish with ice-cold PBS.

5) If sensor transgenic mice are used, identify genotype with a LED lamp (gift of Dr. L. Jaffe) by detecting the sensor fluorescence.

6) Decapitate the embryos; Remove tail, limbs. Wash the carcasses 2 times in PBS. Transfer the torsi to a sheet of PBS-wet filter paper in a lid of Petri dish with its dorsal side up on the paper.

7) Working under a dissecting stereoscope with a magnification of 10-16x, carefully pinch the skin of the embryo above the spinal cord with a pair of fine tipped forceps and gently tear it apart; beginning in the middle, proceed first towards the tail and then resuming from the middle towards the anterior side.

8) Wet the embryo from time to time with two or three drops of PBS to prevent it from drying.

9) Detach the DRGs and the spinal cord from the surrounding cartilaginous vertebral column by horizontal sliding movements with the blade of a fine forceps with inside-polished tips; Transfer the spinal cord to a new Petri dish with cold PBS.

10) Rip off the DRGs and transfer to the 2-mL tube with ice-cold PBS.

D. Dissociation of embryonic DRGs

1) Add 100 µL 10×trypsin/EDTA (0.5/0.2%, Life technologies) to the 2-mL tube with DRGs and incubate 20 min at 37°C; flick tube from time to time; triturate 10 times with a 1 mL pipette at the end of trypsinization.

2) Add 1 mL DRG culture medium without NGF.

3) Centrifuge 4 min at 200 g at RT.

4) Carefully remove supernatant and resuspend in 1.2 mL DRG culture medium

5) Count cells and adjust the cell number to 20,000 cells/mL.

E. Embryonic DRG neuron culture

1) Plate 200 µL cell suspension per 30 mm coverslip in a 6-well plate.

2) Incubate at 37°C and 6% CO_2.

3) Optional: after 4 hours (when cells have attached to the substrate), carefully add 800 µL DRG medium if culture for overnight.

4) Take cultures after 4-16 h for analysis.

F. Isolation of adult DRG neurons.

1) Sacrifice mouse of an age of 6-20 weeks by cervical dislocation.

2) Dissect the spine from the back of the mouse and transfer it into a Petri dish.

3) Coarsely free the spine from surrounding muscle tissue.

4) Cut the spine with appropriate scissors with the spinal cord longitudinally in two halves.

5) Under a stereomicroscope, carefully pull out the spinal cord from the spine to see the DRG attached to the spinal cord.

6) Pick with forceps a DRG and cut through the dorsal root above and below the DRG.

7) Transfer the DRG to 1 mL ice-cold PBS. Repeat for remaining DRGs.

8) Add 10 µL collagenase to the tube with DRGs and incubate 20-30 min at 37°C.

9) Centrifuge 200 g for 2 min.

10) Carefully aspirate supernatant.

11) Add 1 mL 1×trypsin/EDTA and incubate for 20 min at 37°C; flick tube from time to time; Triturate 10 times with a 1 mL pipette at the end of trypsinization.

12) Add 1 mL DRG culture medium without NGF.

13) Centrifuge at 200 g for 4 min.

14) Remove supernatant and resuspend in 1.2 mL DRG culture medium.

15) Plate about 200 µL cell suspension onto a 30 mm coverslip in a 6-well plate.

16) Incubate at 37°C and 6% CO_2.

17) Take culture after 16-24 hours for analysis.

2.3.5 Transfection of primary cells

Isolated R26-CAG-cGi500(L2) primary cells were subjected to Cre excision by transfection of a Cre-expressing plasmid to validate a functional L2 allele. Lipofectamine 2000 (Life Technologies) was used for transfection.

1) Grow cells to a confluence of 80% or higher.
2) Change the medium to 500 µL DMEM prior to transfection.
3) Prepare two 1.5-mL tubes as follows:

for one well of a 24-well plate:

	OptiMEM	DNA (pSG5-Cre)	Lipo 2000
Tube A	50 µL	0.8 µg	
Tube B	50 µL		2.0 µL

for one well of a 6-well plate:

	OptiMEM	DNA (pSG5-Cre)	Lipo 2000
Tube A	250 µL	4.0 µg	
Tube B	250 µL		10 µL

4) Within 5 min, mix Tube B into Tube A; gently mix by tapping the tube.
5) Incubate for 20-30 min, not longer,
6) Add the 100 µL mixture to the cells with 500 µL DMEM,
7) Change medium next morning. Cells are analyzed 48 h after transfection.

2.3.6 Thrombus formation in a flow chamber

Collagen is an important agonist for platelet activation and adhesion *in vivo*. Collagen-induced thrombus formation has been elicited in flow chamber assays. Native blood drawn from an organism flows over immobilized collagen fibrils coated on a coverslip positioned in a parallel-plate perfusion chamber [189].

Murine blood was perfused through a collagen-coated glass coverslip (24 × 60 mm), which forms the bottom of an ibidi flow chamber (ibidi GmbH) with 0.2 mm height. The thrombi formed on the coverslip were used for further imaging analysis (**Figure 7**).

10×Tyrode platelet buffer

Component	Volume/weight
NaCl	80 g
NaHCO$_3$	10.15 g
KCl	1.95 g
H$_2$O	ad to 1 L

Store at 4°C.

1×Tyrode platelet buffer
Prepare freshly from 10×Tyrode platelet buffer in a dilution of 1:10, supplement with 0.1% glucose, and 0.1% BSA, adjust pH to 7.4 with HEPES.

1% BSA
Dissolve 1 g BSA in 100 mL H$_2$O. Filter sterilize and store at 4 °C.

Heparin (20 U/mL in TBS)
Dissolve 20 U/mL heparin in TBS, containing 20 mM Tris/HCl; 137 mM NaCl; pH 7.3.

1) Coat a coverslip (24 × 60 mm) with 200 µg/mL fibrillar type I collagen (Nycomed) overnight at 4°C.

2) Block with 1% BSA solution for at least 30 min at RT.

3) Anesthetize mice by diethylether inhalation.

4) Collect ~700 µL of blood from the retroorbital plexus of each mouse and collect into a tube containing 300 µL of 20 U/mL heparin.

5) Mix 2 parts of blood with 1 part of Tyrode buffer and fill a 1-mL loop using a 1-mL syringe.

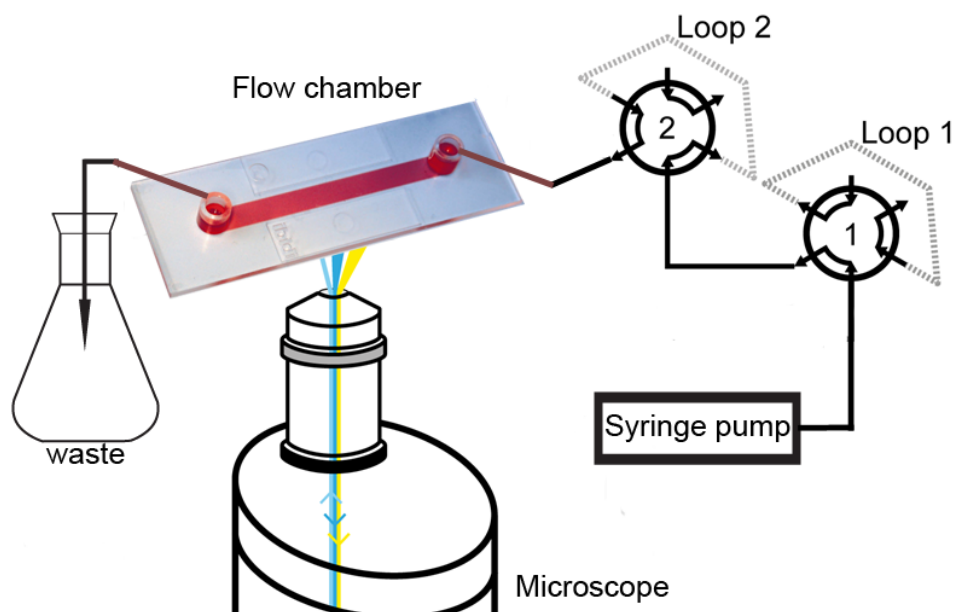6) Flow whole blood over the flow chamber at 15 mL/h with a syringe pump.

Figure 7. Flow chamber system for cGMP and Ca^{2+} visualization.

The thrombus is formed on a coverslip attached to an ibidi flow chamber and superfused with Tyrode buffer using a syringe pump. Two FPLC injection valves are connected between the syringe pump and flow chamber for drug application. Sample loops (loop1 and 2) are attached to injection valve 1 and 2, respectively, and can be loaded with drugs at the same time. By changing the valve position from loading to injection, the drug solution can be delivered continuously to the cells. Note that adherent cells like VSMCs can also be grown on coverslips and attached to the ibidi chamber before measurement under a microscope.

2.3.7 FRET measurement in primary cells

The imaging setup was based on an inverted Axiovert 200 microscope (Carl Zeiss Microscopy GmbH) equipped with LD Plan NeoFluar 20×/0.40 air or Plan NeoFluar40× /1.30 oil objectives and optional 1.6× Optovar magnification, a light source with excitation filter switching device (Oligochrome, TILL Photonics GmbH), a DualView beam splitter with 516 nm dichroic mirror and CFP and YFP emission filters (480/30 nm and 535/40 nm) (Photometrics), and a CCD digital camera (Retiga 2000R, QImaging).

To set up the field of view, cGi500 fluorescence was observed through a YFP filter set (excitation filter 497/16 nm, 516 nm dichroic mirror, and emission filter 535/22 nm). FRET measurements were performed with a CFP excitation filter (445/20 nm) and a 470 nm dichroic mirror as well as the beam splitter device, where emission wavelengths were separated with a 516 nm dichroic filter and 480/30 nm and 535/40 nm emission filters for CFP and YFP fluorescence, respectively. The system was computer-controlled by Live Acquisition software (TILL Photonics GmbH) and imaging data was recorded with arivis Browser 2D (arivis GmbH).

For cGMP imaging of platelet thrombi formed in a flow chamber, or VSMCs grown on a coverslip for shear stress experiments, the cells were superfused with Tyrode platelet buffer at room temperature using a syringe pump (B-Braun) at 15 mL/h with 2-mL and 7-mL sample loops connected in series to apply drugs. For cGMP imaging of primary cells including DRG neurons, adult tail tip fibroblasts and smooth muscle cells, cells were grown on glass coverslips. A coverslip was attached into a custom-built superfusion imaging chamber [135]. Samples were superfused with Tyrode imaging buffer at room temperature using a FPLC pump (Pharmacia P-500, GE Healthcare Europe GmbH) set to 60 mL/h and two injection valves (Pharmacia V-7, GE Healthcare). The solution in the imaging chamber was continuously removed by aspiration with a vacuum pump (Laboport N86, KNF Neuberger).

Tyrode imaging buffer

Component	Final conc.	Volume/weight
NaCl	140 mM	40.91 g
KCl	5 mM	1.86 g
$MgCl_2 \cdot H_2O$	1.2 mM	1.22 g
$CaCl_2$	2.5 mM	1.39 g
Glucose	5 mM	4.5 g
HEPES	10 mM	11.92 g
H_2O		ad to 5 L

The native pH is ~5.3. Adjust pH to 7.4 with NaOH. Autoclave and store at 4°C.

100 µM ANP
Dissolve 0.1 mg ANP (1-28, rat; Sigma-Aldrich) in 0.327 mL H_2O, aliquot to 50 µL and store at −20°C.

100 µM CNP
Dissolve 0.5 mg CNP (Sigma-Aldrich) in 2.275 mL H_2O, aliquot to 50 µL and store at −20°C.

100 mM DEA/NO
Dissolve 50 mg 2-(N,N-diethylamino)-diazenolate-2-oxide diethylammonium salt (DEA/NO, Axxora) in 2.42 mL ice-cold 10 mM NaOH, aliquot to 50 µL and store at −20°C.

100 mM Spermine/NO
Dissolve 25 mg (Z)-1-[N-[3-aminopropyl]-N-[4-(3-aminopropylammonio)butyl]-amino]diazen-1-ium-1,2-diolate (Spermine/NO, Axxora) in 0.95 mL ice-cold 10 mM NaOH, aliquot to 50 µL and store at −20°C.

10 mM DETA/NO
Dissolve 50 mg (Z)-1-[N-(2-aminoethyl)-N-(2-ammonioethyl)amino]diazen-1-ium-1,2-diolate (DETA/NO, Axxora) in 0.61 mL ice-cold 10 mM NaOH, aliquot to 50 µL and store at −20°C.

10 mM EHNA
Dissolve 10 mg erythro-9-(2-hydroxy-3-nonyl)adenine (EHNA, Axxora) in 3.19 mL DMSO, aliquot to 100 µL and store at −20°C.

10 mM BAY 41-2272
Dissolve 5 mg BAY 41-2272 (Santa Cruz) in 1.39 mL DMSO, aliquot to 100 µL and store at −20 °C.

10 mM BAY 60-7550
Dissolve 1 mg BAY 60-7550 (Santa Cruz) in 0.21 mL DMSO, aliquot to 50 µL and store at −20°C.

10 mM Milrinone
Dissolve 10 mg Milrinone (Santa Cruz) in 4.73 mL DMSO, aliquot to 500 µL and store at −20°C.

10 mM Zaprinast
Dissolve 20 mg Zaprinast (Santa Cruz) in 7.37 mL DMSO, aliquot to 500 µL and store at -20°C.

10 mM Pyr3
Dissolve 5 mg Ethyl-1-(4-(2,3,3-trichloroacrylamide)phenyl)-5-(trifluoromethyl)-1H-pyrazole-4-carboxylate (Pyr3, Sigma-Aldrich) in 1.1 mL DMSO, aliquot to 200 µL and store at -20°C.

20 mM ODQ
Dissolve 10 mg 1H-[1,2,4]oxadiazolo[4,3-a]quinoxalin-1-one (ODQ, Axxora) in 2.67 mL DMSO, aliquot to 100 µL and store at −20°C.

30 mM Sildenafil
Dissolve 50 mg Sildenafil (Santa Cruz) in 25 mL H_2O, aliquot to 1.5 mL and store at −20°C.

5 mM Vinpocetine
Dissolve 20 mg Vinpocetine (Biomol) in 11.41 mL DMSO, aliquot to 1.5 mL and store at −20°C.

50 mM Tadalafil
Dissolve 50 mg Tadalafil (Santa Cruz) in 2.57 mL DMSO, aliquot to 150 µL and store at -20°C.

500 mM IBMX
Dissolve 1.0 g 3-isobutyl-1-methylxanthine (IBMX, Sigma-Aldrich) in 9.0 mL DMSO, aliquot to 1.5 mL and store at −20°C.

2.3.8 Simultaneous measurement of Ca^{2+} and cGMP

For independent Ca^{2+} measurement, adherent cells or thrombi formed on a coverslip attached with the ibidi flow chamber were loaded with Fura-2, AM. The optical system including the inverted microscope and a CCD digital camera was the same as the one for FRET measurement as described before (2.3.7). For Fura-2 dual excitation ratio imaging, a filter switching device based on a galvanometer driven mirror (Oligochrome, TILL Photonics) was equipped with two narrow band pass excitation filters, one 340/26 nm and one 387/11nm filter. A 440 nm long pass emission filter was used to attenuate shorter wavelengths than 440 nm and transmitting longer wavelengths. A 410 nm DCLP dichroic mirror was used. Therefore, emission fluorescence was recorded above 440 nm while switching excitation at 340 nm and 380 nm.

For simultaneous Ca^{2+} and cGMP measurement, whole blood from R26-CAG-cGi500(L1) mice was used to form thrombi on a coverslip and then loaded with Fura-2, AM. A combination of filter and mirror sets were used to allow capture of Fura-2 and FRET images simultaneously. A filter switching device with one 340/26 nm and one 387/11 nm narrow band pass filter for Fura-2 excitation, and a CFP excitation filter (445/20 nm) for FRET excitation were used. For both Fura-2 and FRET emission, a

470 nm dichroic mirror and the DualView beam splitter containing a 516 nm dichroic mirror and CFP and YFP emission filters (480/30 nm and 535/40 nm) were used. In every measurement cycle, cells were excited at 340 nm, 380 nm and 445 nm and emitted light was recorded at 480 nm and 535 nm, therefore in total 6 images were captured (**Table 4**). Image 2 was defined as F_{340}, image 4 as F_{380} for Fura-2 measurement, and image 5 as F_{480} and image 6 as F_{535} for FRET measurement.

Table 4. Image acquisition for simultaneous measurement of Fura-2 and FRET

Excitation (Ex.) filter	Emission (Em.) filter	Image No.
340/26 nm	CFP emission filters (480/30 nm)	1
	YFP emission filters (535/40 nm)	2
387/11 nm	CFP emission filters (480/30 nm)	3
	YFP emission filters (535/40 nm)	4
445/20 nm	CFP emission filters (480/30 nm)	5
	YFP emission filters (535/40 nm)	6

Fura-2, AM Tyrode solution

Mix 2.5 µL Fura-2, AM (1 mM in DMSO, Calbiochem) with 1 mL Tyrode buffer. Vortex vigorously to disperse Fura-2, AM in solution. Prepare freshly and avoid light exposure.

1) Load 1 mL Fura-2, AM to the cells in the flow chamber using a 1-mL syringe.
2) Incubate for 45 min at RT in the dark.
3) Wash cells by perfusion with Tyrode buffer for 5 min.
4) Perform imaging with excitation and emission wavelength as required for independent Ca^{2+} imaging or simultaneous Ca^{2+}/cGMP imaging. Generally, record images at 2 s or 5 s interval.

2.3.9 Local application of compounds

DRG neurons were grown on 30 mm coverslips for 4 to 16 h. Each coverslip to be assayed was transferred to a customized superfusion chamber. Local CNP application to compartments of DRG neurons, such as growth cones, was achieved by ejection from a CNP-loaded glass pipette with 10 µm bore width (Biomedical Instruments), which was connected to a microinjector (Femtojet, Eppendorf, kindly provided by Prof. Dr. Gabriele Dodt).

1) Load a glass pipette with CNP solution diluted in Tyrode buffer (100 nM-1 µM).
2) Connect the glass pipette to a Femtojet microinjector.
3) Attach the Femtojet microinjector pipette holder to a micromanipulator.

4) Set up the superfusion chamber with cells, connect the global perfusion system with Tyrode buffer.

5) Search for a neuron for imaging. Position the glass pipette that it is ~50 µm away from the growth cone at an angle of ~45°. The distance can be measured with the FRET Live Acquisition software.

6) Draw regions of interest (ROIs) in the soma, axon and growth cone. Start FRET measurement.

7) Eject CNP from the glass pipette by an air pulse of 20-30 hPa with the microinjector for 20-30 s. Superfuse Tyrode buffer in the same or reverse direction of the glass pipette in order to remove the agonists immediately.

2.3.10   Data analysis and statistics

Live Acquisition software (TILL Photonics) was used for image acquisition and online analysis. Offline image analysis was performed with arivis Browser 2D software (arivis GmbH) or ImageJ [190]; for further data evaluation, Microsoft Excel (Microsoft Corp.), Sigmaplot (Systat Software, Inc.), and Microcal Origin (OriginLab Corp.) were used.

1) Select regions of interest. Cell-free regions were selected as background.

2) Background correction: for FRET measurement, background-corrected F_{480} and F_{535} signals were used to calculate the F_{480}/F_{535} ratio, R.

3) Baseline normalization: $\Delta F_{480}/F_{480}$, $\Delta F_{535}/F_{535}$, and $\Delta R/R$ traces from single cells or thrombus were obtained by normalization to the baseline recorded for 2-5 min at the beginning of each experiment.

4) Optionally, for $\Delta R/R$ peak area estimation, the Peak Analyzer Module of Origin was used; single cell traces were corrected for baseline drifts by subtracting a linear baseline, and peak borders were manually defined.

5) FRET signal $\Delta R/R$ at different time points was reconstructed by ImageJ and represented by pseudocolor.

For Ca^{2+} imaging or simultaneous Ca^{2+} and cGMP imaging, F_{340} and F_{380} from Fura-2 excitation or fluorescence emission of CFP (F_{480}) and YFP (F_{535}) were subjected to similar evaluation, respectively.

Statistical differences between two groups were determined using the two-tailed Student`s t test. Statistical differences among more than two groups were analyzed by one-way ANOVA followed by Tukey's multiple comparison test. P values <0.05 were considered significant. For example, in PDE inhibitor studies, peak areas before and after inhibitor application, and after washout were compared using one-way ANOVA followed by Tukey's multiple comparison test in SigmaPlot 11.

3 Results

3.1 Generation and characterization of cGMP sensor knock-in mice

We used the recently developed FRET-based cGMP sensor, cGMP indicator with an EC_{50} of 500 nM (cGi500), to generate transgenic mice for cGMP imaging. cGi500 is an improved cGMP FRET sensor, which excels in terms of relatively high affinity, exquisite selectivity for cGMP over cAMP and fast cGMP binding and dissociation kinetics [138]. To allow for tissue-specific imaging of cGMP, the Cre-loxP system was used. cGi500 within a Cre recombinase-activatable cassette driven by the ubiquitous CAG promoter was targeted into the Rosa26 locus.

The targeting strategy is illustrated in **Figure 8A**. The targeting vector pR26-CAG-cGi500(L2) was constructed by replacing the mG sequence of pRosa26-mT/mG (Addgene plasmid 17787) [174] with the cGi500 coding sequence [138]. The resulting mT/cGi500 cassette (CAG-loxP-mT-loxP-cGi500) was preceded by the CAG promoter, which drives the expression of a loxP-flanked membrane-targeted tandem-dimer Tomato (mT, red) before and cGi500 (green) after Cre-mediated recombination, respectively.

To perform gene targeting in ES cells, the targeting vector pR26-CAG-cGi500(L2) was linearized by the restriction enzyme KpnI, and 42 µg of purified linear vector was electroporated into ~1.0×10^7 R1 ES cells (genetic background: 129/Sv x 129/Sv-CP) [187]. 24 hours after electroporation, selection with 300 µg/mL G418 was applied to the ES cell culture. After 8 days of G418 selection, 200 clones were isolated and expanded. Genomic DNA from colonies were isolated in 96-well plate and subjected to EcoRV digestion and Southern blot analysis with a 5' probe that binds to the Rosa26 promoter region (**Figure 8A and C**). Three correctly targeted ES cell clones carrying the Cre-activatable L2 allele were identified. To generate ES cells with the 'excised' R26-CAG-cGi500(L1) allele, targeted R26-CAG-cGi500(L2) ES cells were transiently transfected with a Cre-expressing plasmid (pIC-Cre) [157] by electroporation to remove the floxed mT cassette. ES cell clones before Cre excision showed strong mT fluorescence, whereas expression of cGi500 was activated after mT removal, as revealed by YFP fluorescence detection (**Figure 8B**). Isolated ES cells underwent Southern blot analysis, showing a band shift from 20.2 kb (L2 allele) to 17.8 kb (L1

allele), which further confirmed excision of the mT DNA fragment (**Figure 8C**). Therefore, ES cells with targeted insertion of either the R26-CAG-cGi500(L2) allele or the R26-CAG-cGi500(L1) allele were successfully generated.
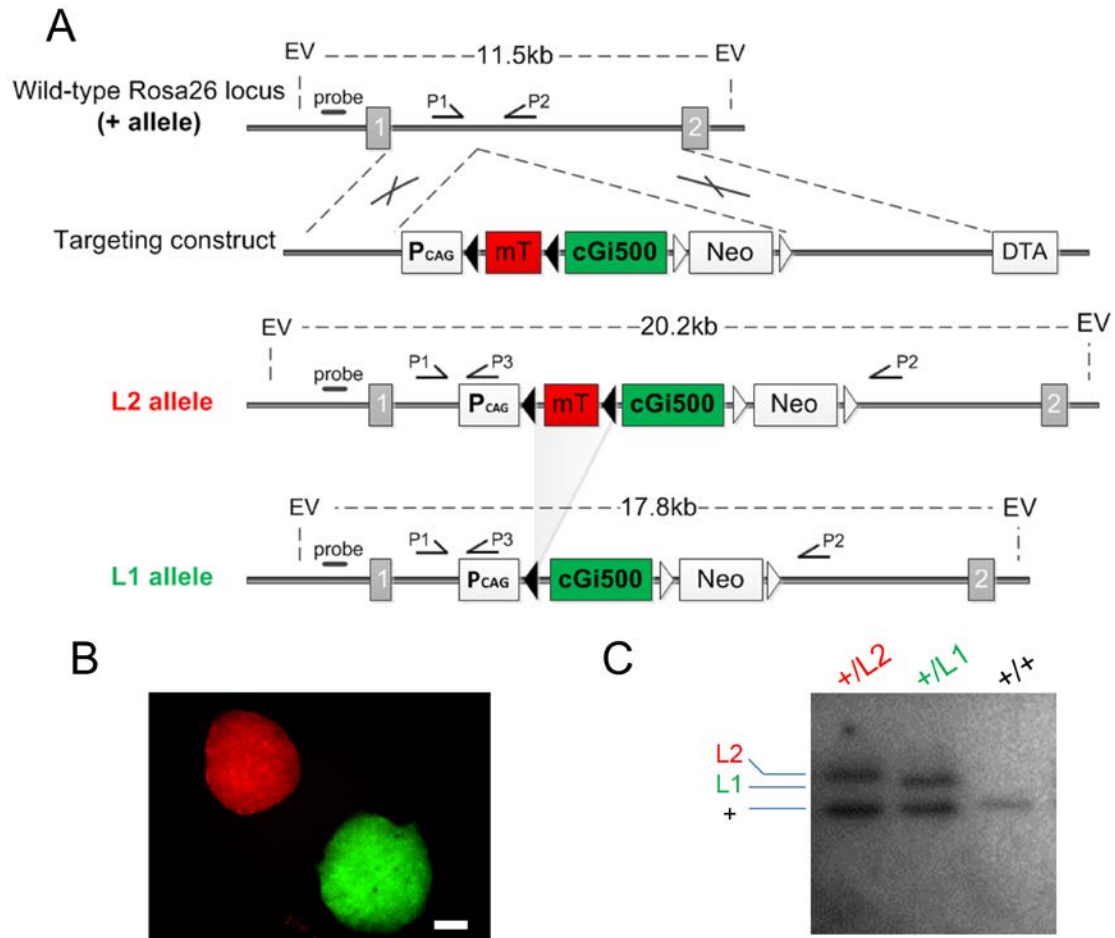

Figure 8. Generation of R26-CAG-cGi500 mice.

A. Schematic representation of the gene targeting strategy to insert a conditional cGi500 construct into the murine Rosa26 locus (+ allele) in the intron between exon 1 and 2 (grey boxes). The targeting construct included the CAG promoter (P_{CAG}) followed by the loxP-flanked (black arrowheads) membrane-targeted tandem-dimer Tomato (mT, red) and cGi500 (green). P_{CAG} drives the expression of mT before and cGi500 after Cre-mediated recombination. Expression cassettes encoding a FRT-flanked (white arrowheads) neomycin resistance gene (Neo) and diphtheria toxin A (DTA) served as positive and negative markers for selection of ES cell clones. Homologous recombination between the targeting construct and the "+ allele" results in a "L2 allele" with two loxP sites, and Cre-mediated excision of mT results in the "L1 allele" with one loxP site. Primers P1, P2, P3 (half arrows) in the diagram correspond to primers ROSA10, ROSA11, ROSA4 used for PCR genotyping of mice described in the text, respectively. The 5` probe and DNA restriction fragments used for Southern blot analysis of ES cell clones are also indicated. EV, EcoRV restriction sites. **B**. Targeted ES cells (+/L2) were transfected with a Cre-expressing plasmid resulting in recombined (+/L1) ES cell clones. Shown is a merged image of ES clones after electroporation excited with a YFP or mT filter set. Scale bar, 100 µm. **C**. Southern blot of EcoRV-digested genomic DNA from wild type (+/+), targeted (+/L2) and Cre-recombined (+/L1) ES cell clones. The expected positions of the DNA fragments originating from the respective alleles are indicated on the left.

R26-CAG-cGi500(L2) ES cells carry the silenced but Cre-activatable "L2 allele", whereas R26-CAG-cGi500(L1) ES cells carry the permanently activated "L1 allele" of the cGi500 sensor transgene. Both L2 and L1 ES cell clones were injected into 3.5 dpc C57BL/6N blastocysts to generate chimeric mice. Chimeras were crossed with wild type mice for germline transmission. Male chimeras were mated to C57BL/6N females to obtain heterozygous R26-CAG-cGi500(L2) mice [B6;129-Gt(ROSA26)Sor[tm1(ACTB-tdTomato,-cGi500)Feil]] or R26-CAG-cGi500(L1) mice [B6;129-Gt(ROSA26)Sor[tm1.1(ACTB-cGi500)Feil]] on a mixed 129Sv/C57BL6 genetic background. Mice were further backcrossed to C57BL/6N animals. Note that the L2 and L1 mouse lines for further experiments were derived from ES cell clone A9 and A7G6, respectively (**Table 5**).

Table 5. Overview of blastocyst injection and chimeric progenies

Clone/ passage	Blastocysts reimplanted	Progeny	Chimera gender (grade of chimerism and GLT)
A9/P22	31	14	8♂ (80-90%, **GLT,** ☆), 2♂ (60-70%), 1♂ (30%),1♀ (70%)
A9/P24	21	4 (†)	no
G12/P23	25	no	no
H10/P24	20	4	no
A3/P22	16	no	no
A7/P23	27	9	no
A7/P23	36	11	2♂ (60-80%), 1♂ (50%)
F1/P23	32	12	1♂ (10%), 1♂ (60%), 1♀ (60%)
A7G6/P29	26	6	1♂ (50%, **GLT**), 1♀ (50%)

Grade of chimerism, an estimation of agouti coat color. GLT, germ-line transmission. ☆, 3 chimeras were examined for GLT and all showed GLT.
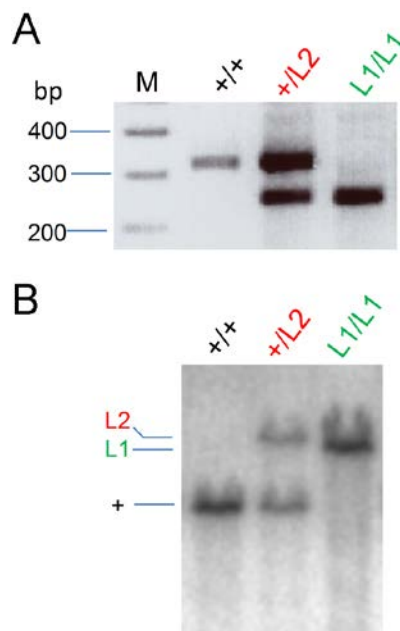
Figure 9. Verification of targeted mouse lines.

A. PCR genotyping of wild type (+/+), targeted (+/L2) and Cre-recombined (L1/L1) mice with genomic DNA from heart tissues. M: 1 kb plus ladder DNA marker. **B**. Southern blot of EcoRV-digested genomic DNA of wild type (+/+), targeted (+/L2) and Cre-recombined (L1/L1) mouse heart tissue. The expected positions of the DNA fragments derived from the respective alleles are indicated on the left.

PCR-based genotyping of ear biopsies was done with primers ROSA10 (P1), ROSA11 (P2), and ROSA4 (P3) [173]. ROSA10 and ROSA11 amplified a 330-bp fragment of the wild type ROSA26 locus, while ROSA10 and ROSA4 amplified a 250-bp fragment of the R26-CAG-cGi500(L2) or R26-CAG-cGi500(L1) allele (**Figure 8A and 9A**). Germline transmission of the targeted alleles was further verified by Southern blot analysis of tail, liver and heart DNA of germline transmitted progeny (**Figure 9B,** shown for heart DNA). Both R26-CAG-cGi500(L2) and R26-CAG-cGi500 (L1) mice were healthy and fertile.
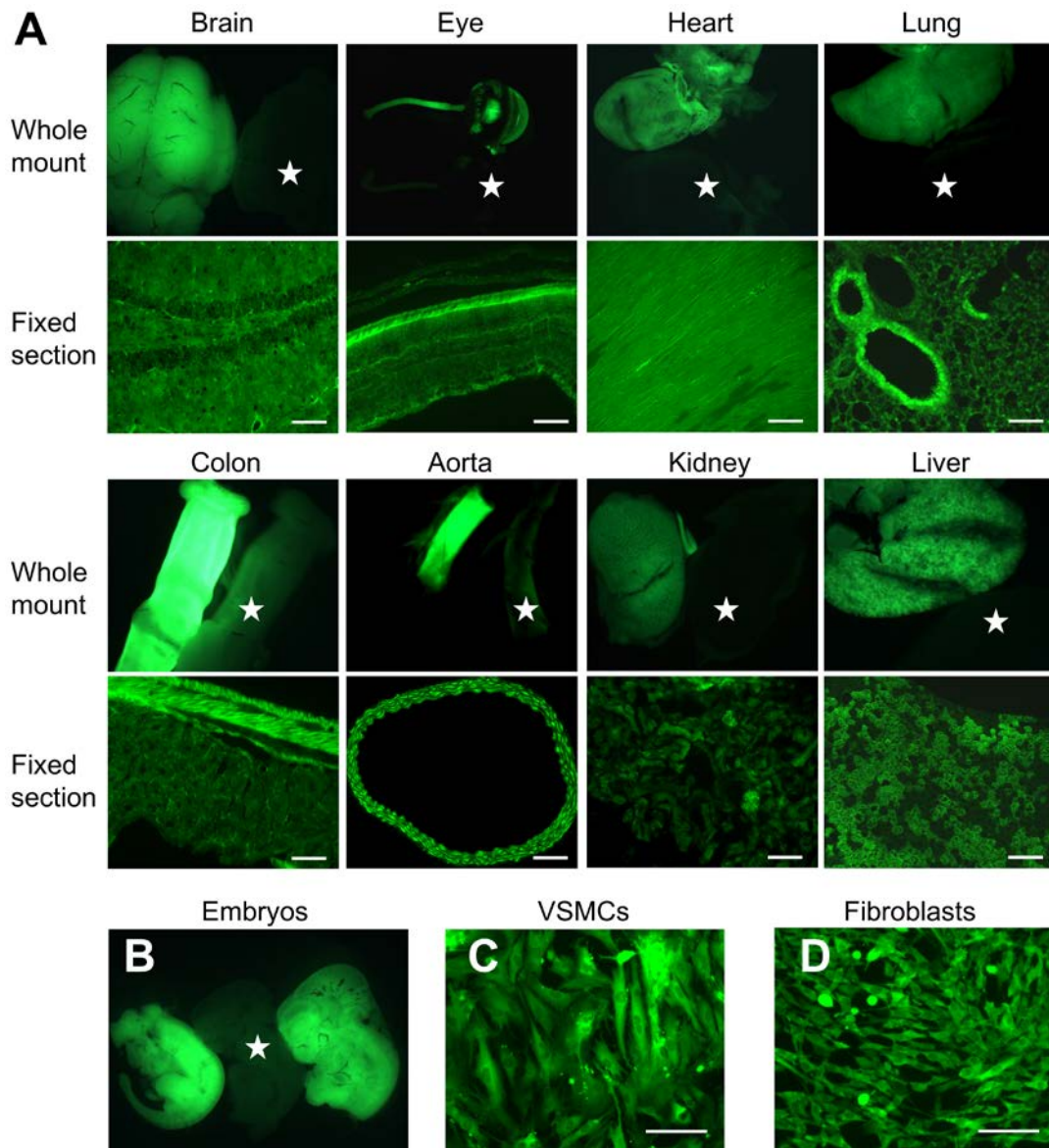
Figure 10. Global expression of cGi500 in R26-CAG-cGi500(L1) mice.
cGi500 sensor fluorescence using an EGFP or YFP filter set was detected in (**A**) live whole mounts (upper panel) and fixed cryosections (lower panel) of various organs from a 6-week-old transgenic mouse, (**B**) transgenic embryos (12.5 dpc), and (**C**) primary aortic VSMCs or (**D**) tail tip fibroblasts from adult animals. Stars indicate the positions of control samples from non-transgenic littermates. Scale bars, 100 µm.

Next, we examined the labeling of mT and cGi500 in both L2 and L1 mouse lines by analysis of live whole mounts and paraformaldehyde-fixed cryosections. In L1 mice, global and robust cGi500 sensor expression was widely detected in organs and tissues of adult mice and in embryos, as well as in primary cells derived from them (**Figure 10**, and data not shown). At the single cell level, the fluorescence was homogeneously distributed in the cytoplasm, without nuclear labeling. Moreover, live visualization of primary neurons isolated from R26-CAG-cGi500(L1) mice showed strong labeling of cell bodies as well as their fine processes (e.g., **Figure 14B**), which enables cGMP imaging at subcellular fine structures like dendrites, axons and growth cones. The red fluorescence of R26-CAG-cGi500(L2) mice showed a similar pattern (upper panel of **Figure 12**, and data not shown), except that mT (a membrane-targeted red fluorescent protein) localized to the cell membrane (**Figure 13**).

FRET-based cGMP imaging was performed with primary VSMCs isolated from heterozygous R26-CAG-cGi500(L1) mice with an epifluorescence microscope. Stimulation of cells with the cGMP-elevating drug CNP led to an increase in CFP fluorescence intensity (F_{480}), and a decrease in YFP fluorescence intensity (F_{535}), as a result of FRET reduction upon cGMP binding to the sensor protein. Overall, the increase of the F_{480}/F_{535} ratio represents intracellular cGMP signals. The cGMP signal was robust; 50 nM CNP induced a ratio change ($\Delta R/R$) up to ~40% in VSMCs, which corresponded to a peak concentration of >3 µM cGMP (**Figure 11**).
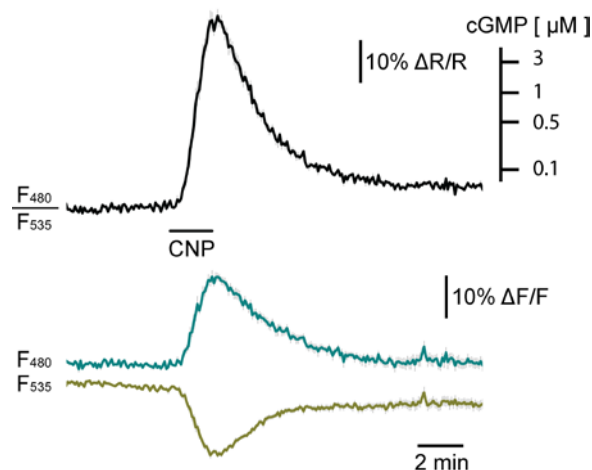
Figure 11. cGMP FRET imaging in primary VSMCs from R26-CAG-cGi500(L1) mice.

Stimulation for 2 minutes with CNP (50 nM) in VSMCs led to a reversible cGMP increase. Cyan, yellow, and black traces correspond to CFP emission (F_{480}), YFP emission (F_{535}), and the CFP/YFP emission ratio (F_{480}/F_{535}), respectively. Emission intensities and ratios were normalized to averaged baseline signals and given as $\Delta F/F$ and $\Delta R/R$, respectively. Data shown are mean ± SEM; n=5 VSMCs. The scale bar of cGMP concentrations was derived from in-cell calibration of the cGi500 sensor [135].

To demonstrate that the L2 allele can be converted into a L1 allele by Cre-mediated recombination *in vivo*, resulting in tissue-specific expression of cGi500, R26-CAG-cGi500(L2) mice were crossed to various Cre mouse lines (e.g., L7-Cre, Pf4-Cre, and SM22-Cre). The L7-Cre line has already been shown to label Purkinje cells in the cerebellum [188, 191, 192]. As expected, R26-CAG-cGi500(L2)[+/-]; L7-Cre[tg/+] mice showed clear labeling of Purkinje cells and axons with cGi500, while mT was complementarily expressed in the surrounding tissue (**Figure 12**).
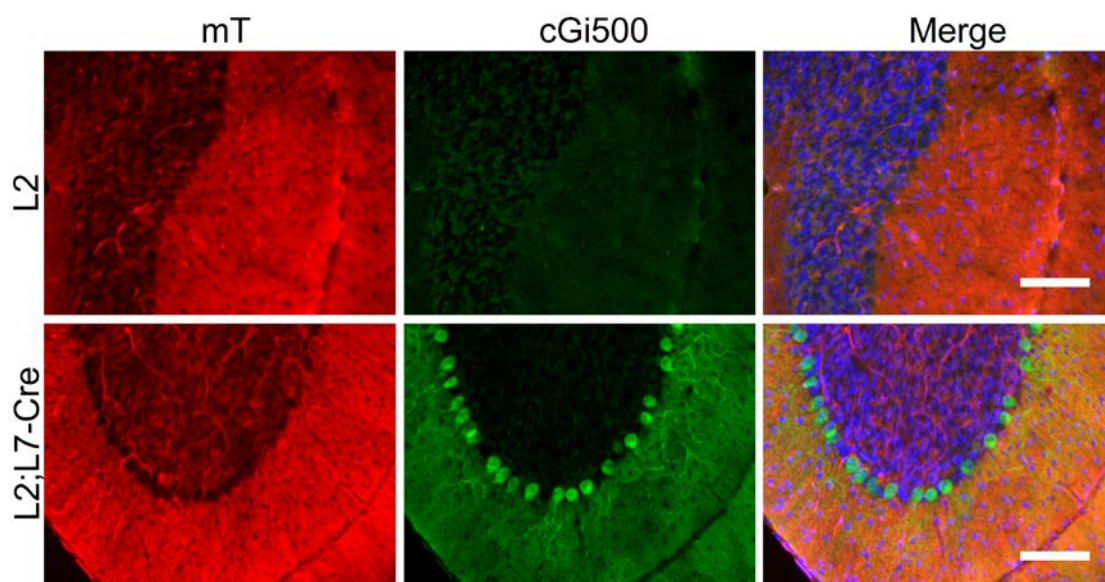

Figure 12. Cell-type specific expression of cGi500.

Sagittal cerebellar sections prepared from 9 week-old R26-CAG-cGi500(L2)[+/-] ; L7-Cre^{+/+} (upper panel, control) or R26-CAG-cGi500(L2)[+/-] ; L7-Cre[tg/+] (lower panel) mice. Specific labeling of cGi500 in Purkinje neurons and mT labeling in the surrounding tissue demonstrated the conversion from mT to cGi500 depending on tissue-specific expression of Cre. Fixed cryosections of both genotypes were processed in the same way and images were taken under the same condition. Scale bars, 100 µm.

Different cell types (VSMCs, CSMCs and tail tip fibroblasts) were isolated from R26-CAG-cGi500(L2) mice and transfected by lipofection with a Cre-expressing plasmid, pSG5-Cre [160]. As early as 12 hours after transfection, green fluorescent cells were detected with a YFP filter set. 30-60% of cells showed green fluorescence 48 hours after transfection (**Figure 13**), indicating the excision of mT and activation of cGi500 expression. Single-cell level detection confirmed mT localization in the plasma membrane, while cGi500 was homogeneously distributed in the cytoplasm without nuclear localization. A small proportion of cells also showed double-labeling of mT and cGi500 (yellow cells; **Figure 13**). In these cells, Cre-mediated recombination caused rapid onset of cGi500 expression, while mT protein was still retained. Overall, these data showed that cGi500 expression in the R26-CAG-cGi500(L2) mouse line was Cre-dependent, and could be conditionally activated in a tissue-specific manner.

To validate the functionality of cGi500 after activation from the conditional L2 allele, the recombined cells were subjected to FRET cGMP imaging. Application of cGMP-elevating drugs resulted in robust FRET changes (up to 40%) and, therefore, cGMP elevation in green cells (**Figure 13**). Isolated VSMCs were superfused for 2 min with CNP, which activates membrane-bound guanylyl cyclase, GC-B. Rapid and reversible CFP/YFP ratio changes indicate CNP-induced cGMP signals in the cells. Similar results were obtained with tail tip fibroblasts stimulated with CNP, and CSMCs stimulated with the NO-releasing compound, DEA/NO. DEA/NO did not induce FRET changes in fibroblasts, indicating the lack of sGC in these cells.
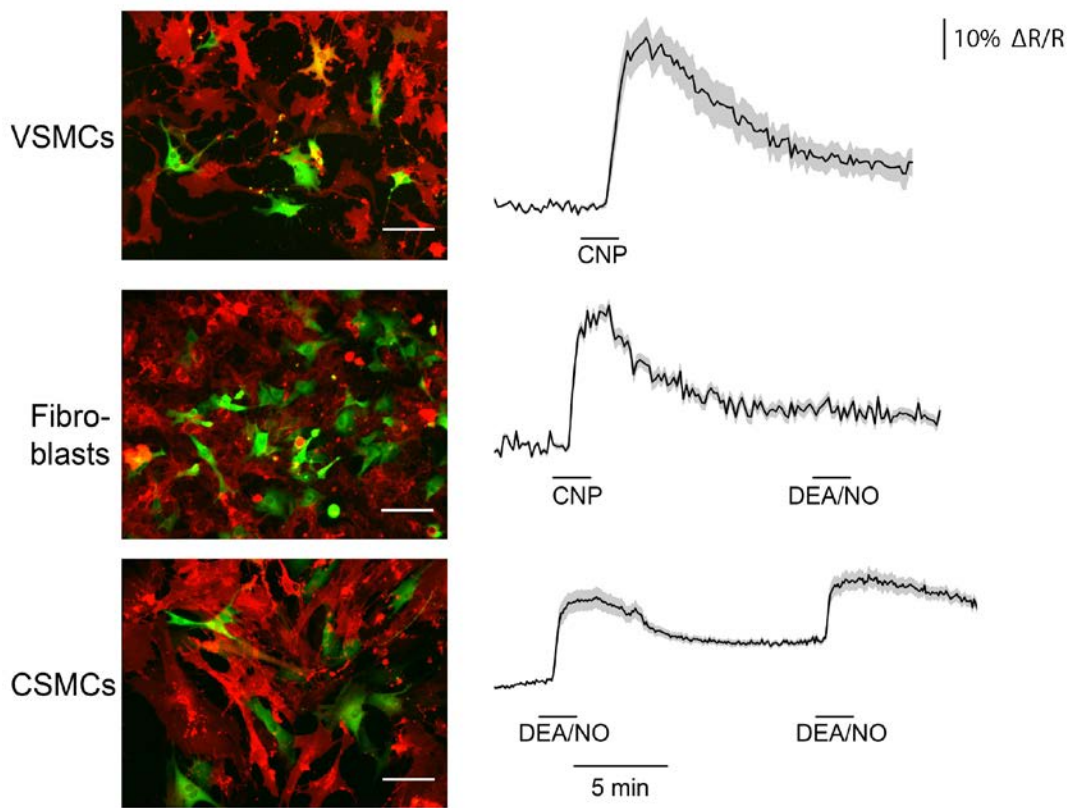
Figure 13. Validation of a functional L2 allele in cells from R26-CAG-cGi500(L2) mice.

VSMCs, fibroblasts, and CSMCs were isolated from R26-CAG-cGi500(L2) mice and then transfected by lipofection with a Cre-expressing plasmid. The detection of green fluorescent cells confirmed that Cre-mediated excision of the mT cassette enables cGi500 expression in all analyzed cell types (left panels). Sustained expression of mT is evidenced by the presence of double-labeled (yellow) cells. FRET imaging (right panels) was performed to test the sensor functionality in cGi500-positive cells. Cells were stimulated with CNP or DEA/NO (VSMCs with 50 nM CNP, fibroblasts with 100 nM CNP followed by 100 nM DEA/NO, and CSMCs two times with 100 nM DEA/NO). Data shown are mean $\pm$ SEM. The number of analyzed VSMCs, fibroblasts, and CSMCs was 8, 10, and 8, respectively. Scale bars, 100 µm.

Taken together, cGMP sensor knock-in mice with global or tissue-specific expression of cGi500 were successfully generated. The widespread sensor expression and robust FRET cGMP signals facilitate cGMP imaging and delineation of the cGMP signaling pathway in various cell types, intact tissues and living mice.

3.2 cGMP imaging in embryonic DRG neurons

Axon branching is critical for the formation of neuronal connectivity. To understand the function of cGMP in sensory axonal guidance and bifurcation, we utilized our newly generated cGi500 sensor knock-in mice to image cGMP signals in embryonic DRG neurons. C57BL/6 female mice were mated with the cGi500 sensor knock-in mice (+/L1 or L1/L1) to obtain E12.5 embryos, from which embryonic DRG neurons were isolated (**Figure 14A and B**).
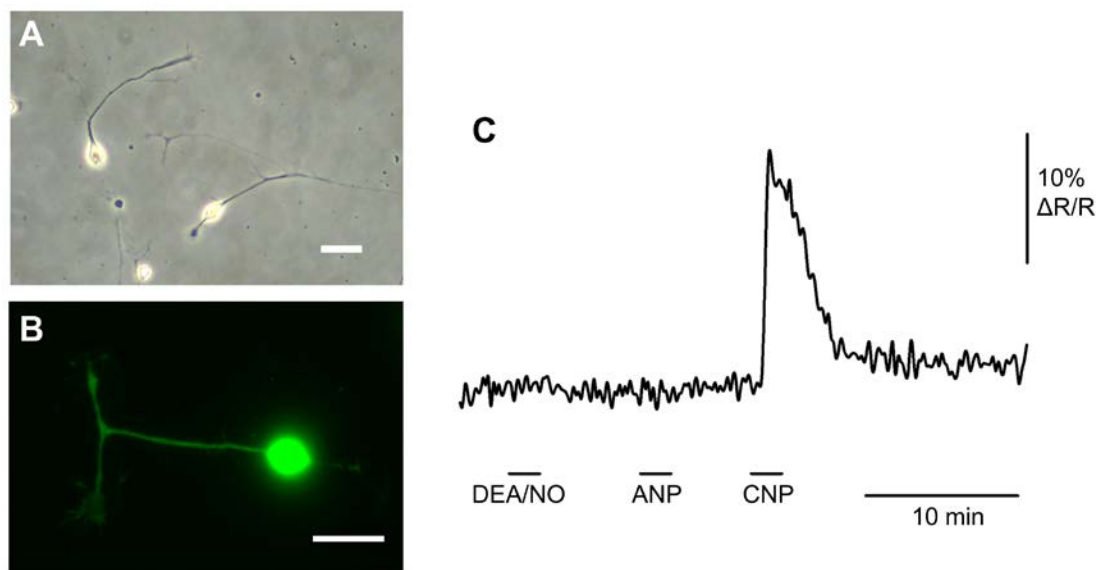

Figure 14. CNP but not ANP or NO stimulates cGMP in embryonic DRG neurons.

A. E12.5 DRG neurons were isolated and grown on glass coverslips coated with 100 µg/mL PDL and 20 µg/mL laminin. Cells were visualized under a phase-contrast microscope. Scale bar, 50 µm. **B**. cGi500 sensor expression was detected in E12.5 DRG neurons from R26-CAG-cGi500(L1) with a YFP filter set. Scale bar, 20 µm. **C**. cGMP imaging in a E12.5 DRG neuron with global perfusion of drugs in the following order: 100 nM DEA/NO, 100 nM ANP, and 100 nM CNP for 2 min each. The region of interest (ROI) for analysis was selected at the soma.

In vivo, DRG neurons are initially bipolar with two axons, one afferent axon projecting into the spinal cord and one efferent axon growing into the periphery (skin, muscles, etc.). Later, the proximal parts of the two axons fuse to form one axon and therefore DRG neurons are called pseudo-unipolar cells. Beside this, DRG neurons are special in that they do not have dendrites [81]. However, *in vitro* cultures of dissociated DRGs display unipolar, bipolar and even sometimes multipolar morphology. This is due to the differences between the two-dimensional *in vitro* culture and the *in vivo* situation. Apart from neurons, DRGs contain also non-neuronal cells (glia and cells from the vasculature). In contrast to post-mitotic neurons, these cells are still dividing. Therefore, anti-mitotic supplements are often used in long-term cultures of DRGs to prevent the non-neuronal cells from overgrowing the neurons. We have seen neurite outgrowth

within 2 hours. In 4 hours, the neurons on the coverslips can already be analyzed. In this study, FRET measurements were performed in DRG neurons after overnight culture. During this short period, we hardly found any non-neuronal cells (**Figure 14A and 16**, upper panel). High expression levels of cGi500 were detected throughout the soma, axon and growth cones of embryonic DRG neurons under an epifluorescence microscope (**Figure 14B**). This strong sensor fluorescence enables cGMP FRET imaging in DRG neurons. Superfusion of the cells with DEA/NO (100 nM) or ANP (100 nM) did not cause any detectable elevation of the intracellular cGMP. In contrast, CNP (100 nM) increased cGMP robustly (**Figure 14C**). This suggests that embryonic DRG neurons express the CNP receptor, GC-B, while the ANP receptor, GC-A, and the NO receptor, sGC, are not present in embryonic DRG neurons. This is also in line with previous studies that GC-B is the only protein responsible for cGMP generation in DRG neurons, whereas no sGC or GC-A transcripts have been detected [67].

The next question we asked is how cGMP in embryonic DRG neurons is degraded. PDEs are important components of the cGMP signaling pathway. They hydrolyze cGMP to GMP, and therefore lower intracellular cGMP levels. By applying different PDE inhibitors, it is possible to specify the PDE subtypes in embryonic DRG neurons. To evaluate the augmentation of cGMP transients by PDE inhibitors, CNP was applied for 2 or 3 times to DRG neurons (**Figure 15**). After the first stimulation, cells were incubated with PDE inhibitors for 5 min and then stimulated again with the same concentration of CNP in the presence of the inhibitor. In addition, in some cases a third application of CNP alone was performed after washing away the respective PDE inhibitor. To evaluate the effect of PDE inhibition on cGMP levels in response to CNP, the peak area of each cGMP transient was taken as a measure and all areas were normalized to the area of the first peak. IBMX is a non-specific PDE inhibitor. Preincubation with 100 µM IBMX significantly potentiated CNP-induced cGMP signals in DRG neurons (**Figure 15A**). Then we started to investigate which PDE subtypes are critical for degradation of CNP-derived cGMP. In the presence of the PDE1 inhibitor vinpocetine, cGMP elicited responses ~3 times larger compared to the stimulation without inhibitors. Inhibition of PDE2 with EHNA led to a ~4-fold cGMP increase of that caused by CNP alone. Similarly, another specific PDE2 inhibitor, Bay 60-7550, potentiated cGMP signals by ~4 fold. In contrast, inhibition of PDE3, 5, and other PDEs by milrinone, sildenafil and zaprinast, respectively, did not significantly change the CNP-induced cGMP transients in comparison to the control stimulations (**Figure 15**). We therefore conclude that PDE1 and PDE2 but not PDE5 or other PDEs catalyze the hydrolysis of cGMP in embryonic DRG neurons.
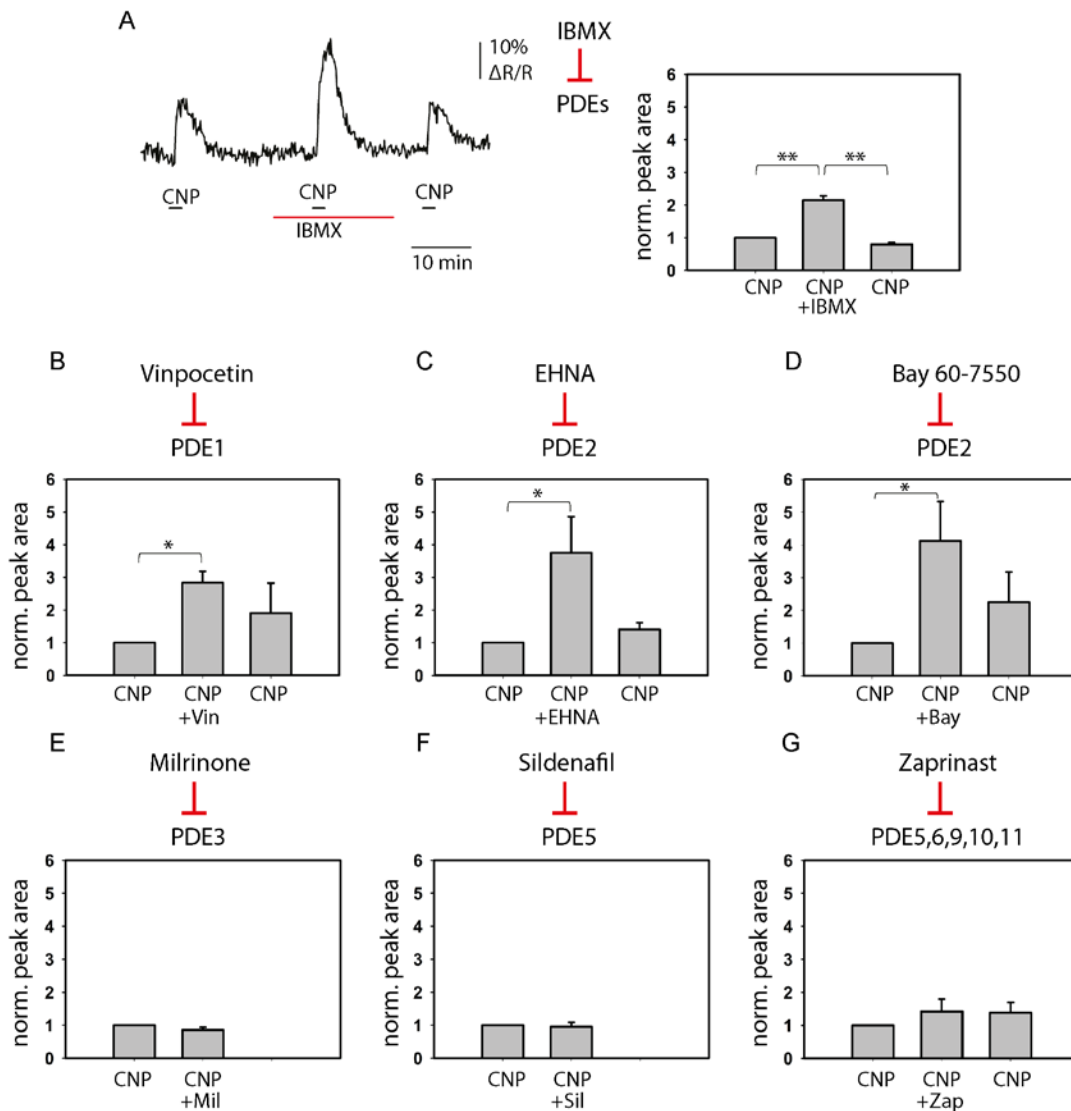
Figure 15. PDE1 and PDE2 are mainly responsible for CNP-derived cGMP degradation in embryonic DRG neurons.

A. PDE inhibition with IBMX potentiates the CNP-induced cGMP responses. Cells were first superfused with 100 nM CNP, and once again in the presence of the PDE inhibitor IBMX. After washing, a third application of CNP was performed. ROIs for analysis were selected at the soma. A summary of CNP-induced cGMP signals before, during and after incubation with IBMX is shown in the bar chart. Peak areas were evaluated and taken as a measure of the cGMP response and normalized to the first peak of each experiment. **B-G**. Similar experiments were performed with different inhibitors: IBMX, 100 µM; Vinpocetine, 5 µM; EHNA, 10 µM; Bay 60-7550, 10 nM; Milrinone, 10 µM; Sildenafil, 20 µM; Zaprinast, 20 µM. ****p<0.01, *p<0.05, n=3 cells from 3 independent measurements.

To ask the question what other signaling components are involved in CNP-derived cGMP signaling in embryonic DRG neurons, immunostaining was performed to detect the important cGMP downstream effector, cGKI. Indeed, cGKI was detcted in the soma, axons and growth cones of embryonic DRG neurons (**Figure 16**, upper panel). The growth cones were strongly labelled, indicating the importance of the cGMP signaling pathway in this compartment. The expression of cGKI is also in line with the *in vivo*

situation, in which cGMP should get elevated firstly in the growth cones, when the DRG sensory axons approach to the DREZ and get exposed to CNP locally. cGKI was also expressed in adult DRG neurons (**Figure 16**, middle panel).
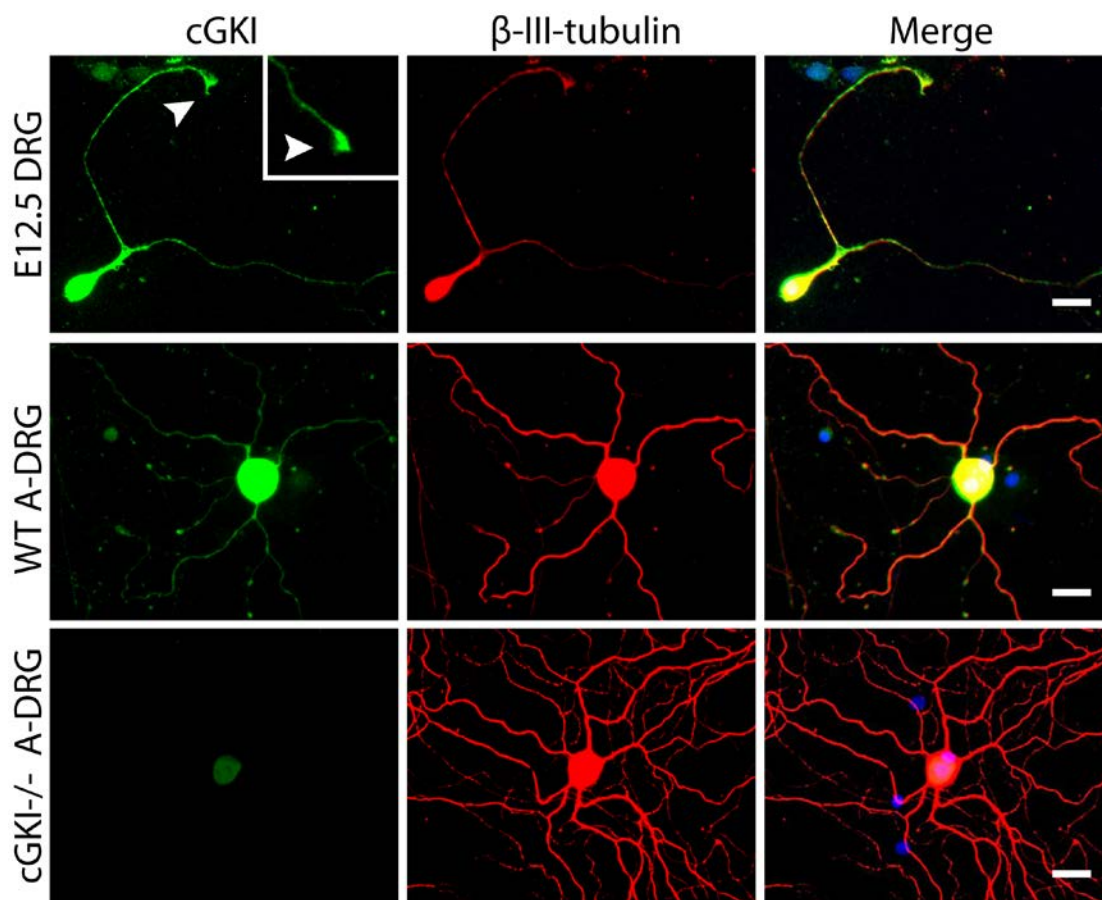
Figure 16. Expression of cGKI in DRG neurons.

Wild type E12.5 DRG neurons (upper panel) were cultured overnight and stained for cGKI (green), β-III-tubulin (red), and with Hoechst 33258 (blue). The same antibodies were used for staining of adult DRG neurons from wild type (WT) or cGKI deficient (-/-) mice cultured for 48 h (middle and lower panel). The inset in the upper left picture shows another tip of the same neuron. Arrowheads indicate the growth cones. β-III-tubulin was used as a marker for neurons. Scale bars, 20 μm.

In order to mimic the *in vivo* situation of embryonic DRG neuron development, CNP was locally applied to the growth cones with a glass pipette, while cGMP levels were monitored by FRET measurements. In one experiment, E12.5 DRG neurons from R26-CAG-cGi500(L1) mice were isolated and cultured overnight (**Figure 17A**). A fine glass pipette with 10 μm bore width was orientated at a 45° angle to the axon and positioned ~50 μm away from the growth cone. The reagent ejected from the pipette was removed immediately by superfusion with Tyrode imaging buffer in the same direction. The pipette was pre-loaded with 1 μM CNP and ejected by an air pulse of 20 hPa for 20 s, resulting in cGMP transients only in the axonal tip but not in the soma (**Figure 17B**). As the pressure or pulse duration increases, the reagents ejected from the pipette

spread over to a larger area [193, 194]. At 20 hPa for 30 s, cGMP production was also detected in the soma. Therefore, by finely orientating the glass pipette and adjusting the air pulse, we were able to achieve the local delivery of CNP to a subcellular region like the growth cone. In another FRET measurement, embryonic DRG neurons were isolated from R26-CAG-mcGi500(L1) mice expressing a version of cGi500 targeted to the plasma membrane (Thunemann et al., unpublished results). The DRG neurons with plasma membrane-targeted cGi500 exhibited reduced differences in fluorescence intensity between the soma, axons and growth cones (**Figure 17C**), and allowed for monitoring of cGMP in these compartments with less noise. A glass pipette loaded with 150 nM CNP was firstly positioned at the growth cone. Applications of CNP at 20 hPa for 20 s reproducibly resulted in cGMP transients at the growth cone (ROI7) but not at the soma (ROI1) or the proximate part of the axon (ROI3) (**Figure 17C and D**). Local elevation of cGMP in the growth cone reveals the local distribution of the cGMP production machinery in the growth cone. Subsequent global bath application of 100 nM CNP led to a global increase of cGMP among the whole DRG neuron including the soma, the axon and the growth cone. The glass pipette was further moved towards the soma. Application at the soma increased cGMP at the soma, but also at the axon and slightly at the growth cone (**Figure 17C and D**). This may be because the CNP application was not confined to the soma, as CNP might flow over to the downstream growth cone. Note that the flow directions of pipette ejection and superfusion were opposite to each other in this experiment. Another possibility was that the cGMP generated at the soma could be immediately transported along the axon down toward the growth cone. Further investigation is needed to unravel this question. Visualization of local or global cGMP elevation is also illustrated in **Figure 17E, F, and G**.

Figure 17. Generation of cGMP in the growth cone independently of the soma.

A, B. Local application of drugs can be achieved by a glass pipette positioned at the tip of a DRG neuron (R26-CAG-cGi500(L1)). 1 μM CNP was ejected at 20 hPa for 20 s or 30 s by the pipette. Tyrode imaging buffer was superfused to remove the drug immediately, as indicated with "flow". ROIs were outlined as shown in **A** and evaluated for cGMP signals. Only the axon close to the pipette but not the soma responded to CNP applied for 20 s, and cGMP increased in the whole DRG neuron including the soma and axon after longer application, for 30 s. **C, D**. A DRG neuron from R26-CAG-mcGi500(L1) mice with a clear soma and growth cone was chosen for FRET imaging. ROIs as outlined in **C** were evaluated for cGMP responses. 150 nM CNP was applied with a glass pipette positioned first at the growth cone (position 1) and later at the soma (position 2). The signal shift due to the movement of the pipette from position 1 to 2 is indicated by asterisks. The red bars 1), 2), 4) indicate the local application at the growth cone, and 5), 6), 7) at the soma, and the bar 3) indicates global bath application of 100 nM CNP for 2 min. Local application of 150 nM CNP resulted in cGMP increase at the region of growth cone but not at the soma and the proximate part of the axon. Shown are also the CFP/YFP emission ratio (F_{480}/F_{535}) images representative of cGMP levels at different time points (indicated in **D**), before and after drug application locally at the growth cone (**E**), globally (**F**), and at the soma (**G**). Scale bars, 20 μm.

A

B

10%
ΔR/R

ROI 1

ROI 2

ROI 3

glass pipette

flow

Soma, ROI 1

Axon, ROI 3

20 s   20 s   30 s   30 s

2 min

C

D

① Pipette at the growth cone   ② pipette at the soma

②

ROI 1
soma

ROI 3
axon

①

ROI 7
growth cone

flow

10%
ΔR/R

Soma, ROI 1

10%
ΔR/R

Axon, ROI 3

5%
ΔR/R

Growth cone,
ROI 7

1)   2)   3)   4)   5)   6)   7)

global appl.   10 min

E   Local appl. at
growth cone / axon

t₀   t₁

F   Global appl.

t₂   t₃

G   Appl. at soma

t₄   t₅

②

①
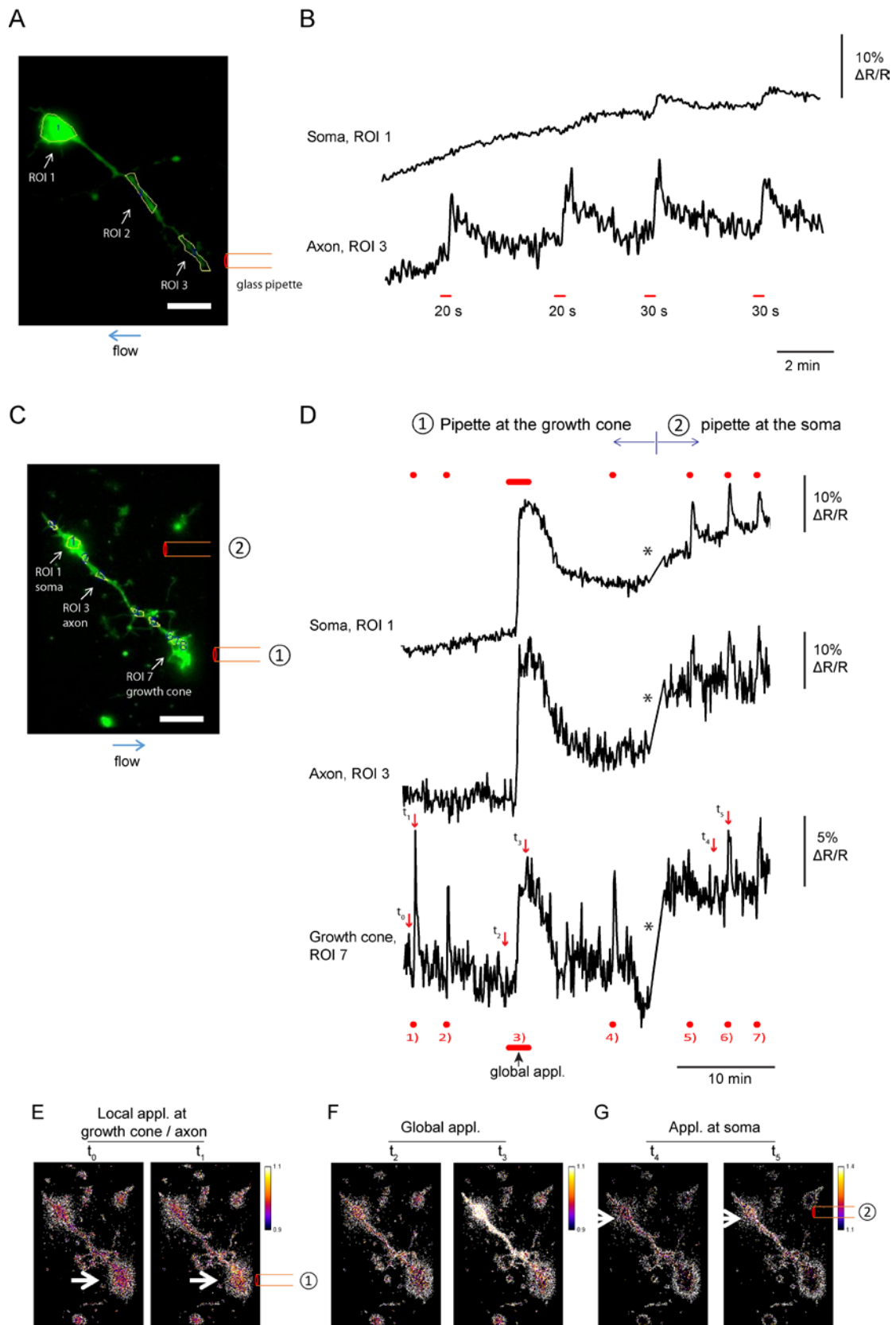
Since sensory neurons are able to sense mechanical force, one question arising from the drug application with air pressure was whether the cGMP was elevated due to the pressure. Therefore, we tried similar measurements under the same condition with PBS as controls. However, no cGMP elevations were detected (data not shown). Also, because the pipette was located ≥50 µm away from the cell, the pressure reached there would be much lower than 20 hPa. Moreover, in an effort to test the possible induction of cGMP in response to touch, we also tried to poke the embryonic DRG neurons with glass pipettes. However, we did not detect cGMP changes (data not shown), indicating that mechanical force did not interfere with cGMP FRET imaging in embryonic DRG neurons.

Altogether, with our newly generated cGMP sensor knock-in mice, we were able to monitor cGMP at the subcellular level. In embryonic DRG neurons, cGMP is produced in response to CNP but not to ANP or NO, and degraded mainly by PDE1 and PDE2. Local cGMP can be generated in the growth cone independently of the soma. The GC-B/cGMP/cGKI machinery at the growth cone may be critical for DRG neurons to sense local CNP in the DREZ of the spinal cord and to bifurcate properly.

3.3 cGMP imaging in platelets

3.3.1 Characterization of cGMP signals in platelets

Platelets are 2-3 µm large cell fragments derived from megakaryocytes residing in the bone marrow. As cells lacking a nucleus, platelets have no transcription machinery to generate mRNA, but can still control protein translation and other cellular processes [92]. We first checked whether cGi500 is expressed in platelets of R26-CAG-cGi500(L1) mice. Whole blood was perfused through a flow chamber attached to a collagen-coated coverslip. Strong sensor fluorescence was observed in single platelets during perfusion and was even more obvious in aggregated thrombi formed on collagen (**Figure 18A**). In contrast, another type of anucleate cells in the blood, the erythrocytes appeared to be negative for cGi500 as fluorescent erythrocytes were not observed during whole blood perfusion (data not shown). The difference may be due to the different lifespans of the two cell types. Billions of platelets circulate in mammalian blood to prevent blood loss in case of tissue injury. The lifespan of platelets is short, 4-6 days in mice and 5-9 days in humans [195, 196], which means several million platelets have to be produced every hour to maintain their physiological counts to fulfill their function. The GFP protein was found to be stable with a half-life of ~1 day [197, 198], and the half-life of engineered proteins like cGi500 is presumably similar. In contrast, mature erythrocytes are anucleate cells with a life span of 40-60 days in mice [199], during which time the sensor protein is probably degraded. Reporter expression in mature erythrocytes has not been reported in other Rosa26 mouse lines either [200].

The strong cGi500 expression in platelets enables cGMP FRET measurement in these cells. FRET imaging of adherent platelets showed that the natriuretic peptides, ANP and CNP did not stimulate cGMP production (**Figure 18B**). Instead, a cGMP elevation was seen in response to DEA/NO. This indicates that only the cytosolic sGC rather than membrane-bound pGCs (GC-A and GC-B) is present in murine platelets and in charge of cGMP production. A response was observed upon application of as low as 10 nM DEA/NO (**Figure 18C**), which releases NO at 20°C, pH 7.4 presumably at a concentration in the physiological range [21]. To characterize the PDE subtypes that are responsible for cGMP degradation in platelets, subtype-specific PDE inhibitors were applied. Preincubation with the PDE2, PDE3, and PDE5 inhibitors, Bay 60-7550, milrinone, and tadalafil alone, respectively, already led to a small cGMP increase and they further potentiated NO-induced cGMP signals (**Figure 18D**). These data support

previous knowledge about the cGMP signaling system in platelets that cGMP is synthesized by sGC and degraded by PDE2, PDE3 and PDE5 [101].
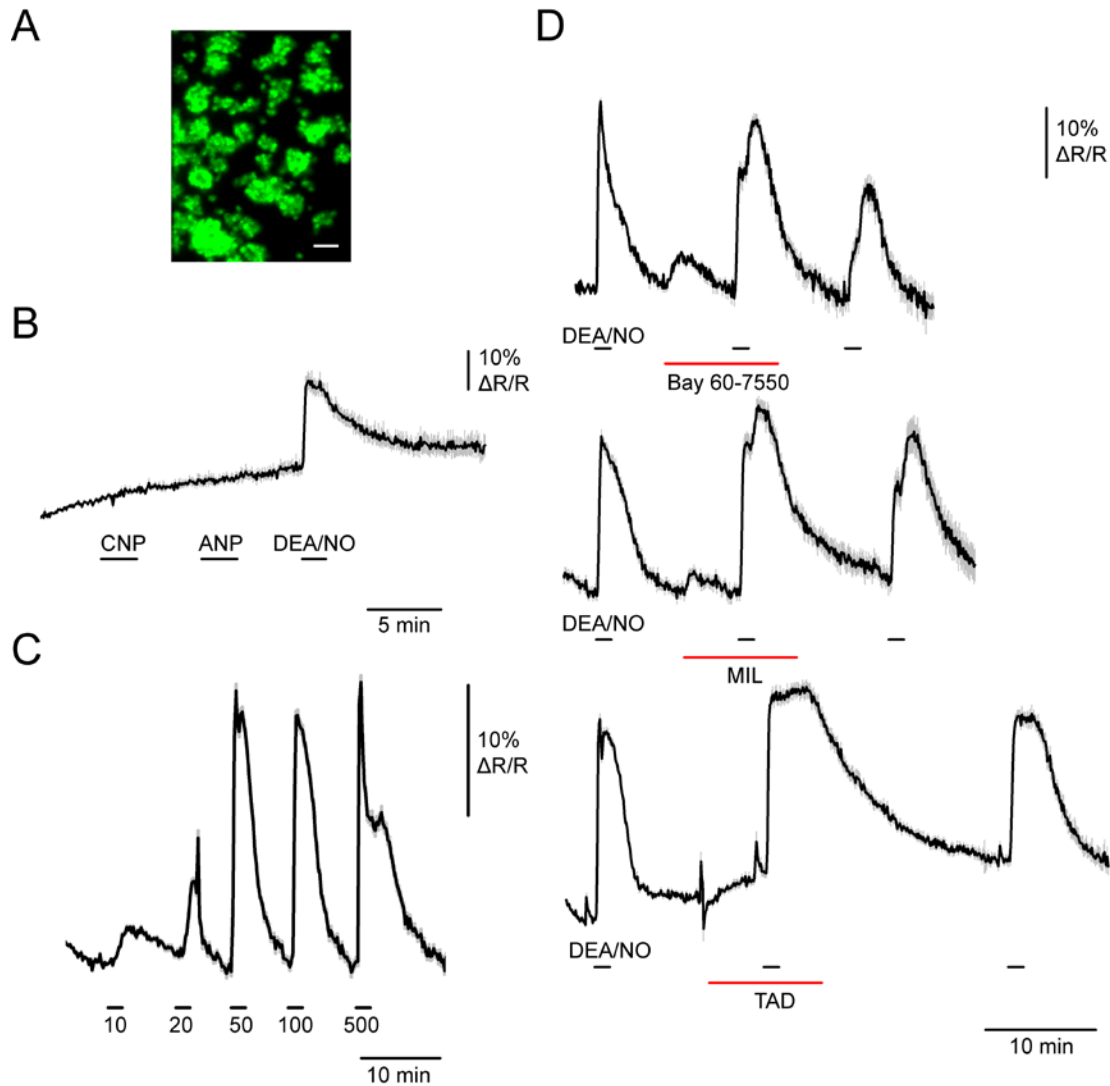

Figure 18. Characterization of platelet cGMP signals.

A. Whole blood from R26-CAG-cGi500(L1) was perfused over a flow chamber at 15 mL/h (corresponding to a shear rate of ~500 s^{-1}) for 10 min resulting in thrombus formation on a collagen-coated coverslip. Sensor fluorescence was detected with a YFP filter set. Scale bar, 10 µm. **B**. cGMP FRET imaging was performed with platelet thrombi on the collagen surface as shown in **A**. A representative recording out of three experiments is shown. Superfusion with DEA/NO led to a reversible cGMP increase in adhered platelets. Superfusion was performed in the following order: 100 nM CNP, 100 nM ANP for 2.5 min each and 100 nM DEA/NO for 1.5 min. **C**. DEA/NO concentration-response experiments; original recordings are shown upon stimulation for 1.5 min with increasing concentrations of DEA/NO (in nM). **D**. PDE inhibition with 10 nM Bay 60-7550, 10 µM milrinone (MIL), or 5 µM tadalafil (TAD) potentiates NO-induced cGMP responses. Cells were superfused with 100 nM DEA/NO for 1.5 min before, during, and after incubation with the respective inhibitor. All FRET data shown are mean ± SEM (n≥8 thrombi).

3.3.2 Flow-regulated cGMP signaling

Strikingly, it was found that NO-induced cGMP production in activated platelets was dependent on fluid flow (**Figure 19**). Superfusing Tyrode buffer containing DEA/NO to platelet thrombi formed on a collagen surface led to cGMP elevation due to sGC stimulation by NO. Continuous application of DEA/NO at 15 mL/h led to sustained cGMP elevation from the basal level to a new plateau. However, upon switching off the fluid flow to zero, cGMP immediately decreased although DEA/NO was still present. The cGMP decrease in platelets started within 2-5 s, and came down to baseline within ~30 s. In the presence of DEA/NO, initiation and cessation of flow ('flow on and off') lead to cGMP increase and decrease, respectively (**Figure 19**).
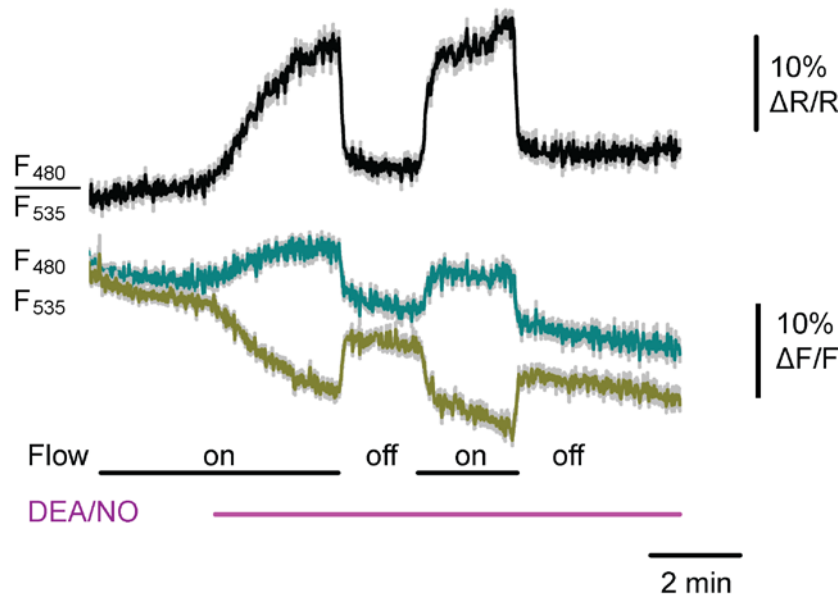

Figure 19. NO-induced cGMP signals are regulated by flow in platelets.

Thrombi were formed on a collagen-coated coverslip mounted to a flow chamber by perfusion with whole blood from R26-CAG-cGi500(L1) mice. cGMP imaging showed that application of 1 µM DEA/NO at 15 mL/h led to cGMP increase in platelets. Flow switch-off to 0 mL/h resulted in a rapid decrease of cGMP to baseline. Cyan, yellow, and black traces indicate CFP emission (F_{480}), YFP emission (F_{535}), and CFP/YFP emission ratio (F_{480}/F_{535}), respectively. Emission fluorescence intensities and ratios were normalized to averaged baseline signals and are given as $\Delta F/F$ and $\Delta R/R$, respectively. Data shown are mean ± SEM; n=11 thrombi. One representative experiment out of 5 experiments is shown. The average decay time of cGMP levels upon flow off of 5 experiments was 28.3 ± 4.8 s.

Further experiments confirmed that the NO-induced cGMP signals were dependent on the flow rate (**Figure 20**). In the presence of DEA/NO, the higher flow rate (45 mL/h) resulted in a higher level of cGMP increase (~15% $\Delta R/R$). When flow is decreased by 9 times from 45 mL/h to 5 mL/h, cGMP signals decreased by ~5%. Further cessation of the flow to zero caused an additional cGMP decrease by 10% to basal levels. This whole flow titration was inversely reproducible, meaning increasing flow rates resulted in corresponding cGMP increases (**Figure 20**).
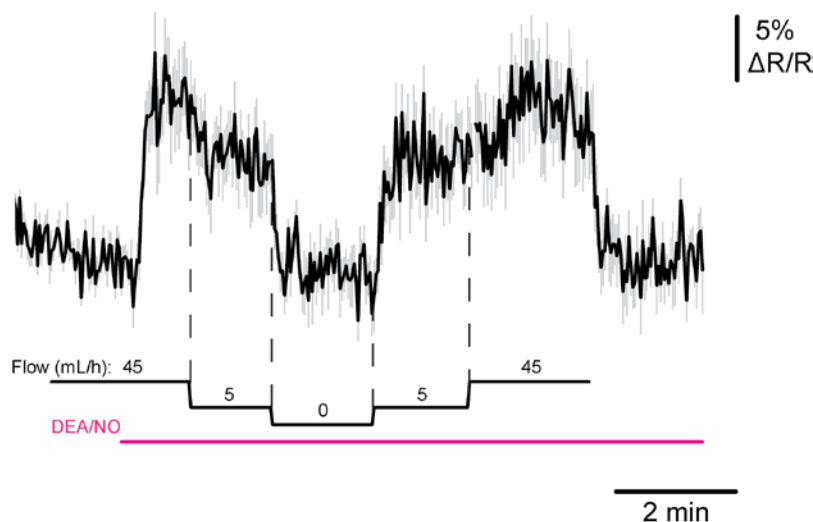
Figure 20. NO-induced cGMP is regulated in a flow rate-dependent manner.

Platelet thrombi on a collagen surface were superfused with 1 µM DEA/NO. The platelets were subsequently subjected to superfusion at a changing rate of 45, 5, 0, 5, 45 mL/h in series. Data shown are mean ± SEM; n=5 thrombi.

Next, the effect of flow in the absence of NO on cGMP levels was examined. Flow off did not cause a change of basal cGMP levels, and cGMP stayed at basal levels after subsequent onset of flow (**Figure 21**). cGMP increased only after superfusing the cells with NO. In contrast, cGMP dropped from the NO-induced plateau after switching off the flow. Interestingly, washout of DEA/NO caused a more delayed cGMP decrease to baseline (~4 min), as compared to that caused by the cessation of flow (~30 s). The slow decay of cGMP is generally observed in all experiments performed with DEA/NO washout (e.g., **Figure 18B, C and D**).
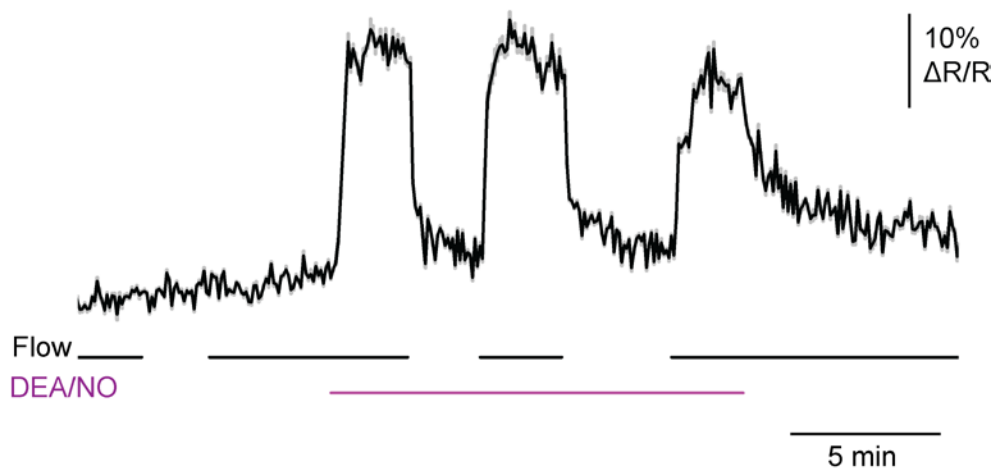
Figure 21. No effect of flow alone on intracellular cGMP levels.

Platelet thrombi on a collagen surface were subjected to flow on and off in the absence or presence of 100 nM DEA/NO. DEA/NO was washed out at the end of the experiment. Data shown are mean ± SEM; n=10 thrombi. One representative experiment out of 10 is shown. The average decay time of cGMP levels upon flow off and upon washout of 5 experiments was 28.3 ± 4.8 s, and 4.4 ± 0.36 min, respectively.

To test if the flow-regulated cGMP relies on flow and NO, rather than the NO-releasing compound itself or its byproducts, different NO donors with distinct half-lives were used for stimulation (**Figure 22**). The NONOates have widely varying half-lives (1.8 s to 20 h). For example, DEA NONOate (DEA/NO) dissociates in a pH-dependent, first-order process to liberate 2 moles of NO per mole of parent compound with a half-life of 2 min and 16 min at 37°C and 22-25°C, pH 7.4, respectively; Spermine NONOate (SPER/NO) has a half-life of 39 minutes and 230 minutes at 37°C and 22-25°C, pH 7.4, respectively; another NO donor, DETA NONOate (DETA/NO), has a half-life of 20 h and 56 h at 37°C and 22-25°C, pH 7.4, respectively [201, 202]. The shorter the half-life of the donor, the shorter it took to stimulate cGMP production, with the sharpest cGMP response to DEA/NO and the slowest to DETA/NO (**Figure 22**). cGMP decreased to baseline upon decrease of flow to zero in the presence of either of the three NO donors, and switching on and off the flow led to cGMP increases and decreases.
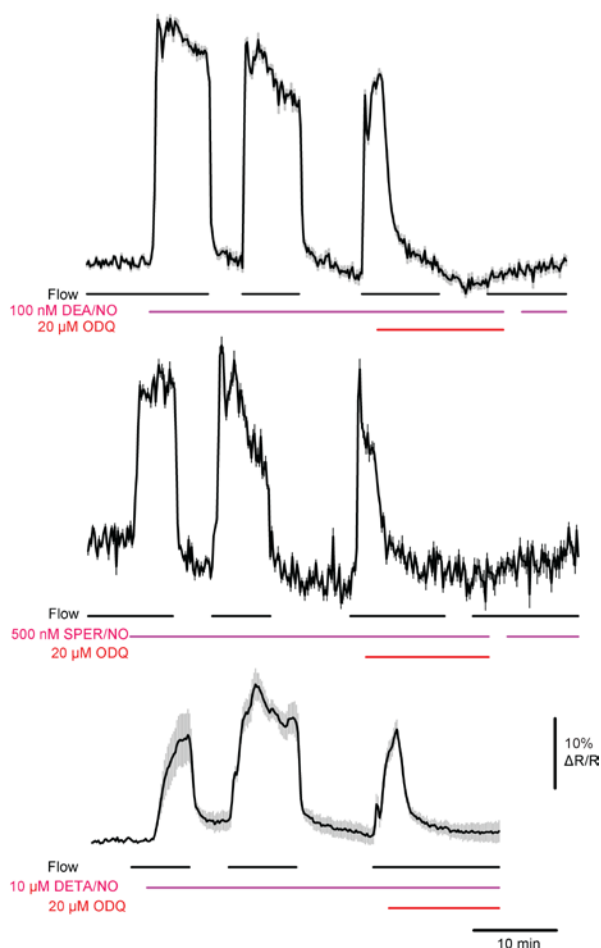
Figure 22. sGC is responsible for cGMP generation in response to NO in platelets.

Platelet thrombi on a collagen surface were used for cGMP imaging. Superfusion of cells at a flow rate of 15 mL/h with different NO donors (100 nM DEA/NO, 500 nM SPER/NO, and 10 µM DETA/NO) resulted in cGMP elevations. Flow switch-on (15 mL/h) and -off (0 mL/h) were performed. At the end of each experiment, 20 µM ODQ was applied in the presence of the respective NO donor with continuous flow. Data shown are mean ± SEM (n≥8 thrombi). Representative results from 3 independent experiments are shown.

To further confirm that the FRET signals were caused by cGMP generation catalyzed by NO-stimulated sGC, ODQ was used to block sGC. ODQ oxidizes the sGC heme iron from Fe^{2+} to Fe^{3+}, resulting in irreversible inactivation of sGC [25]. As expected, application of 20 µM ODQ eliminated cGMP generation completely (**Figure 22**). Even after washout of ODQ, application of NO donors could not increase cGMP production any more. Thus, the NO-induced cGMP FRET change was NO- and sGC-dependent. Intriguingly, the cGMP decreasing kinetics induced by flow off and that by ODQ were very similar (**Figure 22**). For example, the decay time of DEA/NO-induced cGMP after application of ODQ was ~40 s, which was comparable to that caused by flow off (~30 s), implying that sGC might be desensitized after flow off.

Not only NO, but also several synthetic compounds can activate sGC. To test whether the flow-regulated cGMP decrease could also be observed with a NO-independent stimulator of sGC, Bay 41-2272 was applied in similar 'flow on and off' experiments (**Figure 23A**). 1 µM Bay 41-2272 resulted in a much slower increase of cGMP levels compared to DEA/NO, and increase of the concentration of the stimulator to 5 µM caused a faster increase of cGMP. However, cessation of flow resulted in an attenuated decrease (~30%) of peak cGMP in a much delayed time (~3 min) as compared to the decrease of NO-induce cGMP by flow switch-off (~30 s). Switching on and off the flow resulted in reproducible partial increases and decreases of cGMP levels. Removal of Bay 41-2272 by washout with Tyrode buffer without a change in the flow rate resulted in a relatively slow (5-10 min) return of cGMP to basal levels (**Figure 23A**).

The next question we asked was whether sGC or PDEs are regulated by the flow. In theory, the decrease of cGMP can be due to desensitization of sGC and/or activation of PDEs. However, if PDEs were the only ones regulated by flow, then the decrease of Bay 41-2272-induced cGMP upon flow switch-off should have been complete, i.e. to the basal level. Therefore, sGC should be at least partially responsible for the regulation of cGMP by flow. To further elucidate whether cGMP generation or degradation is regulated by flow, we utilized another cGMP-generating cell type, VSMCs, in which cGMP can be produced by both sGC in response to NO as well as pGC in response to ANP and CNP [178], and CNP-induced cGMP can also be degraded by PDE5 (**Figure 23B**). Similar to platelets, delivery of 100 nM DEA/NO to VSMCs resulted in fast cGMP generation, and cGMP decreased after flow switch-off (**Figure 23C**). The decrease from peak cGMP level to baseline took ~2 min, a slower decreasing rate compared to that of NO-induced cGMP in response to flow off (~30 s).

Therefore, NO-induced cGMP signals in VSMCs were also regulated by flow. In contrast, CNP-induced cGMP was not affected by flow switch-off (**Figure 23C**). Considering that PDE5 is involved in degradation of CNP-induced cGMP signals (**Figure 23B**), the lack of a flow effect on CNP-induced cGMP suggests that the cGMP-degrading PDE5 is not responsible for the flow-induced effect. Together with the fact of partial regulation of Bay 41-2272-induced cGMP by flow, these lines of evidence point to sGC as the most likely molecule regulated by flow.
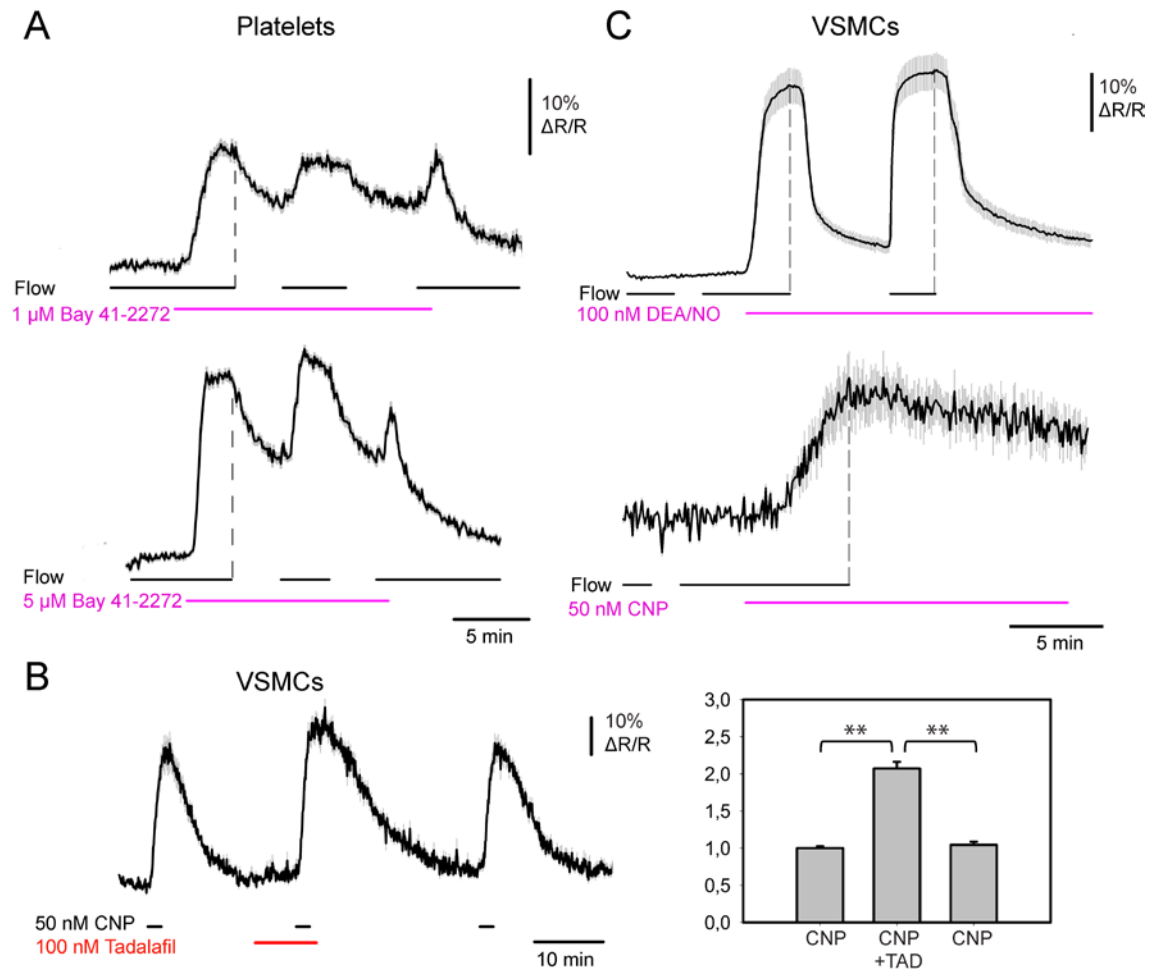
Figure 23. sGC activity is regulated by flow.

A. Bay 41-2272-induced cGMP is regulated by flow. Platelets were superfused with the sGC activator Bay 41-2272 (1 µM or 5 µM) at a rate of 15 mL/h and subjected to flow on and off, and washout. **B**. PDE5 inhibition with tadalafil potentiated the CNP-induced cGMP response in VSMCs. Primary VSMCs were cultured on a coverslip for 7 days and mounted onto the flow chamber and used for cGMP imaging. Cells were first superfused with 50 nM CNP for 2 min, and once again in the presence of the PDE5 inhibitor, tadalafil. After washout, a third application of CNP was performed. A summary of CNP-induced cGMP signals before, during and after incubation with tadalafil is shown in the bar chart. Peak areas were evaluated and taken as a measure of cGMP response and normalized to the first peak. **C**. DEA/NO-induced cGMP signals in VSMCs were regulated by flow, but CNP-induced cGMP was not changed upon flow switch-off. Cells were superfused with Tyrode buffer and later with 100 nM DEA/NO. Data shown are mean ± SEM (n≥ 7 thrombi or 5 VSMCs). **$p<0.01$.

Ca^{2+} is a procoagulant factor in platelets [203]. To assess the physiological relevance of the rapid increase and decrease of the intracellular cGMP concentration in response to flow, the intracellular Ca^{2+} level was also probed. CFP, YFP and Fura-2 have distinct absorption spectra, which allows simultaneous measurement of cytoplasmic Ca^{2+} and cGMP with cGi500-expressing platelets from R26-CAG-cGi500(L1) mice. Simultaneous measurement of cytoplasmic Ca^{2+} and cGMP was performed by loading the thrombi from R26-CAG-cGi500(L1) mice with Fura-2, AM.

As shown before, stimulation of platelets with DEA/NO increased intracellular cGMP, whereas a decrease of flow led to a decrease of cGMP (**Figure 24A and B**). Interestingly, Ca^{2+} signals went opposite of cGMP signals; basal Ca^{2+} levels in the thrombi were comparably high, and DEA/NO application led to a decrease of Ca^{2+}, whereas flow off resulted in Ca^{2+} restoration to the basal level. In both situations, i.e. flow on-induced cGMP increase and flow off-regulated cGMP decrease, cGMP signals preceded Ca^{2+} signals (**Figure 24C**). cGMP signals arised earlier and reached their plateau ~5 seconds earlier than Ca^{2+} signals, and the same was observed for the cGMP decrease upon flow off. Thus, cGMP signaling is an earlier event than Ca^{2+} signaling. Previous studies in knock-out mice have shown that activation of cGKI by NO donors or membrane-permeable cGMP analogs leads to phosphorylation of downstream IP_3 receptor-associated cGKI substrate IRAG protein, which strongly inhibits agonist-evoked Ca^{2+} mobilization from intracellular stores in platelets [98]. Although the NO/cGMP signaling pathway has been demonstrated to attenuate agonist-induced Ca^{2+} release [98, 204-206], the present study shows a direct decrease of Ca^{2+} by NO in the presence of flow. Simultaneous visualization of cGMP and Ca^{2+} revealed that cGMP precedes Ca^{2+} signals, which, coupled with previous findings by others [98, 204-207], further confirms that cGMP inhibits intracellular Ca^{2+} mobilization.
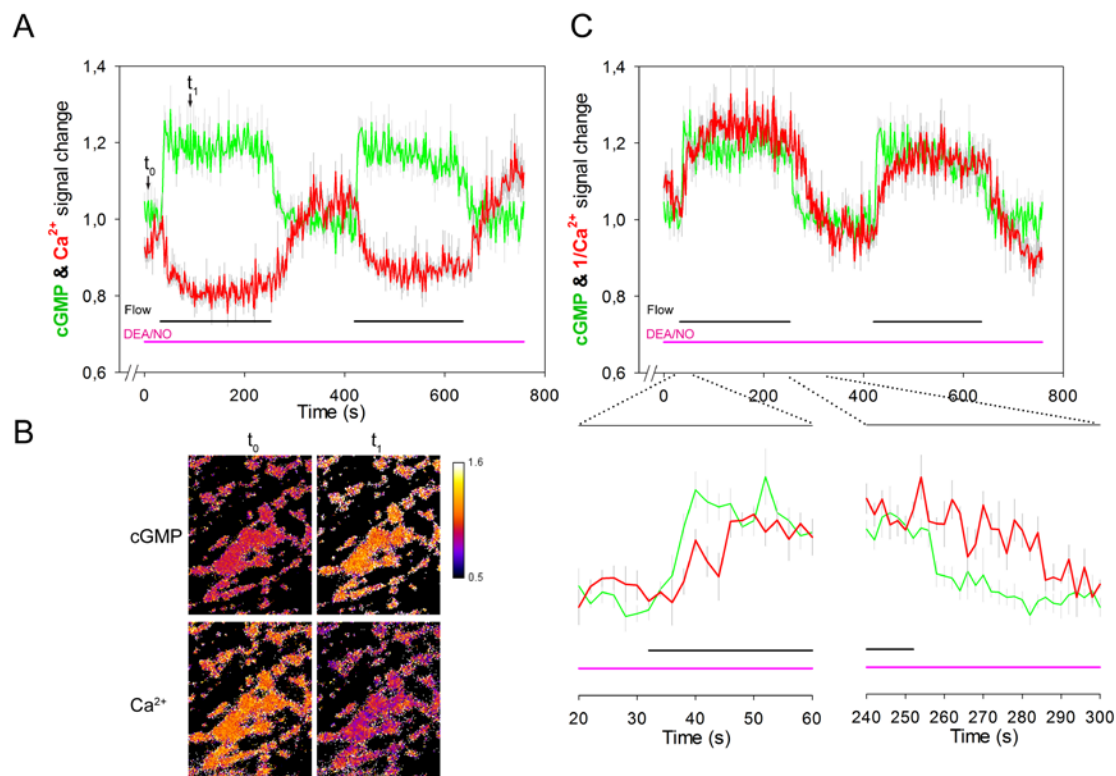
Figure 24. Changes of cGMP signals precede changes of Ca^{2+} signals.

A. Whole blood from Rosa26-CAG-cGi500(L1) mice flowed over a collagen-coated coverslip mounted on a flow chamber and the aggregated thrombi were subsequently loaded with Fura-2, AM. Simultaneous measurement of cGMP (green trace) and Ca^{2+} (red trace) showed the effect of flow on and off on cGMP and Ca^{2+} in the presence of 1 µM DEA/NO. Switching on flow leads to an increase of cGMP and a decrease of Ca^{2+}. **B**. Shown are ratio images of platelets at different times indicated in **A**. cGMP was at the basal level at the time point t_0, while Ca^{2+} was at its peak. Flow-induced cGMP increase and Ca^{2+} decrease in the presence of NO (as shown at t_1). **C**. The same recordings from **A** were shown with cGMP (green) and inverse Ca^{2+} signals (red). R=F$_{480}$/F$_{535}$ were taken as a measure for the cGMP concentration, and R=F$_{340}$/F$_{380}$ as a measure for Ca^{2+}. Ratios for both cGMP and Ca^{2+} were normalized to averaged baseline signals and are given as ΔR/R. Data are shown as mean ± SEM; n=8 thrombi. Results are representative of three independent experiments.

In an effort to search for mediators for flow-regulated cGMP signaling, we tested the roles of several mechanotranducers that have been implicated either in shear stress detection and/or cGMP production. Glycoprotein (GP) Ibα is a platelet membrane receptor for vWF [92]. Platelet activation and adhesion under elevated shear stress requires the binding of vWF to GPIbα [94]. Another main binding site for vWF is the integrin α$_{IIb}$β$_3$ [208]. It is believed that the function of vWF is mainly mediated by its platelet receptor GPIbα [209]. Interaction of vWF/GPIbα induces cGMP elevation, and several groups detected a cGMP increase in response to vWF [104, 210, 211]. Du and colleagues suggested that vWF promotes cGMP through the activation of eNOS and endogenous NO production in platelets elicited by the interaction of vWF and GPIb [94]. Walter et al. did not detect eNOS and found eNOS-independent generation of

cGMP by Src kinase-mediated Tyr^{192} phosphorylation and activation of sGC when platelets were treated with vWF/ristocetin [101, 210].

To determine if GPIbα is mediating flow-regulated cGMP signals in platelets, we evaluated cGMP regulation by flow in IL4Rα/GPIbα-tg mice (kindly provided by Dr. H. Langer), in which the extracellular domain of GPIbα was replaced by that of the human IL-4 receptor [212, 213]. Indirect cGMP imaging was performed by measuring intracellular Ca^{2+} with Fura-2, based on the previous result that Ca^{2+} is a downstream effector of cGMP (**Figure 24**). Ca^{2+} measurements were performed in platelets from IL4Rα/GPIbα-tg mice and wild type controls, respectively (**Figure 25A**). However, flow on and off-induced Ca^{2+} decreases and increases in the presence of DEA/NO showed similar kinetics in both transgenic mice and wild type controls, suggesting that flow-regulated cGMP signals were not affected by GPIbα. Of interest is also that activated platelets showed robust spontaneous Ca^{2+} mobilization. In the presence of NO, flow on not only decreased Ca^{2+} but also inhibited Ca^{2+} mobilization. Flow *per se* did not significantly affect the basal cytoplasmic Ca^{2+} concentration (**Figure 25A**).

Multiple ion channels have been suggested as mechanotransducers or molecular components of a mechanotransduction complex [214]. Transient receptor potential (TRP) channels are a group of ion channels mostly present on the plasma membrane of various eukaryotic cells, which can sense taste, hotness, coldness, and shear stress [215]. These ion channels are non-selectively permeable to cations including Ca^{2+}, Na^+ and Mg^{2+}. In a preliminary screening for the possible involvement of different ion channels, one member of the TRP channel family, TRPC3 was implied to be involved in flow-regulated cGMP signaling (**Figure 25B**). Pyr3 is a pyrazole compound that potently and selectively antagonizes TRPC3 by binding to the extracellular side of the receptor [216]. Pyr3 was applied to thrombi from R26-CAG-cGi500(L1) sensor mice. In the absence of TRPC3 inhibitor, cGMP peaked rapidly in the continuous presence of DEA/NO and returned to basal levels upon flow off. Flow on and off resulted in fast increases and decreases of cGMP. However, preincubation with 1 µM Pyr3 led to a slower increase of cGMP in response to DEA/NO, while the flow off-induced cGMP drop was not significantly affected. Fluid flow might sensitize sGC through TRPC3 activation, whereas inhibition of TRPC3 by Pyr3 should attenuate the increase of cGMP in response to NO. Therefore, these data suggest TRPC3 as a mechano-transducer in flow-regulated cGMP signaling.
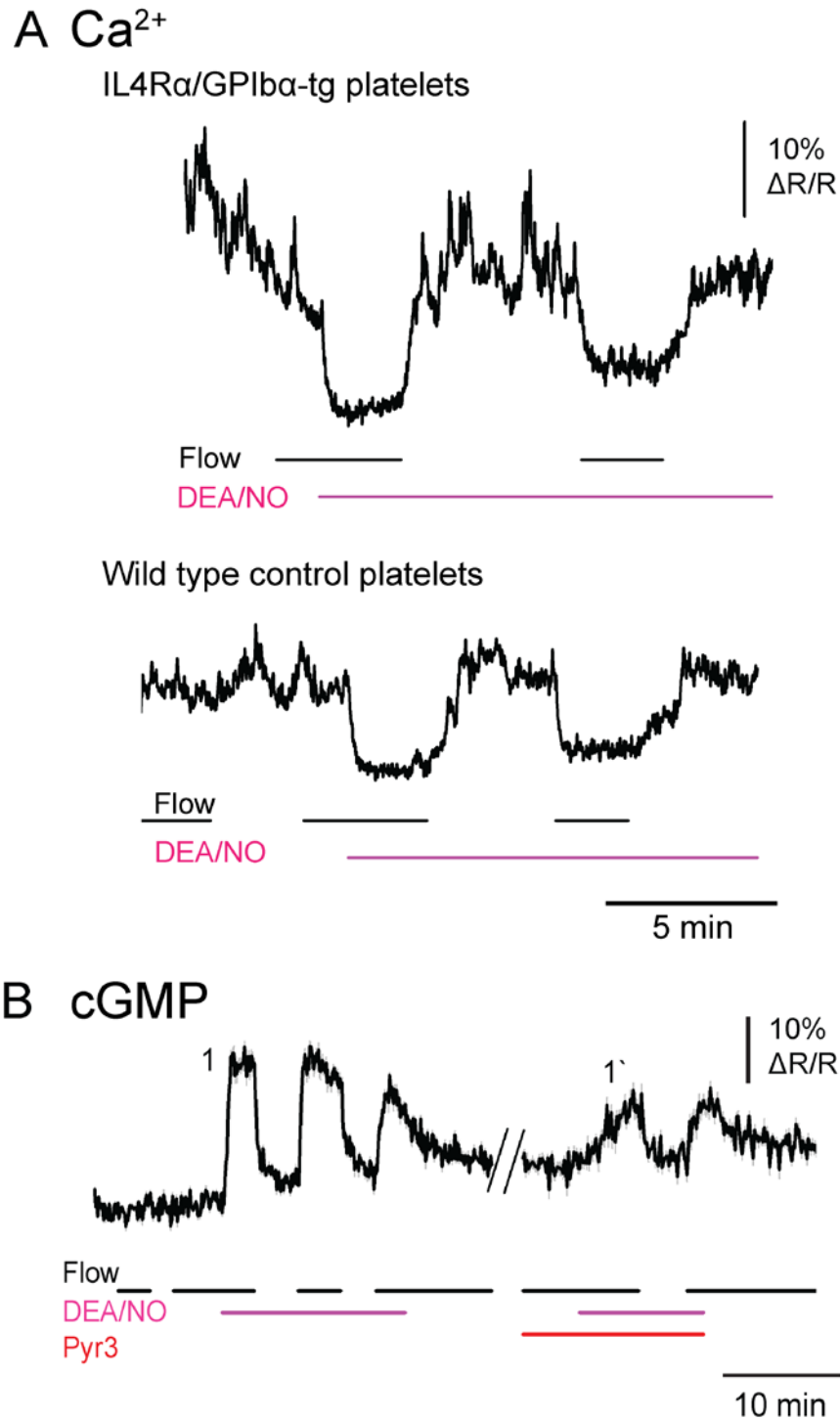
Figure 25. Roles of mechanotransducers in flow-regulated cGMP/Ca^{2+} signals.

A. Effects of GPIbα on flow-regulated cGMP production. Ca^{2+} imaging was performed in Fura-2, AM-loaded platelets from IL4Rα/GPIbα-tg and wild type mice, respectively. Cells were superfused with 100 nM DEA/NO and subjected to flow on and off. Shown are representative traces of a single thrombus from independent experiments with two IL4Rα/GPIbα-tg and three wild type mice, respectively. **B**. TRPC3 inhibition attenuates NO-induced cGMP production. cGMP imaging was performed in platelets from R26-CAG-cGi500(L1) mice. Cells underwent flow on and off in the presence of 100 nM DEA/NO. After removal of DEA/NO, platelets were preincubated with 1 µM Pyr3, and 100 nM DEA/NO was applied subsequently. Data are shown as mean ± SEM; n=7 thrombi. A representative experiment out of three is shown.

4 Discussion

4.1 Generation of cGi500 sensor mice

The present study discloses new cGMP sensor knock-in mouse lines as novel tools for *in vivo* monitoring of cGMP signals in various cell types and tissues with high temporal and spatial resolution. The cGMP sensor mouse lines (R26-CAG-cGi500) were generated by targeted integration of a Cre-activatable cGi500 expression cassette driven by the ubiquitous CAG promoter into the Rosa26 locus. This strategy combines the chromosomal accessibility of Rosa26 locus with the strong and ubiquitous CAG promoter, so that cGi500 could be robustly expressed in a broad range of tissues and cell types.

The random insertion of genetic elements such as a transgene into the mouse genome often leads to the deregulation or misregulation of the expression of endogenous genes. At the same time, the transgene expression pattern may often be restricted by the integration site due to variegation/position effects (e.g., silencing). The unpredictable outcome may result in biased phenotypes. To bypass these limits, we designed knock-in models in which cGi500 was introduced into a well-known permissive locus, the Rosa26 gene locus [166]. With this strategy, we achieved cGi500 sensor expression virtually globally in all tissues (**Figure 10**). On the other hand, it is also important that the expression of the indicator is strong enough so that fluorescence intensity changes can be detected *in vivo*. Note that in our first attempt to generate the sensor knock-in mice, cGi500 was integrated into the endogenous Rosa26 locus (R26-cGi500 mice, data not shown) without the extra CAG promoter, so that cGi500 expression was driven by the endogenous Rosa26 promoter after excision of a STOP cassette by Cre recombinase. However, cGi500 driven by the endogenous Rosa26 promoter exhibited rather low expression levels in adult mice. Nevertheless, FRET measurement in cells isolated from this mouse line can still be achieved, although requiring much longer exposure time to excite the sensor (data not shown).

Strong cGi500 sensor fluorescence was detected in various tissues, including aorta, heart, and brain of R26-CAG-cGi500(L1) mice. Primary cells isolated from these tissues showed strong fluorescence, and cGMP imaging was successfully performed in various cell types, including smooth muscle cells, neurons and platelets. The uniform distribution of cGi500 throughout the cytoplasm enabled detection of robust cGMP signals induced by NO in the cytosol or local cGMP signals induced by natriuretic

peptides presumably near the plasma membrane. cGMP transients have been detected at a concentration as low as 10 nM DEA/NO in platelets, indicating high sensitivity of the cGi500 sensor in response to physiological concentrations of NO stimulation [21]. The maximal FRET change of 40% was observed in both VSMCs and platelets, in line with other studies that were also performed in intact cells, corresponding to a saturating concentration for cGi500 of ≥1-3 µM cGMP [135, 138]. cGMP imaging in embryonic DRG neurons showed high spatial resolution to distinguish signals in the soma, the axon as well as the growth cone, and high temporal resolution of cGMP changes within seconds.

Importantly, the R26-CAG-cGi500(L1) mouse line has also been proved as a powerful tool to study vascular cGMP signals in isolated tissues and live mice; strong and robust cGMP signals in response to DEA/NO were detected in an *in vivo* model of the cremaster muscle. Moreover, using multiphoton FRET microscopy, it was demonstrated in a second *in vivo* model in the L1 mice carrying a dorsal skinfold chamber that cGMP signals induced by intravenous injection of DEA/NO were associated with vasodilation in live mice [178].

The expression of transgenes at high levels always poses the question of potential toxicity. However, both heterozygous R26-CAG-cGi500(L2) and R26-CAG-cGi500(L1) mice are fully viable and fertile without displaying detectable adverse phenotypes, suggesting minimal toxicity of both mT and cGi500 expression. This is also the case for the homozygous R26-CAG-cGi500(L1) mice kept for longer than one year, in which higher levels of cGi500 are expected. No morphological abnormalities were observed in these mice or various cell types derived from them. Notably, another question concerning the overexpression of cGi500 as a buffer molecule for cGMP had also been addressed in the SM22-cGi500 mice (with cGi500 expressed in smooth muscle cells). A "classical" function of cGMP is smooth muscle relaxation and blood pressure regulation [217-220]. The mean arterial blood pressure of SM22-cGi500 mice as measured with a non-invasive tail cuff system was not significantly different from non-transgenic control littermates [178]. Nonetheless, it will be necessary to continue monitoring for potential subtle phenotypes in some specific cell types. In this context, the R26-cGi500 mouse line with much lower expression levels of cGi500 and therefore potentially less detrimental effects may offer a supplementary tool.

Taken together, the newly generated R26-CAG-cGi500(L2) and (L1) mouse lines have opened new experimental routes for studying cGMP signaling in multiple cells, tissues and even *in vivo*. The R26-CAG-cGi500(L1) line with permanent and ubiquitous sensor expression provides a convenient source for primary cell isolation and subsequent cGMP imaging in real time with subcellular resolution. The L1 mouse line may also be used for *in vivo* imaging in tissues and live animals, e.g., to find new cGMP signaling sites with conventional or novel cGMP-elevating drugs. The Cre-activatable L2 mice, when crossed to Cre mouse lines, switch on cGi500 expression in individual cells in a tissue-specific manner, allowing for delineation of cGMP signals in specific tissues or cell types of interest. We expect that this L2 mouse line, combined with intravital imaging and multiphoton FRET microscopy, will find widespread application for *in vivo* analysis of cGMP in the future. In addition, the double marker labeling strategy with R26-CAG-cGi500(L2) mice can also be used for lineage tracing. At a specific time point, cells of interest for fate mapping can be labelled with cGi500 upon tissue-specific Cre recombination; the recombined cells is labelled with cGi500, while the non-recombined cells retain with mT expression. The cGi500-positive cell subpopulation can later be traced, and directly employed for cGMP imaging, therefore dissecting cGMP signaling chronically in physiological conditions or during disease development.

4.2 cGMP in DRG neurons

Connectivity of neurons is established during embryonic and early postnatal development. The establishment of a complex, finely organized axon morphology is a key step for many neurons to receive and transmit information in a circuit network. During the development of the nervous system, the extending growth cones are exposed to a complex and changing environment within the developing tissue. A variety of physical and chemical factors are likely to take part in influencing the direction of nerve growth. Knowledge about how branches get extended from the axons and modulated by molecules is very important for understanding the functional neural circuits [81].

CNP, along with its downstream signaling, is the only factor that has been clearly linked to the bifurcation process of murine DRG neurons *in vivo*. If DRG axons lack a component of the CNP/GC-B/cGKI pathway, then they no longer bifurcate and instead only turn either in a rostral or caudal direction upon entering the spinal cord [80]. Our FRET data showed that CNP elevated cGMP in DRG neurons, but ANP had no effect. This supports exactly the conclusion that GC-B rather than GC-A is expressed in embryonic DRG neurons. GC-B is the only NP receptor expressed in DRG neurons of early developmental stage, whereas GC-A is not detected [67, 86]. There are also studies suggesting that sGC provides an alternative route for cGMP production in DRG neurons, as *in vitro* cultured DRG neurons showed increased branching when being treated with the sGC stimulator YC-1 [87]. However, in our study, acute application of DEA/NO did not show any effect on cGMP generation. Thus, we conclude that sGC is not present in embryonic DRG neurons. The discrepancy may be explained by the lack of specificity of YC-1 as a stimulator of sGC. YC-1 was also reported to inhibit PDE activities [221-223]. Furthermore, our study is also in line with those by Schmidt et al. [67], who showed no or very weak expression of different transcripts of NOS and sGC as revealed by both reverse transcriptase-PCR and *in situ* hybridization. Moreover, no bifurcation errors were found at the DREZ in knock-out mice lacking the β1 subunit of sGC, demonstrating that sGC is dispensable for sensory axon branching.

FRET cGMP imaging could also specify the PDE subtypes that are involved in cGMP degradation by performing experiments with respective PDE inhibitors. Vinpocetine, EHNA and Bay 60-7550, milrinone, and sildenafil are relatively specific inhibitors for PDE1, PDE2, PDE3, and PDE5, respectively. Bath application of vinpocetine, EHNA

and Bay 60-7550 to the DRG neurons showed significant inhibitory effects on CNP-elicited cGMP in comparison to controls, whereas milrinone and sildenafil did not. Therefore, PDE1 and PDE2 are involved in cGMP degradation in embryonic DRG neurons. Zaprinast moderately inhibits PDE5 and PDE6 with IC_{50} values of 0.5-0.76 and 0.15 µM, respectively [224, 225]. In addition, the commonly as selective considered PDE5 inhibitor, sildenafil, inhibits also PDE6 with only 3–10-fold lower potency than PDE5 [226]. Our data show that both zaprinast and sildenafil had no effect on the CNP-induced cGMP increase. Therefore PDE6 is not involved in the degradation of CNP-induced cGMP. Zaprinast also weakly inhibits PDE9, PDE10, and PDE11 with IC_{50} values of 35, 22, and 11-33 µM, respectively [224, 225]. The lack of an inhibitory effect of 20 µM zaprinast also suggests the lack of PDE9, PDE10, and PDE11, although the inhibition of these PDEs by zaprinast, if there is any, may be incomplete. Therefore, PDE1 and PDE2 appear to be the major PDEs responsible for the degradation of CNP-induced cGMP in embryonic DRG neurons. Unpublished data from our collaborator, Dr. H. Schmidt, also show that PDE2A transcripts are detected in these neurons (personal communication). It would be interesting to study cGMP signals and the bifurcation phenotype *in vivo* in PDE1 or PDE2 knock-out and even PDE1 and PDE2 double knock-out mice. One could expect a greater amplitude and longer duration of cGMP in the growth cone after exposure to CNP in the knock-outs compared to the wild type, which may therefore flow over to the whole DRG neuron instead of staying locally in the growth cone, potentially causing branching errors.

It is currently well accepted that the cGMP signaling pathway is critical for sensory DRG axon bifurcation *in vivo* [80]. Recently, it has also been shown to be prominent in the bifurcation of cranial sensory neurons in the hindbrain [227]. A fundamental question remains to be answered is how cGMP signals guide the bifurcation of these neurons. Is cGMP signaling sufficient to induce bifurcation? DRG axons deficient in cGMP signaling no longer bifurcate and instead only turn in one direction after entering the spinal cord. However, bifurcation is observed only in a small proportion of DRG neurons in culture and has never been promoted, although addition of CNP leads to an increase in axon branching [67, 83, 86]. One possible reason is that the drug application in these *in vitro* culture experiments was not optimal. The global addition of CNP or cGMP analogs does not reflect the *in vivo* scenario, where only the growth cone but not the soma is exposed to CNP in the DREZ of the spinal cord during embryonic development. To study the compartmentalized CNP/cGMP signaling in DRG neurons, we established a method to apply drugs to subcellular domains of DRG neurons, such as the axons or growth cones, in combination with cGMP imaging after

local stimulation. Local application of CNP revealed that cGMP can be generated in the growth cone independently of the soma (**Figure 17**). These results suggest that the growth cone can indeed detect CNP when projecting into the DREZ of the spinal cord. The local elevation of cGMP in the growth cone in response to CNP may be important for sensory axon bifurcation during embryonic development.

On the other hand, the fact that the sensory axons in the cGMP signaling-deficient mice still turn longitudinally suggests that repellent signals exist to force the axons to change their growth direction. Filopodia are active protrusions of growth cones, which explore the environment and mediate axon pathfinding [228]. Inhibitory cues may also set a road map for filopodia of growth cones to travel. Operation of these guidance cues is facilitated by subcellular localization of diverse signaling components [229, 230]. Slit proteins have been suggested as repulsive cues for DRG neurons. Slit1 and Slit2 are ligands expressed in the dorsal spinal cord, whereas their receptors Robo1 and Robo2 are expressed in the sensory neurons [231]. The bifurcation of sensory neurons in Slit1 and Slit2 double knock-out as well as Robo1 and Robo2 double knock-out mice was not affected. However, some bifurcated axons of these knock-out mice grew prematurely into the central canal of the spinal cord with a slightly changed angle, which suggests the Slit proteins as repellent axonal guidance cues [81]. The relatively mild phenotypes of the Slit/Robo knock-out mice also imply that Slits are not the only inhibitory cues. Netrin-1 and Semaphorin 3A are also inhibitory factors for sensory axons [232-234]. These cues may act in concert with cGMP to regulate bifurcation. Interestingly, these inhibitory proteins have already been linked to other second messengers, especially cAMP and Ca^{2+} [235]. Optical imaging combined with the growth cone turning assay has revealed the importance of spatially asymmetric Ca^{2+} and cAMP elevation in the growth cone in response to different neurotransmitters or guidance cues [193, 229].

A network of second messengers decodes the cue-derived information as either attractive or repulsive signals that guide the pathfinding of growth cones [235]. With the same cues, nerve growth cones can behave oppositely. One prominent example is that Netrin-1 can function as a chemoattractant for some classes of axons and as a repellent signal for others. The functional difference depends on different levels of cytosolic cAMP, in response to different receptor types in different responsive cells [236]. On the other hand, in the same neuronal population, guidance cues may also have dual roles depending on the cellular level of cAMP and cGMP. Xenopus dorsal neurons switch from attraction to repulsion in response to Netrin-1 after up-regulation

of cAMP, whereas they lose responsiveness after up-regulation of both cAMP and cGMP [236]. It has also been shown that the repellent Semaphorin 3A becomes an attractant for growth cones when cGMP is increased and activates cGKI, which further regulates downstream Ca^{2+} influx and membrane depolarization [237]. In sum, the responsiveness of growth cones to guidance cues is highly complex and depends on both the extracellular context and the internal state of the growth cone, which is strongly linked to the state of the second messengers, Ca^{2+}, cAMP and cGMP.

It is tempting to propose that cGMP acts in DRG sensory axon bifurcation, in concert with cAMP and Ca^{2+}. An inverse correlation between cGMP and cAMP was observed in the freely extending growth cone [238]. The intracellular cGMP level is finely tuned by both GCs and PDEs. We have shown that PDE1 and PDE2 are responsible for cGMP degradation in embryonic DRG neurons. Both PDE1 and PDE2 are implicated in crosstalk with other second messengers: PDE1 is a Ca^{2+}/CaM-stimulated enzyme that hydrolyzes cGMP and cAMP, and PDE2 is cGMP-stimuated and degrades both cGMP and cAMP. The presence of PDE1 and PDE2 implies that an interplay of cGMP, cAMP and Ca^{2+} may occur and could be important in DRG neurons. Intracellular cAMP and Ca^{2+} can also be elevated by various neurotransmitters, or guidance cues [235]. If the state of the second messenger network is the intrinsic factor crucial for the sensory neuron bifurcation, what can be the external factors? In culture, it has been shown that an inhibitory guidance cue can drive the growth cone split [239]. When the signal acts in the center of the growth cone, the cytoskeleton retracts in the center and the two sides of the growth cone proceed to grow into two branches. Bifurcation can be considered as a special kind of axon guidance, when branching occurs at the growth cone in DRG neurons [240]. As cGMP is indispensable for axonal bifurcation *in vivo*, it is probably the state of cGMP in DRG neurons that is fundamental for these cues to exhibit their function to split the growth cones [83, 241]. In sum, the bifurcation of growth cones may require two conditions: 1) an extrinsic repellent signal acts in the center of a growth cone; 2) intrinsic levels of second messengers, e.g., of cGMP alone, or the cGMP/cAMP ratio or the cGMP/Ca^{2+} ratio, should be maintained to shape the motility of the growth cone.

Bringing all together, a model for DRG neuron bifurcation could be proposed as follows (**Figure 26**). During development, DRG neurons project into the spinal cord at the DREZ, where their axons get exposed to a complex environment, containing CNP secreted by dorsal horn neurons [83] as well as multiple guidance cues. CNP elevates cGMP in the whole growth cone, while multiple cues like Netrin-1 cause higher

$cAMP/Ca^{2+}$ in the front side of the growth cones. cGMP and cAMP levels are fine-tuned by PDE1 and PDE2. Additionally, the inhibitory cues set a longitudinal path for the axon, preventing the growth cone from premature growth into the central canal by elevating local cAMP and/or Ca^{2+} in the front side of the growth cone. At the same time, cGMP elevated by CNP at the filopodia in the dorsal and ventral part of the growth cone set a high cGMP/cAMP ratio, which allows the inhibitory cues to steer the growth cone to extend in both caudal and rostral directions.
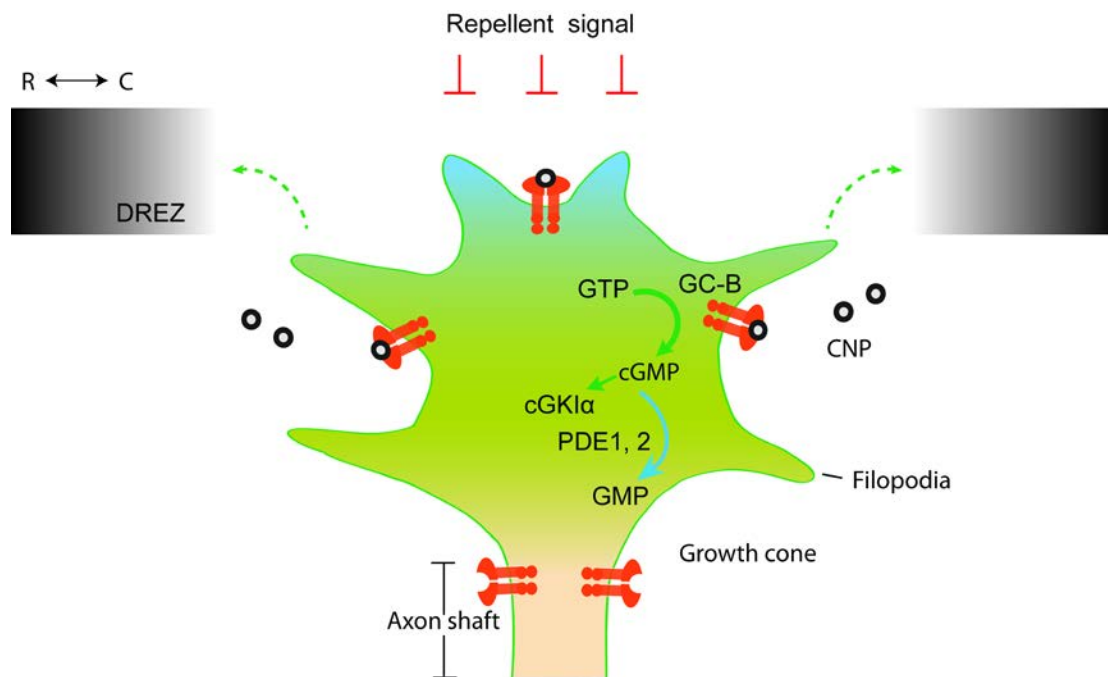

Figure 26. Model for DRG sensory axon bifucation.

The growth cone encounters various physical and chemical cues in the environment. CNP is secreted by cells localized in the dorsal quarter of the spinal cord. Upon arrival at the DREZ, local cGMP in the growth cone is generated by GC-B in response to CNP and degraded by PDE1 and PDE2. The motility of the growth cone may depends on the ratio of cGMP and other second messengers in local domains, especially in the filopodia. CNP increases the motility of the growth cone by affecting the cytoskeletal dynamics, e.g., by cGKIα-mediated phosphorylation of cytoskeleton-related elements. The repellent signals elicited by repulsive proteins, such as Slits and Netrin-1, might act together against the axon extension, probably through elevation of other second messengers such as cAMP and Ca^{2+} (shown in blue). Hence, the extension of the axon is only permitted in rostral and caudal directions. High cGMP levels are indicated in green. R, rostral direction; C, caudal direction. DREZ, dorsal root entry zone.

To scrutinize this model, it is necessary to simultaneously visualize cGMP together with Ca^{2+} and/or cAMP and analyze their spatiotemporal dynamics in growth cones, while CNP and other guidance cues are locally applied. To test this hypothesis, one can try to mimic the local CNP activation and elevation of cGMP by applying CNP locally to the growth cone with glass pipettes. Another *in vitro* culture system to study axon growth, neurite outgrowth and the guidance properties of these molecules in response to different molecules is the stripe assay [242-246]. Active molecules like CNP are immobilized on a surface with silicon matrices to produce striped patterns. A

stripe coated with CNP would reflect the *in vivo* location of CNP in the DREZ, therefore allowing one to examine the axonal growth and signaling behavior of DRG neurons. Moreover, the stripe assay can also be combined with local application with glass pipettes to induce axon bifurcation. Along with these local drug application techniques, cGMP imaging with subcellular resolution deserves a lot of attention in the future. Our sensor mice should also facilitate the time-lapse imaging of cGMP *in vivo* in tissue slices, or even in mouse whole embryo culture, which would hopefully also help resolve the mechanisms of axon bifurcation.

4.3 cGMP in platelets

Platelets play a central role in hemostasis and thrombosis. Without a nucleus, platelets have no control over transcription, making them also resistant to DNA transfection. We established a method for real-time cGMP imaging in activated platelets from cGi500 sensor knock-in mice with a flow chamber system. Collagen is one of the strongest thrombogenic components of the subendothelial matrix responsible for the initiation of platelet adhesion. A number of adhesive receptors on the platelet plasma membrane interact either directly or indirectly with collagen [92]. By flowing whole blood over a collagen-coated coverslip, platelets were activated and arrested on the collagen-coated surface. Platelet thrombi formed in the flow chamber system were used for cGMP FRET imaging. Ca^{2+} is another important second messenger that has been implicated in various cell systems, maintaining physiological homeostasis together with cGMP and cAMP. Due to the distinct spectral properties of Fura-2 and the FRET pair (CFP and YFP) within cGi500, it is possible to measure Fura-2 and FRET at the same time [247, 248]. We describe here a method to visualize cGMP and Ca^{2+} in platelets from R26-CAG-cGi500(L1) mice in parallel. By loading cGMP sensor-expressing cells with Fura-2, cGMP and Ca^{2+} were measured simultaneously.

Characterization of cGMP signaling in platelets with our newly generated R26-CAG-cGi500(L1) mice has shown that cGMP is generated by sGC in response to NO. Our FRET data showed that degradation of cGMP is controlled by PDE2, PDE3 and PDE5. These data are in line with previous reports [95]. PDE2 is a cGMP-stimulated enzyme specific for both cGMP and cAMP, while PDE3 is cGMP inhibited, and preferentially hydrolyzes cAMP, suggesting that fine-tuning of the balance between cGMP and cAMP is important for platelet function. PDE5 is specific for cGMP degradation.

Surprisingly, platelets generated cGMP not only in response to NO, but our real-time FRET measurements also demonstrated that NO-induced cGMP was strongly regulated by flow. This process was very fast; the decrease of cGMP upon flow off occurred within 2-5 seconds. The total decreasing time of NO-induced cGMP was ~30 s. Overall, flow on increased cGMP production, whereas flow off declined cGMP levels (**Figure 19**). Similar results were also observed in VSMCs. However, the decay of cGMP in VSMCs upon flow off took about 2 min, which was slower than in platelets, indicating a slower response to flow change. This may be explained by the smaller size of platelets compared to VSMCs; platelets are cells of 2-3 μm, and a small change in molecules or ions induced by shear stress would result in a rapid change in

concentrations, thereby regulating cGMP in a fast manner. Moreover, the rapid response of cGMP regulation correlates with the functional necessities for platelets to respond immediately to vascular trauma to prevent life-threatening blood loss, whereas VSMCs do not directly sense fluid shear stress, although stretch is present during contraction.

Are sGC and/or PDEs regulated by flow? Intracellular cGMP levels are determined by a balance of its generation and degradation. Theoretically, the flow-induced increase of cGMP concentration in the presence of NO can be attributed to flow-activated sGC or flow-inhibited PDEs, or both. The fact that Bay 41-2272-induced cGMP was only partially decreased after flow off (**Figure 23A**) argues against PDEs as the major mediators of flow regulation; sGC instead may play a critical role. Experiments with VSMCs showed that flow affected NO-induced cGMP signals but not CNP-induced cGMP signals (**Figure 23C**); different cGMP pools induced by DEA/NO or CNP had a differential sensitivity to flow reduction, further pointing to sGC as the likely molecule to be regulated by flow. Therefore, we propose that in the presence of NO, flow on results in sGC sensitization, and cGMP gets elevated. Conversely, flow off gives rise to desensitized sGC, leading to fast cGMP degradation by PDEs.

The decay of cGMP upon flow off in the presence of NO is even faster than that upon washout of NO (**Figure 21**), indicating that flow off results in a state of sGC activity even lower than the basal activity with flow but without NO. Current knowledge suggests a two-step activation of sGC [37]. NO activates sGC through binding to the sixth coordination position of the heme, resulting in a 6-coordinate low-output intermediate activated state. Further scission of the histidine-iron bond produces a 5-coordinate $NO\text{-}Fe^{2+}$-heme complex and induces structural changes within the heme moiety which is considered to trigger the conformational change required to activate the enzyme to a high-output state. Considering the novel mode of cGMP regulation by flow, there might be at least four states of sGC activity *in vivo*: 1) a state with very low to lost sGC activity in the absence of flow, at which the integrity of sGC may be disrupted, possibly due to an event that separates the two subunits of sGC, 2) a state with basal activity of sGC, in the presence of flow, 3) a 6-coordinate NO-heme low output state, 4) a 5-coordinate NO-heme high output state. The four states of sGC may coexist and are inter-convertible, which can well explain the "flow on and off" phenomenon. NO activates sGC to a high output state, resulting in a fast increase of cGMP production. After washout of NO, sGC returns to a basal active state in the presence of flow, and therefore cGMP signals decrease relatively slowly. In contrast,

flow off totally shuts down the sGC activity, while PDE activity is high, leading to a sharp decrease of cGMP levels. On the other hand, the indazole derivatives, including Bay 41-2272 are NO-independent, heme-dependent sGC stimulators. It is proposed that they stimulate sGC by binding to an unknown allosteric site [49]. They also act in synergy with NO by stabilizing the NO-heme complex of sGC in its active state [49, 249]. In our studies, Bay 41-2272-induced cGMP levels only decreased slowly and partially upon flow off, which may be accounted for the stabilization of sGC by Bay 41-2272. Washout of Bay 41-2272 results in the relief of sGC activity back to its basal activity again and cGMP returns to basal levels.

Does shear stress increase cGMP in platelets? It is known that NO also has multiple cGMP-independent effects. NO as a free radical undergoes oxidation into nitrite and nitrate, reacts with the superoxide anion ($\cdot O_2$) to form peroxynitrite ($ONOO-$), or binds to transition metals (NO-M) [250]. Many proteins can be modified by NO through converting thiol groups in proteins into S-nitrosothiols [251, 252]. Recently, S-nitrosylation has been suggested as a mechanism for sGC desensitization [53, 54]. Our finding that flow also regulates Bay 41-2272-induced cGMP suggested that sGC desensitization by flow reduction is an effect not exerted by NO-mediated nitrosylation but rather by fluid shear stress itself.

We showed that NO-induced cGMP was regulated in a flow rate-dependent manner. This cGMP change was not linear to the flow rate. In the presence of NO, a 90% decrease of flow rate from 45 mL/h to 5 mL/h resulted in ~30% decline of peak cGMP, whereas further 10% decrease of flow rate from 5 mL/h to 0 led to ~70% decrease of peak cGMP signals to the basal level (**Figure 20**). In addition, the titration of flow from high flow rate (45 mL/h) to intermediate flow rates (between 45 and 5 mL/h) did not lead to changes of cGMP levels (data not shown). It seems there is a threshold of flow rate for sGC activation; low shear is already sufficient to sensitize the enzyme. This supports the hypothesis by Orr et al. that efficient transmission of small forces to the mechanosensitive elements enhances sensitivity [253]. In conclusion, regulation of sGC activity by shear stress seems to play an important role in flow-regulated cGMP levels in the presence of NO.

How do platelets transduce shear stress to sGC? This is a fundamental question that remains to be answered and can be split into two questions: firstly, how is sGC regulated by shear stress? Secondly, what is the mechanotransducer? It is well known

that sGC activity can be potentiated tremendously by NO and some synthetic compounds that modulate the heme moiety [37]. However, it is barely known how this enzyme is regulated in detail. Many mechanisms of receptor sensitization and desensitization have been suggested, including protein-protein interaction of sGC with Hsp70 [254], PSD95 [255] and PDI [256]. Other mechanisms for regulation of sGC include phosphorylation and S-nitrosylation. Phosphorylation of sGC at serine/threonine residues by PKC [257, 258] and PKA [259] increases the activity of the enzyme, whereas phosphorylation by cGKI [260, 261] leads to inhibition of sGC activity and therefore cGMP formation. Both stimulatory [101, 210] and inhibitory [262] roles of Src kinase on sGC activity have been suggested. Further work will be needed to clarify the role of sGC phosphorylation. Recently, S-nitrosylation, the oxidative modification of cysteine residues of sGC was reported to result in a reduction of NO-stimulated sGC activity, suggesting that the modification of sGC by NO may account for NO tolerance and desensitization [53, 54]. Relocalization of sGC has also been shown in many studies. Translocation of sGC to the membrane occurs in response to a Ca^{2+} signal in human platelets. This membrane association sensitizes sGC to NO [263]. However in our study, shear stress alone did not alter intracellular Ca^{2+}. And in the presence of NO, change of shear stress altered cGMP levels before Ca^{2+} levels (**Figure 24 and 25A**). Ca^{2+} is more likely downstream of cGMP in response to shear stress. Whether shear stress alters translocation and thereby sensitizes sGC independently of Ca^{2+} requires further clarification.

Endothelial cells (ECs) lining the vessel lumen and platelets adhering to the endothelium are directly subjected to blood flow. ECs and platelets are the two major cell types reported to respond to fluid flow. Mechanotranduction in ECs is more extensively investigated, partially due to the easier culture of ECs under flow. Cell-cell junctions [264], ion channels [265], integrins [266], caveolae [267], primary cilia [268], and glycocalyx [269] have been proposed as putative mechanotransducers in sensing flow. Interestingly, many of these proteins or structures that mediate response to shear stress in ECs [253, 270] are also found in platelets. For example, platelet endothelial cell adhesion molecule (PECAM-1), also known as CD31, is abundantly expressed in both platelets and endothelial cells [271]. PECAM-1 transduces the shear response in endothelial cells [122, 264, 272] and has an inhibitory role for platelet aggregation [273]. Platelets and ECs might share common mechanotransducers that convert physical stresses into biochemical signals. Lessons learned from ECs can be applied to platelets and *vice versa*. In platelets, activation and aggregation has been historically evaluated in suspended cells activated by agonists in the absence of interactions with

immobilized substrates, for example, in an aggregometer, where continuous stirring is applied, but the fluid dynamic parameters are poorly defined [92]. Widespread application of the flow chamber system and intravital imaging revealed many adhesion molecules that are involved in platelet aggregation under flow [92, 273]. However, whether and how shear forces are transduced to biochemical signals is still elusive. In this context, it seems not so surprising that shear-regulated cGMP/Ca^{2+} signals were normal in GPIb mutant platelets. The elevation of cGMP induced by vWF [104, 210, 211] might be an effect mediated by binding of vWF to the GPIb receptor rather than an effect of shear stress on GPIb.

Interestingly, preliminary data showed that TRPC3 might affect cGMP generation. Although it is still under debate whether TRP channels themselves work as mechanosensors to detect flow directly, they are widely accepted as molecular components of mechanotransduction [274]. Several TRP channels can also be activated by G protein-coupled receptors. These receptors are themselves often deemed as flow sensors, which activate phospholipase C, and the synthesized diacylglycerol (DAG) mediates TRP channel activation [274]. In this context, shear stress may be transduced via mechanotransducers including TRPC3 to sGC. Pyr3 impairs flow-induced sensitization of sGC and, therefore, slows down NO-induced cGMP production after flow on. sGC desensitization by the blockage of TRPC3 therefore fits well with our model for flow-regulated cGMP signaling (**Figure 27**).

The attenuating effect of Pyr3 on cGMP generation is an important first step towards the understanding of the underlying mechanisms of flow-regulated cGMP signaling. However, it is not known how TRPC3 regulates sGC and whether shear stress regulates TRPC3 by gating the ion channel activity or affecting its physical interaction with sGC. TRPC3 is a non-specific cation channel, allowing influx of Na^+ and Ca^{2+} [274]. It seems unlikely that TRPC3-derived Ca^{2+} affects cGMP production, since Ca^{2+} seems to be the downstream signal of cGMP and flow on and off in the absence of NO does not change cytoplasmic Ca^{2+} as revealed by Fura-2 measurements, unless compartmentalized Ca^{2+} is affected. Although Pyr3 is selective in inhibiting TRPC3 over other TRP channels, it can also have nonspecific effects on other signaling pathways [275], such as store-operated Ca^{2+} entry mediated by Orai channels [276]. However, the concentration of Pyr3 (1 µM) used in this study is relatively low, and seems not likely to exhibit such non-specific effects. Future work to clarify the role of TRPC3 should include: 1) confirmation of the sGC desensitization response by measuring the dose response to NO in the presence and absence of Pyr3; 2)

simulation of the effect of shear stress on TRPC3 activation through application of TRPC3 agonists such as the membrane-permeable DAG analog 1-oleoyl-2-acetyl-sn-glycerol (OAG) [216]; 3) verification of the role of TRPC3 by studying platelets from TRPC3 knock-out mice. Further delineation of the channel activity and its relationship with intracellular cGMP should be performed. Further investigation is needed to unveil whether and, if so, how TRPC3 affects the cGMP level, for example, via ion regulation or physical interaction with sGC.
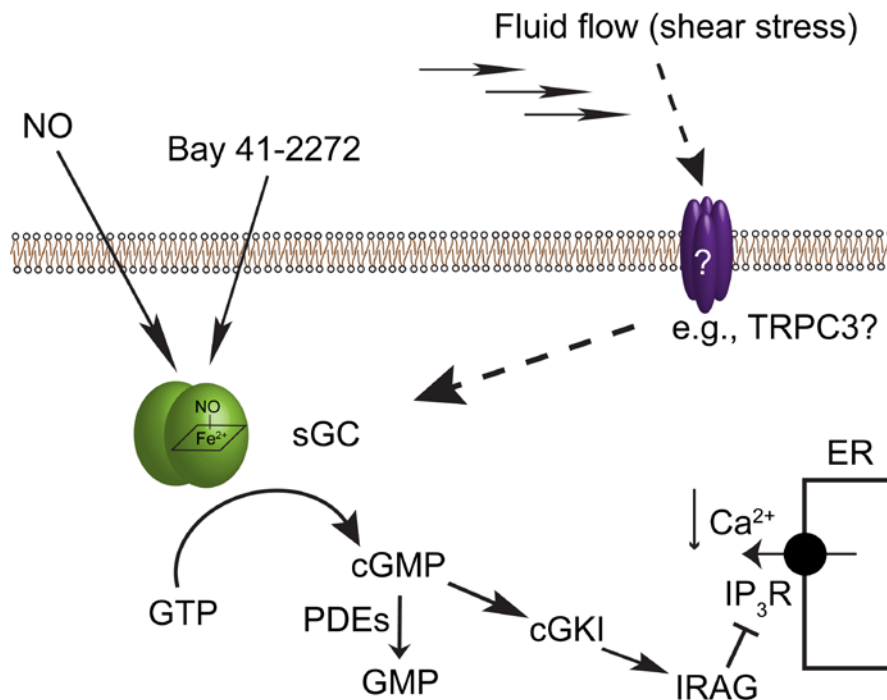

Figure 27. Model for shear stress-regulated cGMP signaling in platelets.

Platelet exposure to fluid shear stress leads to cGMP elevation in response to NO. Fluid shear stress is sensed probably by platelet membrane proteins and transduced by transducers like TRPC3, to sensitize sGC to NO via unknown mechanisms. Acute cessation of flow would result in inhibition of TRPC3, and therefore desensitize the NO receptor sGC, resulting in reduced cGMP levels even in the presence of NO. Inhibition of TRPC3 by inhibitors such as Pyr3 would also inhibit sGC activity, leading to an attenuated cGMP response. cGMP precedes and possibly regulates cytoplasmic Ca^{2+} through inhibition of Ca^{2+} release from the ER. IP_3R, IP_3 receptor; IRAG, IP_3R-associated cGKI substrate protein; ER, endoplasmic reticulum. TRPC3, transient receptor potential channel 3.

What are the functional implications for cGMP modulation by flow? Cytosolic Ca^{2+} is an important prothrombotic factor downstream of most signaling pathways in platelets [203]. Platelet agonists such as collagen and thrombin elevate cytosolic Ca^{2+} levels during platelet activation. Virtually all agonists induce activation of phospholipase C, which generates the second messenger IP_3. IP_3 binds to the IP_3 receptor, an ion channel in the endoplasmic reticulum, mediating Ca^{2+} release from intracellular Ca^{2+} stores and subsequent store-operated Ca^{2+} entry [94, 277]. Sustained cytosolic Ca^{2+} elevation is required for platelet aggregation, and one of the

key steps is phosphatidylserine exposure on the platelet plasma membrane [203]. Phosphatidylserine exposure speeds up thrombin formation via the coagulation cascade, through which fibrinogen is converted into fibrin, thereby stabilizing the thrombus. We have shown that high shear stress leads to sensitized sGC activity which results in high cGMP levels. cGMP lowers intracellular Ca^{2+} levels, which counteracts with the aggregation process, thereby inhibiting thrombus formation.

During thrombus formation, there is a dramatic change of shear rates of blood flow. Shear rates in arteries are in the range of 300-800 s^{-1}, and of 500-1600 s^{-1} in arterioles, whereas that in veins are ten times lower, at 20-200 s^{-1} [278]. However, during vascular stenosis, shear rates can surge up to 10 000 s^{-1} and even higher [279]. During hemostasis, collagen and many other factors at sites of vascular injury trigger platelet activation and subsequent thrombus formation to stop life-threatening bleeding. However, few details are known how thrombus growth is limited at the right time point so that the thrombus gets not too large to occlude the vessels. The growing platelet plug during hemostasis results in a decreasing vessel diameter and elevated shear stress. It is reasonable to propose that elevated shear stress, together with NO supplied by the endothelium, prevents the platelet thrombus from further growth and vessel occlusion, possibly by inhibiting the recruitment of new platelets to the already formed thrombus. Thus, shear stress may function as a dynamic factor to auto-tune the regulation of thrombus growth and stabilization via cGMP signaling.

The novel model of thrombus growth control by shear stress-regulated NO/cGMP signaling fits well with recent knowledge about platelet aggregation under dynamic flow conditions. Jackson and colleagues showed that platelets preferentially adhere in a low-shear zone at the downstream face of the growing thrombus [280]. As high shear induces higher cGMP and inhibits platelet aggregation, it makes sense that the thrombus grows favorably at the low-shear zone. In the future, it would be desirable to understand how the new mode of cGMP regulation by shear stress can be translated to *in vivo* conditions, for example, through cGMP imaging of a thrombus facing different shear exposure. Moreover, the shear-dependent mode of cGMP signaling also suggests that thrombus formation is not a simple progressive process, starting with platelet adhesion and activation, and ending up with the platelet plug at the trauma. Future studies should address a more detailed dissection of this process over time in an *in vivo* context, including adhesion and activation, as well as thrombus growth and stabilization [281].

As also introduced before, Du et al. proposed biphasic effects of cGMP in platelets, i.e. an earlier stimulatory role in platelet activation and a delayed inhibitory role in limiting thrombus overgrowth [104]. Our new model supports the inhibitory effect of cGMP on thrombus growth, although it does not tell if there is any stimulatory effect during platelet activation. For the future, it would be of high interest to monitor cGMP during platelet adhesion and activation, in a flow chamber, and eventually in blood vessels of live animals with intravital microscopy. Ca^{2+} imaging with Ca^{2+} fluorescent dyes in single rolling platelets in a flow chamber [282, 283] or *in vivo* [284] has been described by other groups. A recently described FRET-based calcium indicator ('Twitch' sensor) has also been utilized to image moving T lymphocyte during activation *in vivo* [285]. Therefore, a similar approach based on ratiometric imaging of cGMP with our cGi500 sensor mouse should be feasible in principle. Considering the controversy about the stimulatory or inhibitory role of cGMP in platelet activation, live cell imaging of cGMP during thrombus formation may provide new evidence to settle down the dispute. To develop a fluorometric aggregometer for real-time monitoring of cGMP during aggregation is another potential application to elucidate this question. This method should combine a conventional aggregometer that can be used for monitoring of platelet aggregation and cGMP by fluorometric FRET measurement. A high throughput version of this method may also provide a new route for screening of new cGMP-modulating drugs under more physiological conditions.

Altogether, we have successfully generated and characterized FRET-based cGMP sensor knock-in mice. The mouse lines have already brought us new knowledge about cGMP biology, especially from cGMP imaging in live DRG neurons and platelets. The novel findings of this work highlight the usefulness of the newly generated transgenic mice as important tools for cGMP research. These cGMP sensor mice are expected to find widespread applications in the future.

5 References

1. Kemp-Harper, B. and R. Feil, *Meeting report: cGMP matters.* Sci Signal, 2008. **1**(9): p. pe12.

2. Ashman, D.F., et al., *Isolation of adenosine 3', 5'-monophosphate and guanosine 3', 5'-monophosphate from rat urine.* Biochem Biophys Res Commun, 1963. **11**: p. 330-4.

3. Beavo, J.A. and L.L. Brunton, *Cyclic nucleotide research -- still expanding after half a century.* Nat Rev Mol Cell Biol, 2002. **3**(9): p. 710-8.

4. Katsuki, S., et al., *Stimulation of guanylate cyclase by sodium nitroprusside, nitroglycerin and nitric oxide in various tissue preparations and comparison to the effects of sodium azide and hydroxylamine.* J Cyclic Nucleotide Res, 1977. **3**(1): p. 23-35.

5. Furchgott, R.F. and J.V. Zawadzki, *The obligatory role of endothelial cells in the relaxation of arterial smooth muscle by acetylcholine.* Nature, 1980. **288**(5789): p. 373-6.

6. Ignarro, L.J., et al., *Endothelium-derived relaxing factor produced and released from artery and vein is nitric oxide.* Proc Natl Acad Sci U S A, 1987. **84**(24): p. 9265-9.

7. Palmer, R.M., A.G. Ferrige, and S. Moncada, *Nitric oxide release accounts for the biological activity of endothelium-derived relaxing factor.* Nature, 1987. **327**(6122): p. 524-6.

8. Martin, W., et al., *Blockade of endothelium-dependent and glyceryl trinitrate-induced relaxation of rabbit aorta by certain ferrous hemoproteins.* J Pharmacol Exp Ther, 1985. **233**(3): p. 679-85.

9. Martin, W., et al., *Selective blockade of endothelium-dependent and glyceryl trinitrate-induced relaxation by hemoglobin and by methylene blue in the rabbit aorta.* J Pharmacol Exp Ther, 1985. **232**(3): p. 708-16.

10. Gerzer, R., F. Hofmann, and G. Schultz, *Purification of a soluble, sodium-nitroprusside-stimulated guanylate cyclase from bovine lung.* Eur J Biochem, 1981. **116**(3): p. 479-86.

11. Humbert, P., et al., *Purification of soluble guanylyl cyclase from bovine lung by a new immunoaffinity chromatographic method.* Eur J Biochem, 1990. **190**(2): p. 273-8.

12. Alderton, W.K., C.E. Cooper, and R.G. Knowles, *Nitric oxide synthases: structure, function and inhibition.* Biochem J, 2001. **357**(Pt 3): p. 593-615.

13. Kimura, H. and F. Murad, *Evidence for two different forms of guanylate cyclase in rat heart.* J Biol Chem, 1974. **249**(21): p. 6910-6.

14. Chrisman, T.D., et al., *Characterization of particulate and soluble guanylate cyclases from rat lung.* J Biol Chem, 1975. **250**(2): p. 374-81.

15. Hughes, J.M., et al., *Role of cyclic GMP in the action of heat-stable enterotoxin of Escherichia coli.* Nature, 1978. **271**(5647): p. 755-6.

16. Fischmeister, R., et al., *Compartmentation of cyclic nucleotide signaling in the heart: the role of cyclic nucleotide phosphodiesterases.* Circ Res, 2006. **99**(8): p. 816-28.

17. Cheepala, S., et al., *Cyclic nucleotide compartmentalization: contributions of phosphodiesterases and ATP-binding cassette transporters.* Annu Rev Pharmacol Toxicol, 2013. **53**: p. 231-53.

18. Biel, M., et al., *Structure and function of cyclic nucleotide-gated channels.* Rev Physiol Biochem Pharmacol, 1999. **135**: p. 151-71.

19. Hofmann, F., *The biology of cyclic GMP-dependent protein kinases.* J Biol Chem, 2005. **280**(1): p. 1-4.

20. Xie, Q.W., et al., *Cloning and characterization of inducible nitric oxide synthase from mouse macrophages.* Science, 1992. **256**(5054): p. 225-8.

21. Hall, C.N. and J. Garthwaite, *What is the real physiological NO concentration in vivo?* Nitric Oxide, 2009. **21**(2): p. 92-103.

22. Moncada, S. and E.A. Higgs, *The discovery of nitric oxide and its role in vascular biology.* Br J Pharmacol, 2006. **147 Suppl 1**: p. S193-201.

23. Toledo, J.C., Jr. and O. Augusto, *Connecting the chemical and biological properties of nitric oxide.* Chem Res Toxicol, 2012. **25**(5): p. 975-89.

24. Dierks, E.A. and J.N. Burstyn, *Nitric oxide (NO), the only nitrogen monoxide redox form capable of activating soluble guanylyl cyclase.* Biochem Pharmacol, 1996. **51**(12): p. 1593-600.

25. Schrammel, A., et al., *Characterization of 1H-[1,2,4]oxadiazolo[4,3-a]quinoxalin-1-one as a heme-site inhibitor of nitric oxide-sensitive guanylyl cyclase.* Mol Pharmacol, 1996. **50**(1): p. 1-5.

26. Hashimoto, S. and A. Kobayashi, *Clinical pharmacokinetics and pharmacodynamics of glyceryl trinitrate and its metabolites.* Clin Pharmacokinet, 2003. **42**(3): p. 205-21.

27. Miller, M.R. and I.L. Megson, *Recent developments in nitric oxide donor drugs.* Br J Pharmacol, 2007. **151**(3): p. 305-21.

28. Hess, D.T. and J.S. Stamler, *Regulation by S-nitrosylation of protein post-translational modification.* J Biol Chem, 2012. **287**(7): p. 4411-8.

29. Derbyshire, E.R. and M.A. Marletta, *Biochemistry of soluble guanylate cyclase.* Handb Exp Pharmacol, 2009(191): p. 17-31.

30. Kamisaki, Y., et al., *Soluble guanylate cyclase from rat lung exists as a heterodimer.* J Biol Chem, 1986. **261**(16): p. 7236-41.

31. Yuen, P.S., L.R. Potter, and D.L. Garbers, *A new form of guanylyl cyclase is preferentially expressed in rat kidney.* Biochemistry, 1990. **29**(49): p. 10872-8.

32. Harteneck, C., et al., *Molecular cloning and expression of a new alpha-subunit of soluble guanylyl cyclase. Interchangeability of the alpha-subunits of the enzyme.* FEBS Lett, 1991. **292**(1-2): p. 217-22.

33. Mergia, E., et al., *Major occurrence of the new alpha2beta1 isoform of NO-sensitive guanylyl cyclase in brain.* Cell Signal, 2003. **15**(2): p. 189-95.

34. Russwurm, M., et al., *Functional properties of a naturally occurring isoform of soluble guanylyl cyclase.* Biochem J, 1998. **335 (Pt 1)**: p. 125-30.

35. Hoenicka, M., et al., *Purified soluble guanylyl cyclase expressed in a baculovirus/Sf9 system: stimulation by YC-1, nitric oxide, and carbon monoxide.* J Mol Med (Berl), 1999. **77**(1): p. 14-23.

36. Harteneck, C., et al., *Expression of soluble guanylyl cyclase. Catalytic activity requires two enzyme subunits.* FEBS Lett, 1990. **272**(1-2): p. 221-3.

37. Derbyshire, E.R. and M.A. Marletta, *Structure and regulation of soluble guanylate cyclase.* Annu Rev Biochem, 2012. **81**: p. 533-59.

38. Gerzer, R., et al., *Soluble guanylate cyclase purified from bovine lung contains heme and copper.* FEBS Lett, 1981. **132**(1): p. 71-4.

39. Karow, D.S., et al., *Characterization of functional heme domains from soluble guanylate cyclase.* Biochemistry, 2005. **44**(49): p. 16266-74.

40. Zhao, Y. and M.A. Marletta, *Localization of the heme binding region in soluble guanylate cyclase.* Biochemistry, 1997. **36**(50): p. 15959-64.

41. Wedel, B., et al., *Mutation of His-105 in the beta 1 subunit yields a nitric oxide-insensitive form of soluble guanylyl cyclase.* Proc Natl Acad Sci U S A, 1994. **91**(7): p. 2592-6.

42. Cary, S.P., J.A. Winger, and M.A. Marletta, *Tonic and acute nitric oxide signaling through soluble guanylate cyclase is mediated by nonheme nitric oxide, ATP, and GTP.* Proc Natl Acad Sci U S A, 2005. **102**(37): p. 13064-9.

43. Zhao, Y., et al., *Inhibition of soluble guanylate cyclase by ODQ.* Biochemistry, 2000. **39**(35): p. 10848-54.

44. Ignarro, L.J., K.S. Wood, and M.S. Wolin, *Activation of purified soluble guanylate cyclase by protoporphyrin IX.* Proc Natl Acad Sci U S A, 1982. **79**(9): p. 2870-3.

45. Stone, J.R. and M.A. Marletta, *Soluble guanylate cyclase from bovine lung: activation with nitric oxide and carbon monoxide and spectral characterization of the ferrous and ferric states.* Biochemistry, 1994. **33**(18): p. 5636-40.

46. Stasch, J.P. and A.J. Hobbs, *NO-independent, haem-dependent soluble guanylate cyclase stimulators.* Handb Exp Pharmacol, 2009(191): p. 277-308.

47. Schmidt, H.H., P.M. Schmidt, and J.P. Stasch, *NO- and haem-independent soluble guanylate cyclase activators.* Handb Exp Pharmacol, 2009(191): p. 309-39.

48. Schmidt, P., et al., *Mechanisms of nitric oxide independent activation of soluble guanylyl cyclase.* Eur J Pharmacol, 2003. **468**(3): p. 167-74.

49. Friebe, A. and D. Koesling, *Mechanism of YC-1-induced activation of soluble guanylyl cyclase.* Mol Pharmacol, 1998. **53**(1): p. 123-7.

50. Mullershausen, F., et al., *Inhibition of phosphodiesterase type 5 by the activator of nitric oxide-sensitive guanylyl cyclase BAY 41-2272.* Circulation, 2004. **109**(14): p. 1711-3.

51. Garthwaite, J., et al., *Potent and selective inhibition of nitric oxide-sensitive guanylyl cyclase by 1H-[1,2,4]oxadiazolo[4,3-a]quinoxalin-1-one.* Mol Pharmacol, 1995. **48**(2): p. 184-8.

52. Friebe, A. and D. Koesling, *Regulation of nitric oxide-sensitive guanylyl cyclase.* Circ Res, 2003. **93**(2): p. 96-105.

53. Sayed, N., et al., *Desensitization of soluble guanylyl cyclase, the NO receptor, by S-nitrosylation.* Proc Natl Acad Sci U S A, 2007. **104**(30): p. 12312-7.

54. Sayed, N., et al., *Nitroglycerin-induced S-nitrosylation and desensitization of soluble guanylyl cyclase contribute to nitrate tolerance.* Circ Res, 2008. **103**(6): p. 606-14.

55. Potter, L.R., *Regulation and therapeutic targeting of peptide-activated receptor guanylyl cyclases.* Pharmacol Ther, 2011. **130**(1): p. 71-82.

56. Kuhn, M., *Function and dysfunction of mammalian membrane guanylyl cyclase receptors: lessons from genetic mouse models and implications for human diseases.* Handb Exp Pharmacol, 2009(191): p. 47-69.

57. Suga, S., et al., *Receptor selectivity of natriuretic peptide family, atrial natriuretic peptide, brain natriuretic peptide, and C-type natriuretic peptide.* Endocrinology, 1992. **130**(1): p. 229-39.

58. de Bold, A.J., et al., *The physiological and pathophysiological modulation of the endocrine function of the heart.* Can J Physiol Pharmacol, 2001. **79**(8): p. 705-14.

59. Lopez, M.J., et al., *Salt-resistant hypertension in mice lacking the guanylyl cyclase-A receptor for atrial natriuretic peptide.* Nature, 1995. **378**(6552): p. 65-8.

60. Oliver, P.M., et al., *Hypertension, cardiac hypertrophy, and sudden death in mice lacking natriuretic peptide receptor A.* Proc Natl Acad Sci U S A, 1997. **94**(26): p. 14730-5.

61. John, S.W., et al., *Blood pressure and fluid-electrolyte balance in mice with reduced or absent ANP.* Am J Physiol, 1996. **271**(1 Pt 2): p. R109-14.

62. Skryabin, B.V., et al., *Hypervolemic hypertension in mice with systemic inactivation of the (floxed) guanylyl cyclase-A gene by alphaMHC-Cre-mediated recombination.* Genesis, 2004. **39**(4): p. 288-98.

63. Tamura, N., et al., *Cardiac fibrosis in mice lacking brain natriuretic peptide.* Proc Natl Acad Sci U S A, 2000. **97**(8): p. 4239-44.

64. Pagel-Langenickel, I., et al., *Natriuretic peptide receptor B signaling in the cardiovascular system: protection from cardiac hypertrophy.* J Mol Med (Berl), 2007. **85**(8): p. 797-810.

65. Tamura, N., et al., *Critical roles of the guanylyl cyclase B receptor in endochondral ossification and development of female reproductive organs.* Proc Natl Acad Sci U S A, 2004. **101**(49): p. 17300-5.

66. Pfeifer, A., et al., *Intestinal secretory defects and dwarfism in mice lacking cGMP-dependent protein kinase II.* Science, 1996. **274**(5295): p. 2082-6.

67. Schmidt, H., et al., *The receptor guanylyl cyclase Npr2 is essential for sensory axon bifurcation within the spinal cord.* J Cell Biol, 2007. **179**(2): p. 331-40.

68. Sager, G., *Cyclic GMP transporters.* Neurochem Int, 2004. **45**(6): p. 865-73.

69. Francis, S.H., M.A. Blount, and J.D. Corbin, *Mammalian cyclic nucleotide phosphodiesterases: molecular mechanisms and physiological functions.* Physiol Rev, 2011. **91**(2): p. 651-90.

70. Norris, R.P., et al., *Cyclic GMP from the surrounding somatic cells regulates cyclic AMP and meiosis in the mouse oocyte.* Development, 2009. **136**(11): p. 1869-78.

71. Zhang, M., et al., *Granulosa cell ligand NPPC and its receptor NPR2 maintain meiotic arrest in mouse oocytes.* Science, 2010. **330**(6002): p. 366-9.

72. Rybalkin, S.D., et al., *Regulation of cGMP-specific phosphodiesterase (PDE5) phosphorylation in smooth muscle cells.* J Biol Chem, 2002. **277**(5): p. 3310-7.

73. Rybalkin, S.D., et al., *PDE5 is converted to an activated state upon cGMP binding to the GAF A domain.* EMBO J, 2003. **22**(3): p. 469-78.

74. Rybalkin, S.D., et al., *Cyclic GMP phosphodiesterases and regulation of smooth muscle function.* Circ Res, 2003. **93**(4): p. 280-91.

75. Mullershausen, F., et al., *Rapid nitric oxide-induced desensitization of the cGMP response is caused by increased activity of phosphodiesterase type 5 paralleled by phosphorylation of the enzyme.* J Cell Biol, 2001. **155**(2): p. 271-8.

76. Shimizu-Albergine, M., et al., *Individual cerebellar Purkinje cells express different cGMP phosphodiesterases (PDEs): in vivo phosphorylation of cGMP-specific PDE (PDE5) as an indicator of cGMP-dependent protein kinase (PKG) activation.* J Neurosci, 2003. **23**(16): p. 6452-9.

77. Sopory, S., T. Kaur, and S.S. Visweswariah, *The cGMP-binding, cGMP-specific phosphodiesterase (PDE5): intestinal cell expression, regulation and role in fluid secretion.* Cell Signal, 2004. **16**(6): p. 681-92.

78. Zhu, B., S. Strada, and T. Stevens, *Cyclic GMP-specific phosphodiesterase 5 regulates growth and apoptosis in pulmonary endothelial cells.* Am J Physiol Lung Cell Mol Physiol, 2005. **289**(2): p. L196-206.

79. Burns, M.E. and V.Y. Arshavsky, *Beyond counting photons: trials and trends in vertebrate visual transduction.* Neuron, 2005. **48**(3): p. 387-401.

80. Schmidt, H. and F.G. Rathjen, *Signalling mechanisms regulating axonal branching in vivo.* Bioessays, 2010. **32**(11): p. 977-85.

81. Gibson, D.A. and L. Ma, *Developmental regulation of axon branching in the vertebrate nervous system.* Development, 2011. **138**(2): p. 183-95.

82. Marmigere, F. and P. Ernfors, *Specification and connectivity of neuronal subtypes in the sensory lineage.* Nat Rev Neurosci, 2007. **8**(2): p. 114-27.

83. Schmidt, H., et al., *C-type natriuretic peptide (CNP) is a bifurcation factor for sensory neurons.* Proc Natl Acad Sci U S A, 2009. **106**(39): p. 16847-52.

84. Schmidt, H., et al., *cGMP-mediated signaling via cGKIalpha is required for the guidance and connectivity of sensory axons.* J Cell Biol, 2002. **159**(3): p. 489-98.

85. Schmidt, H. and F.G. Rathjen, *DiI-labeling of DRG neurons to study axonal branching in a whole mount preparation of mouse embryonic spinal cord.* J Vis Exp, 2011(58).

86. Zhao, Z. and L. Ma, *Regulation of axonal development by natriuretic peptide hormones.* Proc Natl Acad Sci U S A, 2009. **106**(42): p. 18016-21.

87. Zhao, Z., et al., *Regulate axon branching by the cyclic GMP pathway via inhibition of glycogen synthase kinase 3 in dorsal root ganglion sensory neurons.* J Neurosci, 2009. **29**(5): p. 1350-60.

88. Gawaz, M., H. Langer, and A.E. May, *Platelets in inflammation and atherogenesis.* J Clin Invest, 2005. **115**(12): p. 3378-84.

89. Marcus, A.J., M.J. Broekman, and D.J. Pinsky, *COX inhibitors and thromboregulation.* N Engl J Med, 2002. **347**(13): p. 1025-6.

90.   Marcus, A.J., et al., *Role of CD39 (NTPDase-1) in thromboregulation, cerebroprotection, and cardioprotection.* Semin Thromb Hemost, 2005. **31**(2): p. 234-46.

91.   Furie, B. and B.C. Furie, *Mechanisms of thrombus formation.* N Engl J Med, 2008. **359**(9): p. 938-49.

92.   Ruggeri, Z.M., *Platelet adhesion under flow.* Microcirculation, 2009. **16**(1): p. 58-83.

93.   Ruggeri, Z.M., *Old concepts and new developments in the study of platelet aggregation.* J Clin Invest, 2000. **105**(6): p. 699-701.

94.   Li, Z., et al., *Signaling during platelet adhesion and activation.* Arterioscler Thromb Vasc Biol, 2010. **30**(12): p. 2341-9.

95.   Haslam, R.J., N.T. Dickinson, and E.K. Jang, *Cyclic nucleotides and phosphodiesterases in platelets.* Thromb Haemost, 1999. **82**(2): p. 412-23.

96.   Schwarz, U.R., U. Walter, and M. Eigenthaler, *Taming platelets with cyclic nucleotides.* Biochem Pharmacol, 2001. **62**(9): p. 1153-61.

97.   Geiselhoringer, A., et al., *Distribution of IRAG and cGKI-isoforms in murine tissues.* FEBS Lett, 2004. **575**(1-3): p. 19-22.

98.   Antl, M., et al., *IRAG mediates NO/cGMP-dependent inhibition of platelet aggregation and thrombus formation.* Blood, 2007. **109**(2): p. 552-9.

99.   Massberg, S., et al., *Increased adhesion and aggregation of platelets lacking cyclic guanosine 3',5'-monophosphate kinase I.* J Exp Med, 1999. **189**(8): p. 1255-64.

100.   Massberg, S., et al., *Enhanced in vivo platelet adhesion in vasodilator-stimulated phosphoprotein (VASP)-deficient mice.* Blood, 2004. **103**(1): p. 136-42.

101.   Walter, U. and S. Gambaryan, *cGMP and cGMP-dependent protein kinase in platelets and blood cells.* Handb Exp Pharmacol, 2009(191): p. 533-48.

102.   Dangel, O., et al., *Nitric oxide-sensitive guanylyl cyclase is the only nitric oxide receptor mediating platelet inhibition.* J Thromb Haemost, 2010. **8**(6): p. 1343-52.

103.   Zhang, G., et al., *Biphasic roles for soluble guanylyl cyclase (sGC) in platelet activation.* Blood, 2011. **118**(13): p. 3670-9.

104.   Li, Z., et al., *A stimulatory role for cGMP-dependent protein kinase in platelet activation.* Cell, 2003. **112**(1): p. 77-86.

105.   Haslam, R.J. and M.D. McClenaghan, *Effects of collagen and of aspirin on the concentration of guanosine 3':5'-cyclic monophosphate in human blood platelets: measurement by a prelabelling technique.* Biochem J, 1974. **138**(2): p. 317-20.

106.   Brooker, G., L.J. Thomas, Jr., and M.M. Appleman, *The assay of adenosine 3',5'-cyclic monophosphate and guanosine 3',5'-cyclic monophosphate in biological materials by enzymatic radioisotopic displacement.* Biochemistry, 1968. **7**(12): p. 4177-81.

107.   Steiner, A.L., et al., *Radioimmunoassay for the measurement of cyclic nucleotides.* Adv Cyclic Nucleotide Res, 1972. **2**: p. 51-61.

108.   Schmidt, P.M., *Biochemical Detection of cGMP From Past to Present: An Overview.* Handb Exp Pharmacol, 2009(191): p. 195-228.

109.   Butt, E., et al., *cAMP- and cGMP-dependent protein kinase phosphorylation sites of the focal adhesion vasodilator-stimulated phosphoprotein (VASP) in vitro and in intact human platelets.* J Biol Chem, 1994. **269**(20): p. 14509-17.

110.   Weber, S., et al., *Rescue of cGMP kinase I knockout mice by smooth muscle specific expression of either isozyme.* Circ Res, 2007. **101**(11): p. 1096-103.

111.   Johansson, K., et al., *Immunohistochemical analysis of the developing inner plexiform layer in postnatal rat retina.* Invest Ophthalmol Vis Sci, 2000. **41**(1): p. 305-13.

112.   Tanaka, J., et al., *Nitric oxide-mediated cGMP synthesis in oligodendrocytes in the developing rat brain.* Glia, 1997. **19**(4): p. 286-97.

113.   Nikolaev, V.O. and M.J. Lohse, *Novel techniques for real-time monitoring of cGMP in living cells.* Handb Exp Pharmacol, 2009(191): p. 229-43.

114. Zhang, J., et al., *Creating new fluorescent probes for cell biology.* Nat Rev Mol Cell Biol, 2002. **3**(12): p. 906-18.

115. Grynkiewicz, G., M. Poenie, and R.Y. Tsien, *A new generation of Ca2+ indicators with greatly improved fluorescence properties.* J Biol Chem, 1985. **260**(6): p. 3440-50.

116. Okumoto, S., A. Jones, and W.B. Frommer, *Quantitative imaging with fluorescent biosensors.* Annu Rev Plant Biol, 2012. **63**: p. 663-706.

117. Mank, M. and O. Griesbeck, *Genetically encoded calcium indicators.* Chem Rev, 2008. **108**(5): p. 1550-64.

118. Lleres, D., S. Swift, and A.I. Lamond, *Detecting protein-protein interactions in vivo with FRET using multiphoton fluorescence lifetime imaging microscopy (FLIM).* Curr Protoc Cytom, 2007. **Chapter 12**: p. Unit12 10.

119. Yasuda, R., et al., *Supersensitive Ras activation in dendrites and spines revealed by two-photon fluorescence lifetime imaging.* Nat Neurosci, 2006. **9**(2): p. 283-91.

120. Harvey, C.D., et al., *A genetically encoded fluorescent sensor of ERK activity.* Proc Natl Acad Sci U S A, 2008. **105**(49): p. 19264-9.

121. Cao, G., et al., *Genetically targeted optical electrophysiology in intact neural circuits.* Cell, 2013. **154**(4): p. 904-13.

122. Conway, D.E., et al., *Fluid shear stress on endothelial cells modulates mechanical tension across VE-cadherin and PECAM-1.* Curr Biol, 2013. **23**(11): p. 1024-30.

123. Lam, A.J., et al., *Improving FRET dynamic range with bright green and red fluorescent proteins.* Nat Methods, 2012. **9**(10): p. 1005-12.

124. T, F., *Intermolecular energy migration and fluorescence.* Ann Physiol, 1948. **2**: p. 55-75.

125. Rich, T.C., et al., *Cyclic nucleotide-gated channels colocalize with adenylyl cyclase in regions of restricted cAMP diffusion.* J Gen Physiol, 2000. **116**(2): p. 147-61.

126. Rich, T.C., et al., *In vivo assessment of local phosphodiesterase activity using tailored cyclic nucleotide-gated channels as cAMP sensors.* J Gen Physiol, 2001. **118**(1): p. 63-78.

127. Biel, M., A. Schneider, and C. Wahl, *Cardiac HCN channels: structure, function, and modulation.* Trends Cardiovasc Med, 2002. **12**(5): p. 206-12.

128. Pfleger, K.D. and K.A. Eidne, *Illuminating insights into protein-protein interactions using bioluminescence resonance energy transfer (BRET).* Nat Methods, 2006. **3**(3): p. 165-74.

129. Biswas, K.H., S. Sopory, and S.S. Visweswariah, *The GAF domain of the cGMP-binding, cGMP-specific phosphodiesterase (PDE5) is a sensor and a sink for cGMP.* Biochemistry, 2008. **47**(11): p. 3534-43.

130. Nausch, L.W., et al., *Differential patterning of cGMP in vascular smooth muscle cells revealed by single GFP-linked biosensors.* Proc Natl Acad Sci U S A, 2008. **105**(1): p. 365-70.

131. Bhargava, Y., et al., *Improved genetically-encoded, FlincG-type fluorescent biosensors for neural cGMP imaging.* Front Mol Neurosci, 2013. **6**: p. 26.

132. Sato, M., et al., *Fluorescent indicators for cyclic GMP based on cyclic GMP-dependent protein kinase Ialpha and green fluorescent proteins.* Anal Chem, 2000. **72**(24): p. 5918-24.

133. Nikolaev, V.O., S. Gambaryan, and M.J. Lohse, *Fluorescent sensors for rapid monitoring of intracellular cGMP.* Nat Methods, 2006. **3**(1): p. 23-5.

134. Niino, Y., K. Hotta, and K. Oka, *Simultaneous live cell imaging using dual FRET sensors with a single excitation light.* PLoS One, 2009. **4**(6): p. e6036.

135. Thunemann, M., et al., *Visualization of cGMP with cGi biosensors.* Methods Mol Biol, 2013. **1020**: p. 89-120.

136. Sprenger, J.U. and V.O. Nikolaev, *Biophysical techniques for detection of cAMP and cGMP in living cells.* Int J Mol Sci, 2013. **14**(4): p. 8025-46.

137. Honda, A., et al., *Spatiotemporal dynamics of guanosine 3',5'-cyclic monophosphate revealed by a genetically encoded, fluorescent indicator.* Proc Natl Acad Sci U S A, 2001. **98**(5): p. 2437-42.

138. Russwurm, M., et al., *Design of fluorescence resonance energy transfer (FRET)-based cGMP indicators: a systematic approach.* Biochem J, 2007. **407**(1): p. 69-77.

139. Pittet, M.J. and R. Weissleder, *Intravital imaging.* Cell, 2011. **147**(5): p. 983-91.

140. Jaenisch, R. and B. Mintz, *Simian virus 40 DNA sequences in DNA of healthy adult mice derived from preimplantation blastocysts injected with viral DNA.* Proc Natl Acad Sci U S A, 1974. **71**(4): p. 1250-4.

141. Copeland, N.G. and N.A. Jenkins, *Harnessing transposons for cancer gene discovery.* Nat Rev Cancer, 2010. **10**(10): p. 696-706.

142. Capecchi, M.R., *Gene targeting in mice: functional analysis of the mammalian genome for the twenty-first century.* Nat Rev Genet, 2005. **6**(6): p. 507-12.

143. Palmiter, R.D., et al., *Dramatic growth of mice that develop from eggs microinjected with metallothionein-growth hormone fusion genes.* Nature, 1982. **300**(5893): p. 611-5.

144. Costantini, F. and E. Lacy, *Introduction of a rabbit beta-globin gene into the mouse germ line.* Nature, 1981. **294**(5836): p. 92-4.

145. Gordon, J.W. and F.H. Ruddle, *Integration and stable germ line transmission of genes injected into mouse pronuclei.* Science, 1981. **214**(4526): p. 1244-6.

146. Palmiter, R.D. and R.L. Brinster, *Germ-line transformation of mice.* Annu Rev Genet, 1986. **20**: p. 465-99.

147. Thomas, K.R. and M.R. Capecchi, *Site-directed mutagenesis by gene targeting in mouse embryo-derived stem cells.* Cell, 1987. **51**(3): p. 503-12.

148. Thomas, K.R. and M.R. Capecchi, *Targeted disruption of the murine int-1 proto-oncogene resulting in severe abnormalities in midbrain and cerebellar development.* Nature, 1990. **346**(6287): p. 847-50.

149. McMahon, A.P. and A. Bradley, *The Wnt-1 (int-1) proto-oncogene is required for development of a large region of the mouse brain.* Cell, 1990. **62**(6): p. 1073-85.

150. Yagi, T., et al., *A novel negative selection for homologous recombinants using diphtheria toxin A fragment gene.* Anal Biochem, 1993. **214**(1): p. 77-86.

151. Copp, A.J., *Death before birth: clues from gene knockouts and mutations.* Trends Genet, 1995. **11**(3): p. 87-93.

152. Kuhn, R. and F. Schwenk, *Conditional knockout mice.* Methods Mol Biol, 2003. **209**: p. 159-85.

153. Sternberg, N. and D. Hamilton, *Bacteriophage P1 site-specific recombination. I. Recombination between loxP sites.* J Mol Biol, 1981. **150**(4): p. 467-86.

154. Abremski, K., R. Hoess, and N. Sternberg, *Studies on the properties of P1 site-specific recombination: evidence for topologically unlinked products following recombination.* Cell, 1983. **32**(4): p. 1301-11.

155. Buchholz, F., P.O. Angrand, and A.F. Stewart, *Improved properties of FLP recombinase evolved by cycling mutagenesis.* Nat Biotechnol, 1998. **16**(7): p. 657-62.

156. Gu, H., *Gene targeting and its application to the study of B-cell development.* Curr Opin Immunol, 1994. **6**(2): p. 308-12.

157. Gu, H., Y.R. Zou, and K. Rajewsky, *Independent control of immunoglobulin switch recombination at individual switch regions evidenced through Cre-loxP-mediated gene targeting.* Cell, 1993. **73**(6): p. 1155-64.

158. Feil, R., et al., *Ligand-activated site-specific recombination in mice.* Proc Natl Acad Sci U S A, 1996. **93**(20): p. 10887-90.

159. Kuhn, R., et al., *Inducible gene targeting in mice.* Science, 1995. **269**(5229): p. 1427-9.

160. Feil, R., et al., *Regulation of Cre recombinase activity by mutated estrogen receptor ligand-binding domains.* Biochem Biophys Res Commun, 1997. **237**(3): p. 752-7.

161. Feil, S., N. Valtcheva, and R. Feil, *Inducible Cre mice.* Methods Mol Biol, 2009. **530**: p. 343-63.

162. Feil, R., *Conditional somatic mutagenesis in the mouse using site-specific recombinases.* Handb Exp Pharmacol, 2007(178): p. 3-28.

163. Luo, L., E.M. Callaway, and K. Svoboda, *Genetic dissection of neural circuits.* Neuron, 2008. **57**(5): p. 634-60.

164. Vagner, S., B. Galy, and S. Pyronnet, *Irresistible IRES. Attracting the translation machinery to internal ribosome entry sites.* EMBO Rep, 2001. **2**(10): p. 893-8.

165. Szymczak, A.L., et al., *Correction of multi-gene deficiency in vivo using a single 'self-cleaving' 2A peptide-based retroviral vector.* Nat Biotechnol, 2004. **22**(5): p. 589-94.

166. Soriano, P., *Generalized lacZ expression with the ROSA26 Cre reporter strain.* Nat Genet, 1999. **21**(1): p. 70-1.

167. Badea, T.C., et al., *New mouse lines for the analysis of neuronal morphology using CreER(T)/loxP-directed sparse labeling.* PLoS One, 2009. **4**(11): p. e7859.

168. Safran, M., et al., *Mouse reporter strain for noninvasive bioluminescent imaging of cells that have undergone Cre-mediated recombination.* Mol Imaging, 2003. **2**(4): p. 297-302.

169. Srinivas, S., et al., *Cre reporter strains produced by targeted insertion of EYFP and ECFP into the ROSA26 locus.* BMC Dev Biol, 2001. **1**: p. 4.

170. Lin, F., et al., *Hematopoietic stem cells contribute to the regeneration of renal tubules after renal ischemia-reperfusion injury in mice.* J Am Soc Nephrol, 2003. **14**(5): p. 1188-99.

171. Madisen, L., et al., *A robust and high-throughput Cre reporting and characterization system for the whole mouse brain.* Nat Neurosci, 2010. **13**(1): p. 133-40.

172. Madisen, L., et al., *A toolbox of Cre-dependent optogenetic transgenic mice for light-induced activation and silencing.* Nat Neurosci, 2012. **15**(5): p. 793-802.

173. Zong, H., et al., *Mosaic analysis with double markers in mice.* Cell, 2005. **121**(3): p. 479-92.

174. Muzumdar, M.D., et al., *A global double-fluorescent Cre reporter mouse.* Genesis, 2007. **45**(9): p. 593-605.

175. Snippert, H.J., et al., *Intestinal crypt homeostasis results from neutral competition between symmetrically dividing Lgr5 stem cells.* Cell, 2010. **143**(1): p. 134-44.

176. Zariwala, H.A., et al., *A Cre-dependent GCaMP3 reporter mouse for neuronal imaging in vivo.* J Neurosci, 2012. **32**(9): p. 3131-41.

177. Dreosti, E., et al., *A genetically encoded reporter of synaptic activity in vivo.* Nat Methods, 2009. **6**(12): p. 883-9.

178. Thunemann, M., and Wen, L., et al., *Transgenic mice for cGMP imaging.* Circ Res, 2013. **113**(4): p. 365-71.

179. Mullershausen, F., et al., *Direct activation of PDE5 by cGMP: long-term effects within NO/cGMP signaling.* J Cell Biol, 2003. **160**(5): p. 719-27.

180. Valtcheva, N., et al., *The commonly used cGMP-dependent protein kinase type I (cGKI) inhibitor Rp-8-Br-PET-cGMPS can activate cGKI in vitro and in intact cells.* J Biol Chem, 2009. **284**(1): p. 556-62.

181. Kuhbandner, S., *Induzierbare Cre-vermittelte Rekombination im glatten Muskel der Maus.* Dissertation. Fakultät Wissenschaftszentrum Weihenstephan, TU München, München, 2001.

182. Thunemann, M., *Generation and characterization of transgenic mice for noninvasive cell tracking with PET and for FRET-based cGMP imaging.* Dissertation. Mathematisch-Naturwissenschaftlichen Fakultät, Universität Tübingen , Tübingen, 2012.

183. Nagy, A., et al., *Manipulating the Mouse Embryo: A Laboratory Manual. Third Edition.* Cold Spring Harbor: Cold Spring Harbor Laboratory Press, 2003: p. 359-452.

184. Tompers, D.M. and P.A. Labosky, *Electroporation of murine embryonic stem cells: a step-by-step guide.* Stem Cells, 2004. **22**(3): p. 243-9.

185. Vachaviolos, I.-A., *Construction of targeting vectors for Cre/lox assisted genome modifications.* Diploma thesis. Department of Life Sciences, Faculty For Biochemistry And Biotechnology, University of Thessaly, Thessaly, 2010.

186. Boiani, M. and H.R. Scholer, *Regulatory networks in embryo-derived pluripotent stem cells.* Nat Rev Mol Cell Biol, 2005. **6**(11): p. 872-84.

187. Nagy, A., et al., *Derivation of completely cell culture-derived mice from early-passage embryonic stem cells.* Proceedings of the National Academy of Sciences, USA, 1993. **90**(18): p. 8424-8.

188. Barski, J.J., K. Dethleffsen, and M. Meyer, *Cre recombinase expression in cerebellar Purkinje cells.* Genesis, 2000. **28**(3-4): p. 93-8.

189. Ruggeri, Z.M. and G.L. Mendolicchio, *Adhesion mechanisms in platelet function.* Circ Res, 2007. **100**(12): p. 1673-85.

190. Rasband, W.S. *ImageJ.* 1997-2012; Available from: http://imagej.nih.gov/ij/.

191. Barski, J.J., et al., *Calbindin in cerebellar Purkinje cells is a critical determinant of the precision of motor coordination.* J Neurosci, 2003. **23**(8): p. 3469-77.

192. Feil, R., et al., *Impairment of LTD and cerebellar learning by Purkinje cell-specific ablation of cGMP-dependent protein kinase I.* J Cell Biol, 2003. **163**(2): p. 295-302.

193. Lohof, A.M., et al., *Asymmetric modulation of cytosolic cAMP activity induces growth cone turning.* J Neurosci, 1992. **12**(4): p. 1253-61.

194. Pujic, Z., et al., *Analysis of the growth cone turning assay for studying axon guidance.* J Neurosci Methods, 2008. **170**(2): p. 220-8.

195. Robinson, M., et al., *In vivo biotinylation studies: specificity of labelling of reticulated platelets by thiazole orange and mepacrine.* Br J Haematol, 2000. **108**(4): p. 859-64.

196. Leeksma, C.H. and J.A. Cohen, *The life-span of thrombocytes determined with radioactive DFP.* Ned Tijdschr Geneeskd, 1955. **99**(47): p. 3563-5.

197. Corish, P. and C. Tyler-Smith, *Attenuation of green fluorescent protein half-life in mammalian cells.* Protein Eng, 1999. **12**(12): p. 1035-40.

198. Verkhusha, V.V., et al., *High stability of Discosoma DsRed as compared to Aequorea EGFP.* Biochemistry, 2003. **42**(26): p. 7879-84.

199. Horky, J., J. Vacha, and V. Znojil, *Comparison of life span of erythrocytes in some inbred strains of mouse using 14C-labelled glycine.* Physiol Bohemoslov, 1978. **27**(3): p. 209-17.

200. Zambrowicz, B.P., et al., *Disruption of overlapping transcripts in the ROSA beta geo 26 gene trap strain leads to widespread expression of beta-galactosidase in mouse embryos and hematopoietic cells.* Proc Natl Acad Sci U S A, 1997. **94**(8): p. 3789-94.

201. Maragos, C.M., et al., *Complexes of .NO with nucleophiles as agents for the controlled biological release of nitric oxide. Vasorelaxant effects.* J Med Chem, 1991. **34**(11): p. 3242-7.

202. Keefer, L.K., et al., *"NONOates" (1-substituted diazen-1-ium-1,2-diolates) as nitric oxide donors: convenient nitric oxide dosage forms.* Methods Enzymol, 1996. **268**: p. 281-93.

203. Jackson, S.P., *Arterial thrombosis--insidious, unpredictable and deadly.* Nat Med, 2011. **17**(11): p. 1423-36.

204. Quinton, T.M., K.D. Brown, and W.L. Dean, *Inositol 1,4,5-trisphosphate-mediated Ca2+ release from platelet internal membranes is regulated by differential phosphorylation.* Biochemistry, 1996. **35**(21): p. 6865-71.

205. Cavallini, L., et al., *Prostacyclin and sodium nitroprusside inhibit the activity of the platelet inositol 1,4,5-trisphosphate receptor and promote its phosphorylation.* J Biol Chem, 1996. **271**(10): p. 5545-51.

206. Eigenthaler, M., et al., *Defective nitrovasodilator-stimulated protein phosphorylation and calcium regulation in cGMP-dependent protein kinase-deficient human platelets of chronic myelocytic leukemia.* J Biol Chem, 1993. **268**(18): p. 13526-31.

207. Schlossmann, J., et al., *Regulation of intracellular calcium by a signalling complex of IRAG, IP3 receptor and cGMP kinase Ibeta.* Nature, 2000. **404**(6774): p. 197-201.

208. Ginsberg, M.H., A. Partridge, and S.J. Shattil, *Integrin regulation.* Curr Opin Cell Biol, 2005. **17**(5): p. 509-16.

209. Andrews, R.K., et al., *Glycoprotein Ib-IX-V.* Int J Biochem Cell Biol, 2003. **35**(8): p. 1170-4.

210. Gambaryan, S., et al., *NO-synthase-/NO-independent regulation of human and murine platelet soluble guanylyl cyclase activity.* J Thromb Haemost, 2008. **6**(8): p. 1376-84.

211. Riba, R., et al., *Von Willebrand factor activates endothelial nitric oxide synthase in blood platelets by a glycoprotein Ib-dependent mechanism.* J Thromb Haemost, 2006. **4**(12): p. 2636-44.

212. Bergmeier, W., et al., *The role of platelet adhesion receptor GPIbalpha far exceeds that of its main ligand, von Willebrand factor, in arterial thrombosis.* Proc Natl Acad Sci U S A, 2006. **103**(45): p. 16900-5.

213. Kanaji, T., S. Russell, and J. Ware, *Amelioration of the macrothrombocytopenia associated with the murine Bernard-Soulier syndrome.* Blood, 2002. **100**(6): p. 2102-7.

214. Arnadottir, J. and M. Chalfie, *Eukaryotic mechanosensitive channels.* Annu Rev Biophys, 2010. **39**: p. 111-37.

215. Nilius, B., et al., *Transient receptor potential cation channels in disease.* Physiol Rev, 2007. **87**(1): p. 165-217.

216. Kiyonaka, S., et al., *Selective and direct inhibition of TRPC3 channels underlies biological activities of a pyrazole compound.* Proc Natl Acad Sci U S A, 2009. **106**(13): p. 5400-5.

217. Carvajal, J.A., et al., *Molecular mechanism of cGMP-mediated smooth muscle relaxation.* J Cell Physiol, 2000. **184**(3): p. 409-20.

218. Lincoln, T.M., N. Dey, and H. Sellak, *Invited review: cGMP-dependent protein kinase signaling mechanisms in smooth muscle: from the regulation of tone to gene expression.* J Appl Physiol, 2001. **91**(3): p. 1421-30.

219. Nakatsu, K. and J. Diamond, *Role of cGMP in relaxation of vascular and other smooth muscle.* Can J Physiol Pharmacol, 1989. **67**(4): p. 251-62.

220. Rees, D.D., R.M. Palmer, and S. Moncada, *Role of endothelium-derived nitric oxide in the regulation of blood pressure.* Proc Natl Acad Sci U S A, 1989. **86**(9): p. 3375-8.

221. Friebe, A., et al., *YC-1 potentiates nitric oxide- and carbon monoxide-induced cyclic GMP effects in human platelets.* Mol Pharmacol, 1998. **54**(6): p. 962-7.

222. Hwang, T.L., S.K. Zhuo, and Y.L. Pan, *YC-1 attenuates homotypic human neutrophil aggregation through inhibition of phosphodiesterase activity.* Eur J Pharmacol, 2008. **579**(1-3): p. 395-402.

223. Galle, J., et al., *Effects of the soluble guanylyl cyclase activator, YC-1, on vascular tone, cyclic GMP levels and phosphodiesterase activity.* Br J Pharmacol, 1999. **127**(1): p. 195-203.

224. Nakamizo, T., et al., *Phosphodiesterase inhibitors are neuroprotective to cultured spinal motor neurons.* J Neurosci Res, 2003. **71**(4): p. 485-95.

225. Gibson, A., *Phosphodiesterase 5 inhibitors and nitrergic transmission-from zaprinast to sildenafil.* Eur J Pharmacol, 2001. **411**(1-2): p. 1-10.

226. Zhang, X., Q. Feng, and R.H. Cote, *Efficacy and selectivity of phosphodiesterase-targeted drugs in inhibiting photoreceptor phosphodiesterase (PDE6) in retinal photoreceptors.* Invest Ophthalmol Vis Sci, 2005. **46**(9): p. 3060-6.

227.   Ter-Avetisyan, G., F.G. Rathjen, and H. Schmidt, *Bifurcation of Axons from Cranial Sensory Neurons Is Disabled in the Absence of Npr2-Induced cGMP Signaling.* J Neurosci, 2014. **34**(3): p. 737-47.

228.   Lowery, L.A. and D. Van Vactor, *The trip of the tip: understanding the growth cone machinery.* Nat Rev Mol Cell Biol, 2009. **10**(5): p. 332-43.

229.   Zheng, J.Q., J.J. Wan, and M.M. Poo, *Essential role of filopodia in chemotropic turning of nerve growth cone induced by a glutamate gradient.* J Neurosci, 1996. **16**(3): p. 1140-9.

230.   Nicol, X., K.P. Hong, and N.C. Spitzer, *Spatial and temporal second messenger codes for growth cone turning.* Proc Natl Acad Sci U S A, 2011. **108**(33): p. 13776-81.

231.   Ma, L. and M. Tessier-Lavigne, *Dual branch-promoting and branch-repelling actions of Slit/Robo signaling on peripheral and central branches of developing sensory axons.* J Neurosci, 2007. **27**(25): p. 6843-51.

232.   Fu, S.Y., et al., *SEMA3A regulates developing sensory projections in the chicken spinal cord.* J Neurobiol, 2000. **45**(4): p. 227-36.

233.   Masuda, T., et al., *Guidance cues from the embryonic dorsal spinal cord chemoattract dorsal root ganglion axons.* Neuroreport, 2007. **18**(16): p. 1645-9.

234.   Watanabe, K., et al., *Dorsally derived netrin 1 provides an inhibitory cue and elaborates the 'waiting period' for primary sensory axons in the developing spinal cord.* Development, 2006. **133**(7): p. 1379-87.

235.   Tojima, T., et al., *Second messengers and membrane trafficking direct and organize growth cone steering.* Nat Rev Neurosci, 2011. **12**(4): p. 191-203.

236.   Ming, G.L., et al., *cAMP-dependent growth cone guidance by netrin-1.* Neuron, 1997. **19**(6): p. 1225-35.

237.   Nishiyama, M., et al., *Membrane potential shifts caused by diffusible guidance signals direct growth-cone turning.* Nat Neurosci, 2008. **11**(7): p. 762-71.

238.   Kobayashi, T., et al., *Crosstalk between second messengers predicts the motility of the growth cone.* Sci Rep, 2013. **3**: p. 3118.

239.   Zhou, F.Q., C.M. Waterman-Storer, and C.S. Cohan, *Focal loss of actin bundles causes microtubule redistribution and growth cone turning.* J Cell Biol, 2002. **157**(5): p. 839-49.

240.   Dent, E.W., F. Tang, and K. Kalil, *Axon guidance by growth cones and branches: common cytoskeletal and signaling mechanisms.* The Neuroscientist, 2003. **9**(5): p. 343-353.

241.   Polleux, F., T. Morrow, and A. Ghosh, *Semaphorin 3A is a chemoattractant for cortical apical dendrites.* Nature, 2000. **404**(6778): p. 567-73.

242.   Walter, J., S. Henke-Fahle, and F. Bonhoeffer, *Avoidance of posterior tectal membranes by temporal retinal axons.* Development, 1987. **101**(4): p. 909-13.

243.   Walter, J., et al., *Recognition of position-specific properties of tectal cell membranes by retinal axons in vitro.* Development, 1987. **101**(4): p. 685-96.

244.   Knoll, B., et al., *Stripe assay to examine axonal guidance and cell migration.* Nat Protoc, 2007. **2**(5): p. 1216-24.

245.   Shelly, M., et al., *Local and long-range reciprocal regulation of cAMP and cGMP in axon/dendrite formation.* Science, 2010. **327**(5965): p. 547-52.

246.   Yates, P.A., et al., *Topographic-specific axon branching controlled by ephrin-As is the critical event in retinotectal map development.* J Neurosci, 2001. **21**(21): p. 8548-63.

247.   Palmer, A.E., et al., *Bcl-2-mediated alterations in endoplasmic reticulum Ca2+ analyzed with an improved genetically encoded fluorescent sensor.* Proc Natl Acad Sci U S A, 2004. **101**(50): p. 17404-9.

248.   Harbeck, M.C., et al., *Simultaneous optical measurements of cytosolic Ca2+ and cAMP in single cells.* Sci STKE, 2006. **2006**(353): p. pl6.

249.   Russwurm, M., et al., *Inhibition of deactivation of NO-sensitive guanylyl cyclase accounts for the sensitizing effect of YC-1.* J Biol Chem, 2002. **277**(28): p. 24883-8.

250. Lundberg, J.O., E. Weitzberg, and M.T. Gladwin, *The nitrate-nitrite-nitric oxide pathway in physiology and therapeutics.* Nat Rev Drug Discov, 2008. **7**(2): p. 156-67.

251. Irwin, C., W. Roberts, and K.M. Naseem, *Nitric oxide inhibits platelet adhesion to collagen through cGMP-dependent and independent mechanisms: the potential role for S-nitrosylation.* Platelets, 2009. **20**(7): p. 478-86.

252. Lima, B., et al., *S-nitrosylation in cardiovascular signaling.* Circ Res, 2010. **106**(4): p. 633-46.

253. Orr, A.W., et al., *Mechanisms of mechanotransduction.* Dev Cell, 2006. **10**(1): p. 11-20.

254. Balashova, N., et al., *Characterization of a novel type of endogenous activator of soluble guanylyl cyclase.* J Biol Chem, 2005. **280**(3): p. 2186-96.

255. Russwurm, M., N. Wittau, and D. Koesling, *Guanylyl cyclase/PSD-95 interaction: targeting of the nitric oxide-sensitive alpha2beta1 guanylyl cyclase to synaptic membranes.* J Biol Chem, 2001. **276**(48): p. 44647-52.

256. Heckler, E.J., et al., *Protein disulfide-isomerase interacts with soluble guanylyl cyclase via a redox-based mechanism and modulates its activity.* Biochem J, 2013. **452**(1): p. 161-9.

257. Zwiller, J., M.O. Revel, and A.N. Malviya, *Protein kinase C catalyzes phosphorylation of guanylate cyclase in vitro.* J Biol Chem, 1985. **260**(3): p. 1350-3.

258. Louis, J.C., M.O. Revel, and J. Zwiller, *Activation of soluble guanylate cyclase through phosphorylation by protein kinase C in intact PC12 cells.* Biochim Biophys Acta, 1993. **1177**(3): p. 299-306.

259. Zwiller, J., M.O. Revel, and P. Basset, *Evidence for phosphorylation of rat brain guanylate cyclase by cyclic AMP-dependent protein kinase.* Biochem Biophys Res Commun, 1981. **101**(4): p. 1381-7.

260. Murthy, K.S., *Activation of phosphodiesterase 5 and inhibition of guanylate cyclase by cGMP-dependent protein kinase in smooth muscle.* Biochemical Journal, 2001. **360**: p. 199-208.

261. Murthy, K.S., *Modulation of soluble guanylate cyclase activity by phosphorylation.* Neurochemistry International, 2004. **45**(6): p. 845-851.

262. Murthy, K.S., *Inhibitory phosphorylation of soluble guanylyl cyclase by muscarinic m2 receptors via Gbetagamma-dependent activation of c-Src kinase.* J Pharmacol Exp Ther, 2008. **325**(1): p. 183-9.

263. Zabel, U., et al., *Calcium-dependent membrane association sensitizes soluble guanylyl cyclase to nitric oxide.* Nat Cell Biol, 2002. **4**(4): p. 307-11.

264. Tzima, E., et al., *A mechanosensory complex that mediates the endothelial cell response to fluid shear stress.* Nature, 2005. **437**(7057): p. 426-31.

265. Barakat, A.I., *Responsiveness of vascular endothelium to shear stress: potential role of ion channels and cellular cytoskeleton (review).* Int J Mol Med, 1999. **4**(4): p. 323-32.

266. Jalali, S., et al., *Integrin-mediated mechanotransduction requires its dynamic interaction with specific extracellular matrix (ECM) ligands.* Proc Natl Acad Sci U S A, 2001. **98**(3): p. 1042-6.

267. Yu, J., et al., *Direct evidence for the role of caveolin-1 and caveolae in mechanotransduction and remodeling of blood vessels.* J Clin Invest, 2006. **116**(5): p. 1284-91.

268. Hierck, B.P., et al., *Primary cilia sensitize endothelial cells for fluid shear stress.* Dev Dyn, 2008. **237**(3): p. 725-35.

269. Pahakis, M.Y., et al., *The role of endothelial glycocalyx components in mechanotransduction of fluid shear stress.* Biochem Biophys Res Commun, 2007. **355**(1): p. 228-33.

270. Hahn, C. and M.A. Schwartz, *Mechanotransduction in vascular physiology and atherogenesis.* Nat Rev Mol Cell Biol, 2009. **10**(1): p. 53-62.

271. Fujiwara, K., *Platelet endothelial cell adhesion molecule-1 and mechanotransduction in vascular endothelial cells.* J Intern Med, 2006. **259**(4): p. 373-80.

272. Conway, D. and M.A. Schwartz, *Lessons from the endothelial junctional mechanosensory complex.* F1000 Biol Rep, 2012. **4**: p. 1.

273. Falati, S., et al., *Platelet PECAM-1 inhibits thrombus formation in vivo.* Blood, 2006. **107**(2): p. 535-41.

274. Storch, U., M. Mederos y Schnitzler, and T. Gudermann, *G protein-mediated stretch reception.* Am J Physiol Heart Circ Physiol, 2012. **302**(6): p. H1241-9.

275. Harteneck, C. and M. Gollasch, *Pharmacological modulation of diacylglycerol-sensitive TRPC3/6/7 channels.* Curr Pharm Biotechnol, 2011. **12**(1): p. 35-41.

276. Schleifer, H., et al., *Novel pyrazole compounds for pharmacological discrimination between receptor-operated and store-operated Ca(2+) entry pathways.* Br J Pharmacol, 2012. **167**(8): p. 1712-22.

277. Geiger, J., et al., *Role of cGMP and cGMP-dependent protein kinase in nitrovasodilator inhibition of agonist-evoked calcium elevation in human platelets.* Proc Natl Acad Sci U S A, 1992. **89**(3): p. 1031-5.

278. Kroll, M.H., et al., *Platelets and shear stress.* Blood, 1996. **88**(5): p. 1525-41.

279. Sakariassen, K.S., *Thrombus formation on apex of arterial stenoses: the need for a fluid high shear stenosis diagnostic device.* Future Cardiol, 2007. **3**(2): p. 193-201.

280. Nesbitt, W.S., et al., *A shear gradient-dependent platelet aggregation mechanism drives thrombus formation.* Nat Med, 2009. **15**(6): p. 665-73.

281. Cosemans, J.M., et al., *The effects of arterial flow on platelet activation, thrombus growth, and stabilization.* Cardiovasc Res, 2013. **99**(2): p. 342-52.

282. Nesbitt, W.S., et al., *A live cell micro-imaging technique to examine platelet calcium signaling dynamics under blood flow.* Methods Mol Biol, 2012. **788**: p. 73-89.

283. Nesbitt, W.S., et al., *Distinct glycoprotein Ib/V/IX and integrin alpha IIbbeta 3-dependent calcium signals cooperatively regulate platelet adhesion under flow.* J Biol Chem, 2002. **277**(4): p. 2965-72.

284. Dubois, C., et al., *Thrombin-initiated platelet activation in vivo is vWF independent during thrombus formation in a laser injury model.* J Clin Invest, 2007. **117**(4): p. 953-60.

285. Thestrup, T., et al., *Optimized ratiometric calcium sensors for functional in vivo imaging of neurons and T lymphocytes.* Nat Methods, 2014. **11**(2): p. 175-82.

6 Acknowledgements

I would like to give my sincere thanks to Prof. Robert Feil for giving me the opportunity to work on such an interesting and challenging project in his lab. Thank you for your continuous support on my work, especially for those understanding and motivation in front of challenges and for the help on my living in Tübingen.

I would also like to acknowledge Dr. Hannes Schmidt for sharing protocols, ideas and suggestions in the DRG neuron project. I thank Dr. Harald Langer for providing me with GPIb mutant mice and Dr. Marcus Olbrich for helping me set up the platelet flow chamber assay. Thanks to Prof. Gabriele Dodt for supporting with the microinjector and Prof. Ralf Jansen for the cryostat.

I am also grateful to Dr. Susanne Feil for performing blastocyst injections and for help with starting my life in Tübingen.

Many thanks go to Dr. Martin Thunemann for always being so kind to help around, his contribution to the present study and critical reading of the thesis. I thank Dr. Markus Milde for commenting on the thesis. Many thanks go also to Shen Lu, Sinziana Pop, Angelos Vachaviolos and Feride Kaşıkçı for contributing to this work.

I would also like to thank Sandeep Dhayade for interesting discussions and company, and Raghavan Vallur for friendly support.

I thank Barbara Birk for excellent assistance. Thanks to Stefanie Peters, Hyazinth Dobrowinski, Moritz Lehners, and all other past and present members in the Feil lab for the discussions and nice time spent together.

妈妈，谢谢您！Any words would never be too exaggerated to express my gratefulness to my family, my beloved parents, sisters and brothers-in-law for always being so supportive, whatever we have been going through. I thank Xiaocui, for continuous support, encouragement and patience whenever it was needed.

All my friends, in and out of Tübingen, are always invaluable to me, to name a few, Yanmei Qi, Qifeng Zhou and Qi Wang; thanks for helpful discussions and company.

7 Resume

Name: Lai Wen

Gender: Male
Birth: 12.10.1985, Jiangxi, China

Education

2009-Present   Ph.D, University of Tuebingen, Germany

2006-2008   M.Sc. in Cell Biology, Sun Yat-sen University, China

2002-2006   B.E. in Biological Engineering, Nanchang University, China

Honors

2013   Poster award, 6th International Conference on cGMP, Erfurt, Germany

2009   Travel grant, Boheringer Ingelheim Fonds, Germany

Publications

1. **Wen L.**, Thunemann M., Langer H., Gawaz M., de Wit C., Feil R. *Shear stress-regulated cGMP signals in thrombosis.* (in preparation)

2. Thunemann M.*****, **Wen L.***, Hillenbrand M., Vachaviolos A., Feil S., Ott T., Han X., Fukumura D., Jain R.K., Russwurm M., de Wit C., Feil R. *Transgenic mice for cGMP imaging.* Circ Res. 2013, 113, 365-371. **[*, contributed equally]**

3. Fan G., **Wen L.**, Li M., Li C., Luo B., Wang F., Zhou L., Liu L. *Isolation of mouse mesenchymal stem cells with normal ploidy from bone marrows by reducing oxidative stress in combination with extracellular matrix.* BMC Cell Biol. 2011, 12:P30.

4. **Wen L.**, Schwamborn J.C. *Cellular reprogramming and its implications for therapeutic applications.* Euro Pharm Rev. 2009, 3, 36-40.

Abstracts

1. **Wen L.,** Lu S., Thunemann M., Pop S., Schmidt H., Feil R. *cGMP imaging in embryonic dorsal root ganglion neurons with FRET-based cGMP sensor knock-in mice.* 80. Jahrestagung der Deutschen Gesellschaft für Experimentelle und Klinische Pharmakologie und Toxikologie e. V. (DGPT 2014) in Hannover.

2. Thunemann M., **Wen L.**, Feil S., Birk B., Russwurm M., Jaffe L., de Wit C., Han X., Fukumura D., Jain R., Feil R. *cGMP indicator mice: Generation, characterization and first in vivo results.* 80. Jahrestagung der Deutschen Gesellschaft für Experimentelle und Klinische Pharmakologie und Toxikologie e. V. (DGPT 2014) in Hannover.

3. **Wen L.***, Thunemann M.*****, Feil S., Hillenbrand M., Vachaviolos A., Ott T., Han X., Fukumura D., Jain R.K., de Wit C., Russwurm M., Feil R. *Analysis of cGMP signalling with transgenic mice expressing FRET-based cGMP sensors.* BMC Pharmacology and Toxicology. 2013, 14(Suppl 1):P76. **[*, contributed equally]**

4. Jaffe L., Efgbert J., Shuhaibar L., **Wen L.**, Thunemann M., Feil R., Nikolaev V., Robinson J., Potter L. *Cyclic GMP-mediated intercellular communication in mammalian ovarian follicles.* BMC Pharmacology and Toxicology. 2013, 14(Suppl 1):P31.